UNIVERSITÀ DI PARMA

UNIVERSITA' DEGLI STUDI DI PARMA

Dottorato di Ricerca in
Scienze del Farmaco, delle Biomolecole
e dei Prodotti per la Salute

CICLO XXXI

Inhibition of cysteine biosynthesis for the development of enhancers of antibiotic therapy

Coordinatore:
Chiar.mo Prof. Marco Mor

Relatore:
Chiar.mo Prof. Andrea Mozzarelli

Dottoranda: Nina Franko

Anni 2015/2019

The research was supported by MSCA-ITN-2014-ETN project INTEGRATE, grant number 642620. Nina Franko was a MSCA INTEGRATE Early Stage Researcher (ESR).

The thesis contains unpublished results and results that have been published in the following papers:

Magalhães J, **Franko N**, Annunziato G, Pieroni M, Benoni R, Nikitjuka A, Mozzarelli A, Bettati S, Karawajczyk A, Jirgensons A, Campanini B, Costantino G. *Refining the Structure–Activity Relationships of 2-Phenylcyclopropane Carboxylic Acids as Inhibitors of O-Acetylserine Sulfhydrylase Isoforms*. J Enzyme Inhib Med Chem. 2019;34:31-43.

Franko N, Grammatoglou K, Campanini B, Costantino G, Jirgensons A, Mozzarelli A. *Inhibition of O-acetylserine sulfhydrylase by fluoroalanine derivatives*. J Enzyme Inhib Med Chem. 2018;33:1343-1351.

Magalhães J, **Franko N**, Annunziato G, Welch M, Dolan SK, Bruno A, Mozzarelli A, Armao S, Jirgensons A, Pieroni M, Costantino G, Campanini B. *Discovery of novel fragments inhibiting O-acetylserine sulphhydrylase by combining scaffold hopping and ligand–based drug design*. J Enzyme Inhib Med Chem. 2018;33:1444-1452.

the original work is properly cited. The thesis contains figures, tables and texts, adapted from these papers.

Nina Franko performed part of her experiments during secondments in partner laboratories of INTEGRATE project:

- August – December 2016: University of Cambridge, Department of Biochemistry. Supervisor: Prof. Martin Welch.
  Nina Franko carried out optimization of expression constructs for StOASS and crystallization of proteins with automatic setup.
- May – July 2017: Aptuit Verona, Department of Microbiology. Supervisor: Dr. Antonio Felici.
  Nina Franko performed preliminary microbiological assays with potent protein inhibitors and optimized the method for measurement of intracellular reduced thiols.

Reversible inhibitors of OASS and SAT were synthesized in Prof. Costantino's group (University of Parma). Irreversible inhibitors of OASS were synthesized in Prof. Jirgensons' group (Latvian Institute of Organic Synthesis). Nina Franko carried out biochemical and microbiological assays with these compounds. Received compounds were stored at -20 ^{o}C and solubilized in DMSO and/or water. Stock solutions were stored at -20 ^{o}C. Received compounds were used for the assays without any further purification. High-throughput screening of ChemDiv library, performed in Prof. Tammela's group (University of Helsinki), was carried out with SAT, purified by Nina Franko. Activity assay, used for high-throughput screening, was developed based on Nina Franko's protocol.

TABLE OF CONTENTS

ABSTRACT

Emerging antibiotic resistance represents a major hazard for public health. The necessity for the development of new antibiotics is high, especially against Gram-negative bacteria. However, for their development many issues must be faced, such as bacterial intrinsic protection by a complex outer membrane, deficit of knowledge regarding its permeability, low number of identified targets and lack of molecule diversity in libraries used for screening campaigns. Unsuccessful outcomes of numerous projects focused on the identification of new antibiotics led several big pharmaceutical companies to completely abolish their antimicrobial research. A promising strategy to fight bacterial resistance is to use enhancers of antibiotic therapy. Enhancers either block the main bacterial resistance mechanism or potentiate the action of a chosen antibiotic.

Cysteine is a multifunctional amino acid and its auxotrophs are not able to grow on minimal medium. It is the organic source of sulfur that is donated for biosynthesis of sulfur containing molecules, while cysteine itself stabilizes protein tertiary structure by disulfide bonds formation and maintains intracellular redox status. It has been shown that deletion mutants of cysteine biosynthetic pathway have attenuated virulence, elevated levels of intracellular oxidative stress and they have been linked to decreased antibiotic resistance. Oxidative stress is one of the common mechanisms by which antibiotics affect bacteria, and therefore inhibition of bacterial enzymes involved in biosynthesis of cysteine, that are absent in mammals, presents a promising strategy for the development of

enhancers of antibiotic therapy. The project was focused on the inhibition of the last two enzymes in this pathway, serine acetyltransferase (SAT) and *O*-acetylserine sulfhydrilase (OASS) that, in enteric bacteria, exists in two isoforms, A and B. The chosen proteins were from *Salmonella enterica* serovar Typhimurium, which presents a major health risk all over the world and has been listed as a high priority pathogen by World Health Organization for the development of novel inhibiting compounds.

In the course of the project we optimized the conditions for expression and purification of target enzymes as recombinant proteins in *E. coli*. Expression constructs for OASS were prepared during the secondments at the University of Cambridge (supervisor Prof. Martin Welch). The proteins were later used for *in vitro* testing of novel reversible and irreversible inhibitors.

For OASS, potent reversible inhibitors had been identified previously. A cocrystal between OASS-A and the most potent inhibitor UPAR-415 was prepared which allowed us to confirm binding interactions and understand the molecular basis of enzyme inhibition. Since existing inhibitors presented issues in the permeability through the Gram-negative membrane, several derivatives were prepared in Prof. Costantino's group (University of Parma) in order to improve their drug-likeness and penetration in bacteria. We determined their binding affinity and mechanism of action via enzyme assays and fluorimetric titrations. We identified novel potent inhibitors and the most promising ones were later selected for microbiological testing.

In a collaboration with Prof. Jirgensons' group (Latvian Institute of Organic Synthesis), we investigated covalent modification of OASS by

mechanism-based inactivators. Fluoroalanine derivatives were assayed in order to determine their inactivation potency, mechanism of action and structure-activity relationship.

Inhibitors of SAT were tested in our laboratory for the first time. For this purpose, we optimized and validated an indirect activity assay that can be used for inhibitors testing on a small and large scale. We screened novel SAT inhibitors, selected by Prof. Costantino's group (University of Parma) based on the *in silico* screening of an *in house* compound library and high-throughput screening of ChemDiv libraries, evaluated their potency and determined the mechanism of action. With this approach we identified the most potent SAT inhibitors reported so far.

Promising protein inhibitors were later tested in microbiological assays to evaluate their effect on bacterial viability. This part of the project was partially carried out during the secondments in Aptuit Verona (supervisor Dr. Antonio Felici). We found out that they have issues in the permeability through the bacterial membrane, although in the presence of the permeability enhancer they were able to interfere with bacterial growth. To investigate their mechanism of action when inside bacteria, we developed a method for the measurement of the bacteria intracellular reduced thiols as a marker of cysteine availability.

Keywords:

antibiotic resistance, cysteine biosynthesis, enzyme inhibition, intracellular reduced thiols, pyridoxal 5'-phosphate, *O*-acetylserine sulfhydrylase, serine acetyltransferase.

GENERAL INTRODUCTION

1. ANTIBIOTICS AND ANTIBIOTIC RESISTANCE

1.1. THE GLOBAL THREAT OF ANTIBIOTIC RESISTANCE

Antibiotics are medicines used to treat bacterial infections [1]. The modern era of antibiotics started in 1928 with the discovery of penicillin by Sir Alexander Fleming and they were first prescribed to treat serious infections in 1940s [2]. Besides saving lives of infected patients, antibiotics have enabled major medical achievements, such as surgical procedures, transplantations, advances in neonatal medicine and chemotherapy for cancer treatment [3]. Following the penicillin, several classes of antibiotics with different mechanisms of actions were discovered fruitfully and rapidly in the middle of the 20th century.

The period between 1940s and 1960s was the golden era of antibiotic discovery and these antibiotics or their derivatives are still in use today. Soon after the beginning of antibiotics use for treatments of the infections, bacteria started to show antibiotic resistance. Acquired resistance is a natural process that evolves as an evolutionary response of bacteria to the antibiotics, enabling the survival of the species [4,5]. However, the overuse and misuse of antibiotics in medicine and agriculture led to a rapid occurence of acquired bacterial resistance and nowadays resistance emergance is so fast, that it is often observed even before the antibiotic is approved by regulatory agencies to be marketed. Currently, it is so widespread that it presents a unique challenge to both science and medicine [6]. For example, Gram-negative *Acinetobacter baumannii* is already resistant to all currently available antibiotics [7,8]

and European Centre for Disease Prevention and Control estimates that every year 25.000 Europeans die due to the resistant bacterial infections [9]. In 2017, World Healthcare Organization (WHO) published a *Global priority list of antibiotic-resistant bacteria to guide research, discovery, and development of new antibiotics* where bacterial strains were divided in three groups based on the priority for the development of antibiotics against them (Table 1). In this list, *Mycobacterium tuberculosis* is not specified as it is already considered as a top global health priority [10].

Table 1. WHO priority pathogens list for R&D of new antibiotics [10].

priority	bacterial strains
critical	• *Acinetobacter baumannii*, carbapenem-resistant • *Pseudomonas aeruginosa*, carbapenem-resistant • *Enterobacteriaceae**, carbapenem-resistant, 3rd generation cephalosporin-resistant
high	• *Enterococcus faecium*, vancomycin-resistant • *Staphylococcus aureus*, methicillin-resistant, vancomycin intermediate and resistant • *Helicobacter pylori*, clarithromycin-resistant • *Campylobacter*, fluoroquinolone-resistant • *Salmonella spp*., fluoroquinolone-resistant • *Neisseria gonorrhoeae*, 3rd generation cephalosporin-resistant, fluoroquinolone-resistant
medium	• *Streptococcus pneumoniae*, penicillin-non-susceptible • *Haemophilus influenzae*, ampicillin-resistant • *Shigella spp*., fluoroquinolone-resistant

** Enterobacteriaceae include: Klebsiella pneumonia, Escherichia coli, Enterobacter spp., Serratia spp., Proteus spp., and Providencia spp, Morganella spp.*

Besides the occurence of bacterial antibiotic resistance, the worrying fact is that no new major classes of antibiotics have been found and introduced to the market for over 50 years [11,12]. Several big pharmaceutical companies have carried out large studies that failed in the identification of new antibiotics and consequently have completely abolished the antimicrobial research. On the other hand, investment in the antibiotics research and development is not attractive, since antibiotics are low-profitable drugs and is expected that bacteria will sooner or later develop resistance mechanisms against them, thus rendering drugs inefficient. That said, the fight against resistant microbes is extremely challenging. Bacteria are becoming more and more resistant to the existing drugs while we do not have an arsenal to fight the resistant strains. It is predicted that without a major improvement in the antibiotic development accompanied by the increase of microbial resistance and antibiotic misuse, by 2050 10 million people will die yearly due to the bacterial infections [5].

1.2. INTRINSIC AND ACQUIRED RESISTANCE OF GRAM-NEGATIVE BACTERIA

A careful look at Table 1 shows that most of the resistant bacteria are Gram-negative. Development of antibiotics against them is particularly difficult due to their two-membrane cell envelopes which are protecting the cell and building a barrier for the external compounds, making them intrinsically resistant to antimicrobials.

The outer membrane (OM) of Gram-negative bacteria is an asymmetric and rigid bilayer of lipopolysaccharides (LPS). LPS consists of a saturated lipid A, core oligosaccharide and distal polysaccharide, which is also referred as O-antigen and is immunogenic. The LPS bilayer is very rigid since in it several proteins are inserted, for example:

- general diffusion porins,
- specific uptake channels (e. g. LamB),
- OmpAs (connecting the outer membrane with a peptidoglycan layer and are essential for OM integrity and stability)
- other translocators, enzymes and structural proteins [13].

Underneath the OM lies a fiber-like periplasmic space, consisting of a peptidoglycan that provides rigidity to the overall cell membrane. The cytoplasmic space of Gram-negative bacteria is surrounded by an inner membrane (IM) which is a symmetrical bilayer of glycerolphospholipids and is more fluid comparing to the OM [14,15].

The complexity of Gram-negative membrane presents a unique challenge for the permeation of drugs in the cytoplasmic space where the biggest issue is the OM. LPS is highly functionalized with anionic charges, stabilized by divalent cations and subsequently cross-linked to create a large defensive web which can block the entry of molecules as the first line of bacterial defence [14,16]. It is more rigid than normal bilayers, slowing passive diffusion of hydrophobic compounds, and narrow pores limit by size the penetration of hydrophilic drugs [17].

However, the intrinsic bacterial resistance due to the efficient OM is not the only issue for the inefficiency of antibiotics. A unique challenge presents the acquired resistance, which is the ability of bacteria to escape the action of antibiotics that were once effective against them. Its origin is attributed to the overuse and misuse of these medications. The evolutionary drive is leading bacteria to exploit every source of resistance genes and every possible way of horizontal gene transfer to develop and inherit multiple resistance mechanisms for basically all antibiotics introduced into practice [2,8,18]. There are several modes of acquired resistance, which are dependent on the antibiotic target. Closely related to the permeability are efflux pumps which are overexpressed in the resistant strains and therefore extremely efficient in exporting drugs from cytoplasm and periplasm in the external medium. Other types of acquired resistance are enzymatic inactivation or modification of drug (for example acetylation, phosphorylation, hydrolysis etc), target modification or its overexpression and introduction of bypass pathways [8,17].

1.3. STRATEGIES TO OVERCOME ANTIBIOTIC RESISTANCE

Taking into account the emergence of resistance crisis and a low number of new antibiotic agents in the pipeline, the situation is alarming. Since 1990s, the pharmaceutical industry has been focusing on the development of synthetic antibiotics based on genomics, combinatorial chemistry, high-throughput screening and rational drug design without any major success. This led several big pharmaceutical companies to

completely abandon the antimicrobial research [8,19]. The review by Kim Lewis [8] suggests several reasons for the failure of antibiotic discovery in recent years:

- Studies are focused on antibiotic identification rather than the knowledge of how antibiotics work. For example, there are approximately 200 conserved essential proteins in bacteria, but the number of currently targeted proteins is very small (ribosomes, cell wall synthesis linked enzymes, DNA gyrase and topoisomerase);
- The research is focused on the identification of synthetic antibiotics rather than the ones of natural origins. However, having a look at the current antibiotic classes it is evident that only fluoroquinolones are a successful example of synthetic antibiotics and all the other major classes are derived from natural compounds;
- Nowadays, antibiotics are searched by using *in vitro* assays, in which is easy to miss the prodrugs;
- There are not many studies focused on species-specific antibiotic research. Several species share conserved essential proteins, but the sequences of orthologues are not identical. These variable parts are attractive targets – for example, recently approved drug for *M. tuberculosis*, bedaquiline, targets highly conserved F_1F_0-ATPase, present also in mammals [20];
- The big issue presents the lack of knowledge regarding the permeability of drugs through the outer membrane.

Based on these observations, new platforms for antibiotic discovery are suggested:

- Identification of rules of permeation and design of molecules with permeability-like properties, including prodrugs [8];
- Screening of drug candidates using models that mimic better mammalian *in vivo* conditions, thus allowing the identification of prodrugs (suggested it is the use of *C. elegans*) [8];
- Returning to the source of natural compounds, that could be identified by turning on silent operons and by exploitation of currently uncultivable organisms [8];
- To stimulate research on a primary level in order to identify new targets [3];
- To invest in the development of antibiotic enhancers [21].

Antibiotic enhancers or adjuvants have little or no antibiotic activity themselves but when they are co-administered with the antibiotic, they either block the main bacterial resistance mechanism or enhance the antimicrobial action of the drug. In the sense of drug discovery, enhancers can compensate for the identification of new targets and antibiotics and potentiate the activity of existing drugs. By now, three major classes of antibiotic enhancers have been developed [21]. First of them are β-lactamase inhibitors that are co-administered with penicillin antibiotics and are the only class of antibiotic enhancers that are currently used in clinical practice. However, their constant development is essential since bacteria are becoming resistant to the existing ones and new β-lactamase inhibitors are being tested in clinical trials [6,21]. In the

second group are efflux pumps inhibitors that besides the potentiation of antibiotic activity can also decrease the virulence in some strains [22,23]. However, they have problems entering the market due to their high toxicity related to cross-reactivity with efflux pumps present in human cells [3,24]. Lastly, outer membrane permeabilizers are mechanistically limited for the treatment of Gram-negative infections and are disrupting the rigid structure of LPS bilayer, thus facilitating the drug transport. Commonly used on laboratory scale are cationic agents such as polymyxins [21,25].

Nowadays, several studies are focused on the identification of new antibiotic adjuvants. For example, new peptides have been identified that act on the bacterial membrane without having any effect on bacterial viability, but when used with penicillin antibiotics they potentiate the drug action in methicillin resistant *S. aureus* [26]. 2-aminoimidazole derivatives are inhibitors of response regulator protein BfmR and when added to *A. baumannii*, they inhibit biofilm formation and increase the sensitivity to carbapenem antibiotics [27]. CeO_2 nanoparticles are non-specific outer membrane permeabilizers and it has been shown that they can synergistically enhance the activity of β-lactam antibiotics in resistant *K. pneumoniae* clinical isolates [16].

Few recent achievements in antibiotic discovery should also be highlighted. Murepavadin is currently the only drug candidate against Gram-negative bacteria with novel mechanism of action that is in clinical trials, it recently entered in phase 3 [6,28]. It is a peptidomimetic agent

that binds to the lipopolysaccharide transport protein D (LptD), present in the OM and involved in the lipopolysaccharide biogenesis. By binding to LptD, murepavadin inhibits its transport function thus causing such alternations in the OM structure, that are resulting in cell death. It is being tested for the treatment of hospital-acquired and ventilator-associated bacterial pneumonia caused by *Pseudomonas aeruginosa* [29]. By investigation of secondary metabolites of not-commonly used bacteria, a new class of antibiotics, odilorhabdins, has been identified. These non-ribosomal peptides have been found in Gram-negative genus *Xenorhabdus* and they bind to a new ribosome site, leading to a miscoding of proteins. They are active against Gram-positive and Gram-negative bacteria in *in vitro* assays as well as in animal models [30]. Recent advances in the cultivation of 'uncultivable' bacteria have also been achieved – the iChip enables the growth of bacteria on an artificial plate, covered with soil from which they are obtaining all needed nutrients [31]. Using this method, scientists have been able to grow *Eleftheria terrae*, from which they have isolated teixobactin, a new peptidoglycan synthesis inhibitor effective against Gram-positive bacteria [32]. An encouraging new class of new antibiotics, active against Gram-positive and Gram-negative bacteria has been discovered recently. Arylomycins covalently inhibit membrane-bound signal peptidase LepB. They exhibit low resistance frequency and are effective against ESKAPE pathogens in pre-clinical models [12].

1.4. *Salmonella enterica* serovar Typhimurium

The PhD project is focused on the development of antibiotic adjuvants targeting metabolic enzymes, present in *Salmonella enterica* serovar Typhimurium (*S*. Typhimurium) due to its clinical relevance. *Salmonellae* is a genus belonging to the family Enterobacteriaceae. It is a rod-shaped Gram-negative facultative anaerobe, that spreads predominantly by contaminated food and water and presents a major health threat in both developed and developing countries. In the United States it causes 1.2 million illnesses, 23.000 hospitalizations and 450 deaths each year [33]. Based on the major clinical symptoms, *Salmonella* species can be divided into typhoidal and non-typhoidal. *S*. Typhimurium is non-typhoidal, enteric pathogen species, triggering an innate immune response after the colonization of M cells and enterocytes [34]. Consequently, patients suffer for gastrointestinal disease with symptoms as fever, abdominal pain, cramping, large bowel inflammation and diarrhea. Infections are normally treated with fluoroquinolones and wide-spectrum cephalosporins [35,36].

The *Salmonellae* resistance to existing drugs has been emerging since 1990 and based on data from 2006 presented by the National Antimicrobial Resistance Monitoring System, 84 % of clinical isolates of non-typhoidal *Salmonellae* displayed multidrug resistant phenotype and 4.1 % of the isolates had reduced susceptibility to cephalosporins in the USA [36]. Specifically for *S*. Typhimurium, a recent study of clinical isolates from Brazil population foud that majority of strains were resistant to different antibiotic classes and the study also identified genes

that were responsible for the emergence of resistance [37]. The mentioned studies are originating from developed countries, where the management of infections with antibiotics is better monitored comparing to the third world countries. Therefore, in high-income countries *S*. Typhimurium is mostly causing self-limiting diarrhoeal illness in healthy individuals; bloodstream or focal infection are only observed in immunocompromised patients. By contrast, in sub-Saharan Africa antibiotic misuse already caused the emergence of extremely resistant genotype ST313, that predominantly causes bacteremia associated with fatal outcome in 20-25 % [38].

Taking into account a high number of infections caused by *Salmonellae* and its high resistance to existing antibiotics, the WHO listed it in a high priority pathogen list [10], stating the urgent necessity for the development of novel treatments for this bacterium.

2. TARGETING SULFUR ASSIMILATION FOR THE DEVELOPMENT OF ANTIBIOTIC THERAPY ENHANCERS

A new approach for the development of antibiotic therapy enhancers is inhibition of bacterial cysteine biosynthesis. While mammals are obtaining cysteine from methionine via trans-sulfuration pathway, bacteria and plants have developed a cysteine biosynthetic pathway in which they are able to incorporate inorganic sulfur into an amino acid. Since enzymes of this pathway are absent in humans, they are attractive targets for antibiotic development.

Cysteine is an amino acid of many functions and is required for viability of bacteria. It has been shown that cysteine auxotrophs are not able to grow in the minimal medium if cysteine is not supplied [39]. One of its most important functions is being organic source of sulfur, that is in free inorganic form toxic for bacteria [40]. Cysteine is able to donate sulfur for biosynthesis of Fe-S clusters, modified tRNAs, thiamine, biotin, glutathione and mycothiol when needed [41–44]. Besides that, cysteine stabilizes protein tertiary structure by forming disulfide bonds. Cysteine also has an important role in regulation of intracellular redox state. While it has the ability to scavenge reactive oxygen species itself, it is also a precursor of major intracellular nonenzymatic antioxidants glutathione and mycothiol [45,46]. Taking into account that some pathogens need to survive under extremely challenging conditions during colonization in humans (macrophages, gastric mucosa), any disruption of intracellular redox balance leads to a decrease of bacterial fitness and reduction of

infectivity. For example, *ΔcysI* and *ΔcysK Brucella melitensis* and *ΔcysH M. tuberculosis* exhibit attenuated virulence, and *ΔcysI Brucella melitensis* exhibits increased sensitivity to oxidative stress [47,48]. In *S.* Typhimurium, deletion mutants of cysteine biosynthetic pathway have been shown to have higher degree of intracellular oxidative stress and in swarm populations decreased resistance to antibiotics [49,50]. Antibiotic-induced oxidative stress is one of the many identified antimicrobial mechanisms and thus the inhibition of cysteine synthesis could enhance their efficacy [51]. Therefore, several research groups have focused their attention on the inhibition of the enzymes involved in the cysteine biosynthesis in γ-proteobacteria and actinomycetales due to their clinical relevance [52].

The cysteine biosynthetic pathway in enteric bacteria is shown on Figure 1.

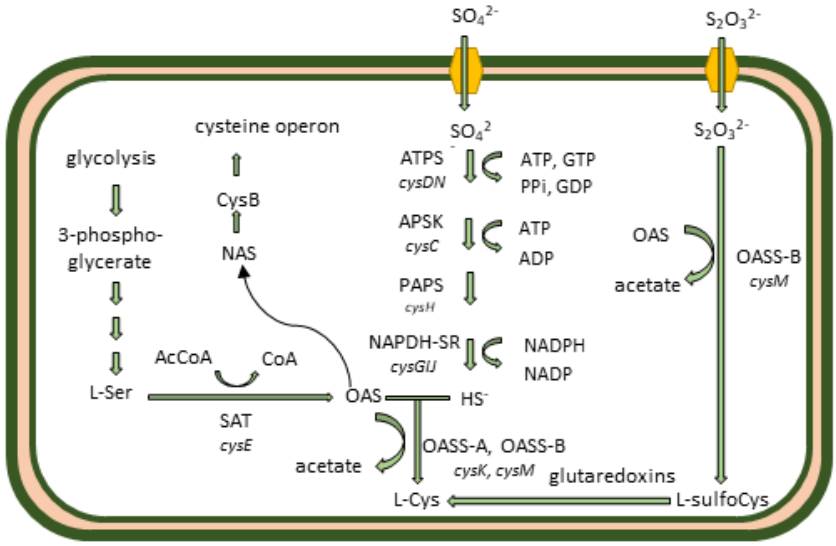

Figure 1. Schematic presentation of cysteine biosynthetic pathway in enteric bacteria. Abbreviations used: ATPS – ATP sulfurylase; APSK – 5-phosphosulfate kinase; PAPS R - 3-phosphoadenosine 5-phosphosulfate reductase; NADPH-SR - NADPH-dependent sulfite reductase; OAS – O-acetylserine; AcCoA – acetyl coenzyme A; CoA – coenzyme A. Adjusted from [44].

Cysteine biosynthesis is considered a two-phase process. The first phase is the so called Reductive Sulfate Assimilation Pathway (RSAP) that starts when a sulfate molecule is transported into the cell. Sulfate itself is not reactive and it needs to be converted to the active bisulfide form before the incorporation into the cysteine. The reduction of sulfate into bisulfide is a four-step process, that is highly energetically consuming since it requires one mole of GTP, two moles of ATP and three moles of NADPH for each mole of cysteine produced. Once the sulfur source is activated, the second phase of the biosynthesis can proceed [40,44,53]. The backbone of cysteine originates from the activated form of L-serine, that can be either *O*-acetylserine (OAS) or *O*-phosphoserine (OPS). OAS is commonly present in enteric bacteria, while OPS is found in organisms

that live under more extreme conditions, where OAS would be unstable [54–57]. In enteric bacteria, L-Ser is activated to OAS by serine acetyltransferase (SAT). The last step in the cysteine biosyntheis is catalized by *O*-acetlyserine sulfhydrylase (OASS), that in enteric bacteria exists in two isoforms, A and B. This enzyme substitutes the acetoxy moiety of OAS with bisulfide, producing L-cysteine [40]. The B isoform of OASS is also able to use thiosulfate as a sulfur source and catalyses the production of L-sulfocysteine, that is later converted to L-cysteine by glutaredoxins [58–60].

Since *Mycobacterium tuberculosis* is one of the most investigated organisms for the sulfur metabolism, it is worthwhile mentioning that this organism possesses three enzymes for the final step of cysteine synthesis. CysK1 catalyses cysteine formation from OAS and bisulfide [61], while CysK2 synthesizes S-sulfocysteine from OPS and thiosulfate [54]. On the other hand, CysM uses OPS as a first substrate, while the sulfur source is delivered to it via thiocarboxylated sulfur carrier protein CysO [62].

Inhibition of enzymes involved in the biosynthesis of cysteine and other sulfur containing molecules has been extensively reviewed [52]. Research groups have been focusing their attention on the inhibition of APS reductase (CysH), SAT and OASS, as well as on an inhibition of sulfotransferases and mycothiol biosynthesis. Recently, novel APS reductase [63] and CysM [64] inhibitors have been identified that displayed bactericidal activity in a nutrient-starvation model of dormancy in *Mycobacterium tuberculosis*.

3. *O*-ACETYLSERINE SULFHYDRILASE

Our group has been focusing on the inhibition of the last two enzymes in the biosynthetic pathway of cysteine in *S.* Typhimurium, that are StOASS-A, StOASS-B and StSAT. StOASS is a PLP-dependent enzyme, with the cofactor bound to the active site lysine 41 via a Schiff base. The enzyme catalises a β-replacement reaction, following the ping-pong catalytic mechanism shown in Figure 2.

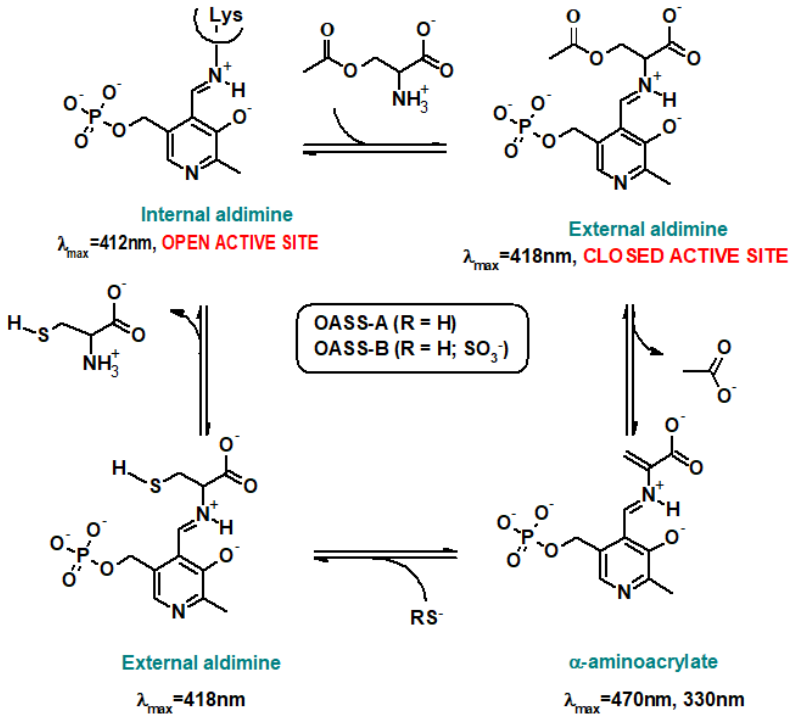

Figure 2. Catalytic cycle of OASS. Adjusted from [65].

The reaction starts with a nucleophilic attack of α-amine of OAS to C4' of PLP, forming an external aldimine and the simultaneous closure of the active site. Then, the active site lysine deprotonates the Cα, causing the

β-elimination of acetate group and formation of α-aminoacrylate intermediate. The nucleophilic attack of sulfide to the Cβ of aminoacrylate forms the cysteine, that is released from the active site and the initial Schiff's base between lysine and cofactor is reformed [66–68]. Structurally, OASS is a homodimer. Each subunit consists of a large and small domain and the active site is placed between them (40). The A and B isozymes catalyze the same reaction, they share 43 % sequence identity and have almost superimposable three-dimensional structure, while the active site of the B isoform is a bit bigger and more polar, but apparently less accessible compared to the A isozyme [67]. Several crystal structures, such as native form [67,69], K41A mutant for mimicking the closed conformation of external aldimine intermediate [70] and inhibited form with chloride bound to an allosteric anion binding site [71], accompanied by fluorescence studies [72–74], revealed high flexibility and conformational dynamics of both isozymes of OASS, that are important for catalytic cycle as well as for understanding of enzyme behaviour during inhibition.

Besides the synthesis of cysteine, OASS-A (encoded by *cysK*) has several other functions related to bacterial physiology. For example, in Gram-positive bacteria it binds the CymR, that is a transcription factor involved in cysteine metabolism. When OASS-A is bound to CymR, its affinity for DNA binding increases up to seven-fold, thus repressing the transcription of the operon [75]. In contact-dependent growth inhibition (CDI), CDI^+ bacteria deliver CdiA-CT toxin into neighboring bacteria and produce specific immunity proteins that protect against self-intoxication. In

uropathogenic *E. coli* the CdiA-CT toxin is active only when in the complex with OASS-A [76]. Finally, importantly for the antibiotic development, *ΔcysK* mutants of *Vibrio fischeri* exhibit defects in biofilm formation, that cannot be complemented by cysteine [77].

Despite good knowledge and thorough characterization of OASS-A, the function of OASS-B (encoded by *cysM*) remains controversial. It has been reported that OASS-B in *Salmonella typhimurium* LT contributes only up to 20 % of total cysteine biosynthesis [58], leaving the question about its necessity unanswered. On the other hand, OASS-B is indispensable when bacteria are growing on thiosulfate as a sole sulfur source since OASS-A is not able to take it as a substrate [58,60]. Early studies suggested that OASS-B is differentially expressed under anaerobic conditions [78,79], but recent findings did not confirm these observations [80].

4. SERINE ACETYLTRANSFERASE

SAT (encoded by *cysE*) is responsible for the first step in biosynthesis of cysteine in higher plants and bacteria. It catalyses acetylation of β-hydroxyl group of L-serine by acetyl coenzyme A (AcCoA), giving the OAS and coenzyme A as products, shown on Figure 3 [81,82]. Reaction mechanism follows the rule of random-order ternary complex [83,84].

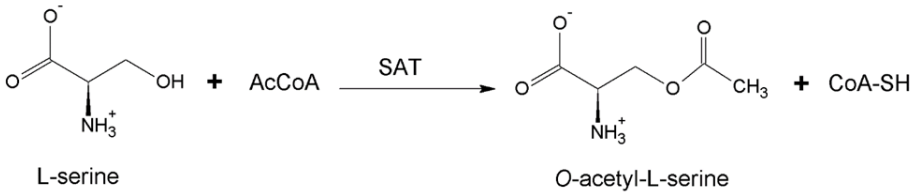

Figure 3. Reaction catalysed by SAT.

SAT is a member of bacterial *O*-acetyltransferases subfamily of *O*-acyltransferases. These enzymes contain repeating hexapeptide motifs that are responsible for the folding of the protein, forming a left-handed β-helix [83,85,86]. Even though the majority of members of this family exists as trimers, biochemical [84,86] and structural studies [87] have revealed that SAT exists in a hexameric form as a dimer of trimers. Left-handed β-helix is positioned on the C-terminal part, while N-terminal part forms an α-helix. Subunits are organized in a trimer, forming a three-sided pyramid shape that interact with each other predominantly by hydrophobic interactions and hydrogen bonds. Two trimers form a hexamer by interactions on their N-terminal sides, and the oligomer interactions are of a similar nature as those between monomers. The

active site is positioned in a small cleft at the junction of two adjacent subunits of the trimer.

StSAT has not been crystallized yet, however the structures of its *Haemophilus influenzae* and *E. coli* orthologues are available. Besides the native structure [88], the complexes of SAT with cysteine [85] or AcCoA bound [86] have been obtained, allowing insight in its conformational dynamics that is also related to its inhibition.

SAT controls the cysteine biosynthesis in three ways – by L-cysteine feedback inhibition, OAS/NAS production and cysteine synthase complex formation.

- **Feedback inhibition by L-cysteine:** SAT is feedback inhibited by L-cysteine, that is competitive versus L-serine. Therefore, elevated levels of cysteine prevent unnecessary OAS production [84,89]. Crystallization studies have revealed that upon cysteine binding to L-serine site, SAT undergoes a large conformational change, in which its C-terminal part occupies acetyl-CoA binding site and consequently the affinity for both substrates is decreased [86].
- **OAS/NAS production:** The product of SAT reaction, OAS, is a substrate of OASS, the last enzyme involved in the biosynthesis of cysteine. This way, cysteine biosynthesis is directly limited by the amount of OAS [66]. On the other hand, OAS is unstable at physiological pH and if it is not being consumed by OASS, it is non-enzymatically converted to *N*-acetylserine (NAS). NAS binds CysB, a promoter of cysteine regulon, and functions as an inducer of the

cysteine regulon after being activated by NAS. Derepression of cysteine regulon leads to upregulated transcription of *cys* genes and consequently to higher cysteine production [90].

- **CS complex formation:** SAT is able to interact with OASS-A, forming a widely studied assembly called cysteine synthase complex (CS complex). Even though there is no structural data about this complex, biochemical and spectroscopic approaches have revealed that in CS complex the C-terminal part of SAT is inserted in the active site of OASS-A [91,92]. Precisely, the C-terminal isoleucine of SAT is essential for binding and it is highly conserved between the species that form CS complex [93,94]. The stoichiometry of the complex was determined to be 3:2, that is, one hexamer of SAT binds 2 dimers of OASS-A [92]. The complex can be disrupted by OAS and stabilized by bisulfide, likely by binding to the allosteric site on OASS-A [95]. Kinetic studies have revealed that in the complex the activity of OASS-A is partially inhibited, suggesting that only one active site of this enzyme is occupied by SAT, while the other is partially closed. When OASS-A is partially inhibited, the bisulfide cannot be consumed and the CS complex is therefore stabilized by it [95]. This leads to (apparently) elevated activity of SAT in the complex and maximized OAS production, leading to the dissociation of the complex and recovered activity of OASS-A. Besides that, maximized OAS production will also result in higher concentration of NAS and therefore induced cysteine operon. It also should be mentioned that SAT undergoes substrate inhibition by L-serine,

that is decreased in the complex (Km of L-ser 3.7 mM for free SAT and 16 mM for SAT within the complex) and consequently its activity in CS complex is apparently elevated. Its kinetic parameters in the CS complex are not affected [84]. Importantly, SAT is not able to form the complex with OASS-B [94].

5. OASS AND SAT INHIBITORS

5.1. OASS REVERSIBLE INHIBITORS

The fact that SAT inhibits OASS inspired our group for development of low-molecular weight OASS inhibitors by mimicking the C-terminal part of SAT. Firstly, SAT peptidomimetics were designed with a purpose to identify the important residues for binding [96]. Taking into account the interacting residues and orientation of peptides in the active site of OASS-A, a design of low-molecular weight inhibitors was performed. These molecules are substituted cyclopropanes with a carboxylic group at Cα that is mimicking the C-terminal isoleucine of SAT, and a tolyl group on the same carbon that is mimicking the SAT backbone. On the Cβ a phenyl group is attached that is mimicking the side chain of SAT's isoleucine. A cyclopropane scaffold was chosen to keep the molecule in trans configuration, that was essential for maintaining the affinity. Rational design of these molecules produced OASS inhibitors, that exhibit K_d in nanomolar range not only towards the A isoform but also against the B isoform that naturally does not form a complex with SAT. UPAR-415 (Figure 4) is the most potent inhibitor of StOASS identified so far, exhibiting K_d StOASS-A = 0.028 ± 0.005 μM and K_d StOASS-B = 0.49 ± 0.05 μM [97].

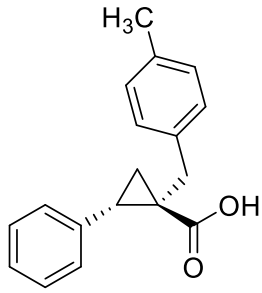

Figure 4. The structure of UPAR-415, the most potent reversible inhibitor identified so far. K_d *StOASS-A = 0.028 ± 0.005 µM;* K_d *StOASS-B = 0.49 ± 0.05 µM* [97].

Unfortunately, microbiological assays have revealed that these inhibitors are lacking *in vivo* efficacy, in particular they do not have any effect on bacterial viability when tested against wild type *E. coli*. However, inhibition of bacterial growth was observed when assays were carried out in the presence of polymyxin B nonapeptide, an enhancer of membrane permeability. These observations suggested that compounds have issues in the permeability through the Gram-negative membrane, that is a common obstacle in the antibiotics development. Therefore, our project was focused on design and identification of UPAR-415 derivatives that would retain the affinity towards the target while possessing the physico-chemical properties favoring the permeability through the Gram-negative bacteria.

Designing permeable molecules is problematic due to the lack of knowledge regarding the permeability. Nowadays, there are no clear rules that would connect the molecular structure with the permeation and this gap is likely one of the biggest issues in the antibiotic discovery [8]. However, few studies extracted the useful properties from sets of permeable molecules – such as logP, polarity, geometry, charges and

importance of side groups [98–100]. These rules were applied in the synthesis of UPAR-415 derivatives. The newly designed molecules were tested with biochemical assays for the evaluation of their potency and structure-activity relationship. The most potent ones were selected as potential candidates for microbiological evaluation.

5.2. OASS IRRVERSIBLE INHIBITORS

Compounds that form covalent bonds with their targets have been raising large concerns regarding their use as medicines considering the possibility of their off-target effects. Indeed, random covalent binding to cellular macromolecules can cause side effects, acute tissue injury and reactive immune response against modified structures. On the other hand, highly specific and selective molecules have been recognized as safe and profitable drugs, for example aspirin, penicillin and omeprazole have made a major positive impact on human health [101]. In comparison with reversible inhibitors, irreversible molecules exhibit a number of benefits, such as high potency, low therapeutic dose and correlated high therapeutic index, accompanied by the extended duration of action. Unlike the reversible inhibitors, covalent drugs can target proteins with shallow binding sites [102].

Two types of covalent inhibitors have been developed: affinity labels and mechanism based inactivators. Affinity labels are *per se* reactive molecules that covalently modify an amino acid residue in a single binding step. They are considered as non-specific, since they can bind to several residues. Mechanism based inactivators are intrinsically not reactive

molecules. However, when they are modified by the catalytic action of the target enzyme, they are converted into reactive molecule that covalently modifies the active side of the protein. Thus, they are also called suicide substrates and are more specific [103,104].

While reversible inhibition of OASS has been widely exploited, there are no current data about its irreversible inhibition. On the other hand, several other PLP dependent enzymes have been studied for the inactivation by mono-, di- or trihalogenated alanines [105–113], making these molecules promising candidates for inactivation of OASS. In the present study, we investigated the reactivity of mono- and trifluoroalanine derivatives with StOASS-A and StOASS-B in order to identify suitable mechanism-based irreversible inhibitors [65].

5.3. SAT INHIBITORS

Taking into account the importance of SAT in cysteine biosynthesis, we were encouraged to identify its novel inhibitors. Despite its key role in cysteine biosynthetic pathway, only three inhibitors of SAT have been reported so far. Agarwal et al [114] performed virtual screening of National Cancer Institute chemical database against *E. coli* and identified three hits (Table 2). The most potent compound (C3) exhibited IC_{50} = 72 µM for EcSAT. The same study also evaluated the effect of compounds on the growth of *Entamoeba histolytica* whose SAT shares 49 % identity in amino acid level with EcSAT. Compound C3 showed IC_{50} = 0.61 µM for *E. histolytica* trophozoites, suggesting target unspecificity.

Table 2. Known inhibitors of serine acetyltransferase [114].

Compound	Structure	EcSAT inhibition at 0.05 µg/µL (%)	IC_{50} for *E. histoytica* proliferation (µM)
C1	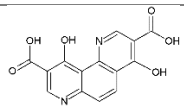	24	1.07
C2	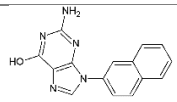	38	1.52
C3	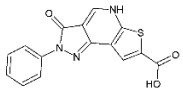	50 (IC_{50} = 72 µM)	0.61

AIM OF THE THESIS

The aim of the thesis was to inhibit StOASS and StSAT with a purpose of development of enhancers of antibiotic therapy. Therefore, the following activities were carried out:

- Preparation of expression constructs and optimization of purification conditions for StOASS-A, StOASS-B and StSAT;
- Crystallization of StOASS-A in the complex with potent reversible inhibitor in order to gain deeper insight into the protein-ligand complex and guide further medicinal chemistry efforts;
- Determination of binding/inhibitory potency of StOASS reversible inhibitors designed for improved permeability and identification of candidates for microbiological evaluation;
- Investigation of reactivity between StOASS and fluoroalanine derivatives as mechanism based inactivators, determination of their mechanism of action and structure-activity relationship;
- Development of an indirect activity assay of StSAT, suitable for the identification and characterization of inhibitors on a large and small scale;
- Determination of the potency of StSAT inhibitors, their mechanism of action and structure-activity relationship;
- Evaluation of intracellular thiol concentration as a marker of cysteine biosynthesis inhibition.

PREPARATION OF PROTEINS AND ACTIVITY ASSAY DEVELOPMENT

1. INTRODUCTION

The project required the use of StOASS (EC 2.5.1.47) and StSAT (EC 2.3.1.30). Expression systems and purification conditions for StOASS-A and StOASS-B isozymes were already available in the laboratory. However, these were constructs for expression of His_{10}-OASS from pET16b, where the histidine tags were removed by Factor Xa. During the secondment at University of Cambridge (supervisor Prof. Martin Welch), expression systems were changed to pET19m in order to replace the restriction site with the one for TEV protease that is more efficient and economical. On the other hand, the expression system for StSAT was not available, so it was newly prepared and expression and purification conditions were identified and optimized. Additionally, a new, indirect continuous activity assay for StSAT was developed for the identification of inhibitors in a cuvette based assays as well as in high-throughput screening.

This chapter describes preparation of expression constructs, identification and optimization of purification conditions for all required proteins and activity assay development for StSAT.

2. MATERIALS AND METHODS

2.1. MATERIALS

All reagents, if not otherwise specified, were obtained from Sigma Aldrich (St. Louis, MO, USA) at the best commercial quality available. Tris (2-carboxyethyl) phosphine (TCEP) was purchased from Apollo Scientific (Stockport, UK). Acetyl coenzyme A (AcCoA) and ninhydrin were purchased from AppliChem GmbH.

2.2. EXPRESSION AND PURIFICATION OF TEV PROTEASE

For the removal of histidine tags from StOASS and StSAT fusion proteins, His_6-TEV protease was expressed and purified. MBP-His_6-TEV protease was expressed from plasmid pRK793 (Addgene plasmid # 8827) in *E. coli* BL21 (DE3). This protease is expressed as a fusion protein with MBP (maltose binding protein), that was added to the construct to increase its stability, although the fusion protein cleaves itself *in vivo* to yield His_6-TEV protease [115]. Histidine tag remains attached to the protease, resulting in its simple separation from the cleaved substrate enzyme (OASS or SAT). For the expression of TEV protease, cells were grown O/N in 2XYT broth with 150 μg/mL ampicillin, 34 μg/mL chloramphenicol and 1 % glucose. Overnight culture was diluted 1:100 in 2XYT broth + 150 μg/mL ampicillin + 34 μg/mL chloramphenicol + 1 % glucose and grown until OD_{600} = 0.5 – 0.6 at 30 ^{o}C, when the protein expression was induced by the addition of 1 mM IPTG. Expression of TEV protease was performed for 4 h at 30 ^{o}C. Cells were pelleted by 10 min centrifugation at 5000 RPM at 4 ^{o}C and washed once with PBS before storage at -80 ^{o}C.

Cells were suspended in lysis buffer (50 mM NaP, 200 mM NaCl, 10 % glycerol, 5 mM TCEP pH=8.0) in the presence of 1 mg/mL lysozyme. Cell lysis was performed by pulsed sonication until about 80 % of cells were lysed. Cell lysis was monitored using turbidimetric method. 10 µL of cell suspension was diluted in 990 µL of lysis buffer and the optical density at 590 nm was measured. Measurements were performed before the sonication and after every sonication cycle, allowing to calculate the % of cell lysis using equation (1).

$$\%\ lysis\ = (\ 1 - \frac{OD_{590}^{sonicated\ cells}}{OD_{590}^{suspended\ cells}}) \cdot 100 \qquad (1)$$

The suspension was centrifuged for 45 min at 13000 g at 4 ^{o}C and crude extract was loaded on pre-equilibrated IMAC with Co^{2+} bound to the resins (Talon™, Clontech Laboratories, Inc., Mountain View, CA, USA). Unspecifically bound proteins were eluted with 25 mM imidazole, 50 mM NaP, 200 mM NaCl, 10 % glycerol, 5 mM TCEP pH=8.0. His_6-TEV protease was eluted with 500 mM imidazole, 50 mM NaP, 200 mM NaCl, 10 % glycerol, 5 mM TCEP pH=8.0 and dialysed O/N in a storage buffer 50 mM NaP, 200 mM NaCl, 10 % glycerol, 5 mM TCEP, 2 mM EDTA pH=8.0. His_6-TEV protease concentration was calculated by using extinction coefficient ε_{280} = 32290 M^{-1} cm^{-1} and MW = 28600 g/mol.

Protein purity was estimated from the SDS-PAGE gel using software ImageLab 5.2.1, Bio-Rad Laboratories.

When His_6-TEV protease was eluted from Co^{2+} resins, the first fractions of the peak were contaminated with DNA (based on the strong absorbance of fractions at 260 nm). Consequently, these protein fractions were not used for proteolytic cleavage of fusion proteins. Later fractions were not contaminated with DNA and based on the SDS PAGE analysis, they were 90 % pure (Figure 5). The yield of purification was 5 mg of His_6-TEV protease from 1 L of bacterial culture.

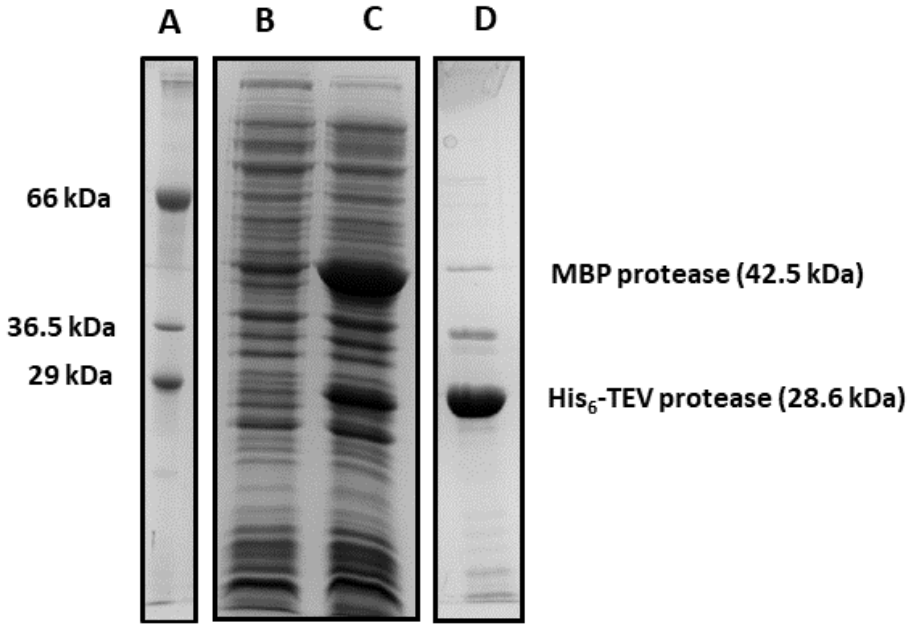

Figure 5. Expression and purification of His_6-TEV protease. A-molecular weight marker; B-Crude extract before the induction; C-Crude extract after completed expression of His_6-TEV protease; D-pure His_6-TEV protease.

2.3. *O*-ACETYLSERINE SULFHYDRILASE

2.3.1. PREPARATION OF EXPRESSION CONSTRUCTS AND PROTEINS

EXPRESSION AND PURIFICATION OF OASS FROM pET16b

Expression and purification of both isoforms of OASS from pET16b were performed as previously described [97]. pET16b plasmids containing genes for both isoforms as fusion proteins His_{10}-OASS were transformed in *E. coli* BL21(DE3) TUNER. For the expression, cells were grown in LB broth with 150 µg/mL ampicillin at 37 °C. Overnight culture was diluted 1:100 in LB + 150 µg/mL ampicillin and grown until OD_{600} = 0.5 – 0.6, when the protein expression was induced by the addition of 1 mM IPTG. Expression of OASS-A and OASS-B was performed for 5 and 4 h, respectively. Cells were pelleted by 10 min centrifugation at 5000 RPM at 4 °C and washed once with PBS before storage at -80 °C.

Cells were suspended in lysis buffer (50 mM NaP, 300 mM NaCl, pH=7.0) in the presence of intracellular protease inhibitors (0.2 mM PMSF, 0.2 mM benzamidine, 1.5 µM pepstatin A), 0.2 mM PLP and 1 mg/mL lysozyme. Cell lysis was performed by pulsed sonication until about 80 % of cells were lysed, which was determined by the turbidimetric method described in chapter 2.2. Suspension was centrifuged for 45 min at 13000 g at 4 °C and crude extract was loaded on pre-equilibrated IMAC with Co^{2+} bound to the resins (Talon™, Clontech Laboratories, Inc., Mountain View, CA, USA). Unspecifically bound proteins were eluted with 20 mM imidazole, 50 mM NaP, 300 mM NaCl, pH = 7.0. OASS-A was eluted with 250 mM imidazole and OASS-B was eluted with 600 mM imidazole. His_{10}-

tagged proteins were digested by factor Xa in 20 mM Hepes, 100 mM NaCl, 4 mM $CaCl_2$, pH = 7.5 at 37 ^oC. Cleavage was completed in 5 h for OASS-A and in 72 h for OASS-B. His tags were removed by bench Co^{2+} affinity chromatography. OASS-A was stored in 10 mM Hepes pH=8 and OASS-B in 5 mM Hepes pH=8.

Protein purity was estimated from the SDS-PAGE gel using software ImageLab 5.2.1, Bio-Rad Laboratories.

PREPARATION OF EXPRESSION CONSTRUCTS IN pET19m

pET16b-cysK and pET16b-cysM were extracted and purified from *E. coli* XL1blue cells by miniprep (Gene EluteTM Plasmid Miniprep kit, Sigma Aldrich). PCR was carried out with the primers listed in Table 3 in order to attach them to the inserts for OASS cut from the pET16b and amplify them. DNA was purified from PCR reaction mixture (GeneJET PCR Purification Kit, Thermo Scientific). New inserts were separated from the vectors using agarose electrophoresis followed by gel extraction. Amplicons were digested with NdeI and BamHI. Inserts were ligated with digested pET19m using T4 ligase in molar ratio insert:vector = 7:1 and *in vivo* amplified in *E. coli* DH5α. Extracted plasmids were sequenced to confirm the correctness of the new constructs. pET19m-STcysK and pET19m-STcysM were transformed in *E. coli* Rosetta^{TM} (DE3) competent cells for the expression.

pET19m is a modified version of a commercially available vector pET19b (Novagen) and it was a kind gift from Prof. Martin Welch [116,117].

Table 3. Sequence of oligonucleotide primers for PCR of cysK and cysM genes and insertion of restriction sites. The nucleotide sequence for NdeI is shown in bold brown and the one for BamHI is shown in bold green.

primer	Sequence
$cysK_f$	5'-AAAAAA**CATATG**AGTAAGATTTATGAAGATAACTCG-3'
$cysK_r$	5'-ACGC**GGATCC**TCACTGTTGCAGTTCTTTCTCA-3'
$cysM_f$	5'-AAAAAA**CATATG**AATACATTAGAACAAACCATCG-3'
$cysM_r$	5'-ACGC**GGATCC**TTAAATCCCTGCCCCCTGG-3'

EXPRESSION AND PURIFICATION OF OASS FROM pET19m

Recombinant proteins from pET19m were purified following the purification protocol for proteins expressed from pET16b with few modifications. After the elution of His_6-OASS-A, *in house* produced TEV protease was added to the protein in the ratio 1 OD_{280} TEV protease : 100 OD_{280} His_6-OASS-A (this results in mass ratio ~ 1 mg TEV protease : 150 mg His_6OASS-A). Cleavage of the fusion protein was performed O/N during the dialysis in 10 mM HEPES, 1 mM EDTA, pH = 8.0 at room temperature. Then, EDTA was removed by ultrafiltration. Protein was loaded on pre-equilibrated Co^{2+} resins, where it was incubated for 1 h in rotations. Pure OASS-A remained unbound to the resins, allowing its removal from TEV protease and histidine tag. StOASS-A concentration was calculated by using extinction coefficient ε_{412} = 9040 M^{-1} cm^{-1} and MW = 34670 g/mol.

After the elution from IMAC, His_6-OASS-B was dialized in 20 mM HEPES, 100 mM NaCl, 1 mM EDTA, pH=7.5 O/N on 5 ^oC and concentrated by

ultrafiltration to about 5 mg/mL. Initially, cleavage of fusion protein with TEV protease was observed to be problematic and unefficient, and therefore several digestion conditions were tested:

- Digestion at different temperatures from 5 °C to 37 °C
- Digestion for different incubation times from 4 h to 24 h
- Digestion in the presence of chaotropic agent - 1 M UREA
- Digestion in different ratios of fusion protein and TEV protease

Most efficient digestion conditions were found to be ratio 1 OD_{280} TEV protease : 4 OD_{280} His_6StOASS-B (this results in mass ratio ~ 1 mg TEV protease : 5 mg His_6OASS-B) at 5 °C for 24 h in static incubation. Protein was then dialyzed O/N in 20 mM HEPES, 100 mM NaCl pH = 7.5 to remove EDTA. TEV protease and His_6 were removed by bench Co^{2+} affinity chromatography. StOASS-B concentration was calculated by using extinction coefficient ε_{414} = 6800 M^{-1} cm^{-1} and MW = 32780 g/mol.
Protein purity was estimated from the SDS-PAGE gel using software ImageLab 5.2.1, Bio-Rad Laboratories.

PROTEIN CHARACTERIZATION WITH ACTIVITY ASSAYS

Activity of proteins expressed in different constructs was compared by their specific activities, measured by a previously described discontinuous method for the measurement of cysteine production by ninhydrin, adjusted to 96-well plate format [84,97,118]. Assays were performed in 100 mM HEPES pH=7.0 at room temperature in the final volume of 500 µL. Briefly, 6 nM OASS in the presence of 10-times concentration excess of BSA (to prevent unspecific protein binding on the tube) was incubated with 1 mM OAS for about 3 min in order to allow

temperature stabilization and reaching the steady state. The reaction was started by the addition of 600 µM Na_2S. 60 µL aliquots were withdrawn from the reaction mixture at regular time intervals and the reaction was stopped in 60 µL of acetic acid. At least 7 time-points were measured for each kinetics. 60 µL of ninhydrin reagent was added to the strips by multichannel pipette and the reaction between cysteine and ninhydrin was completed during 10 min incubation at 100 ^{o}C. 46 µL of the reaction mixture was diluted in 156 µL of ice cold EtOH and the absorbance was measured at 550 nm. Absorbance values were corrected for the blank contribution and converted to cysteine concentration by a calibration curve. Cysteine concentration was plotted against time and kinetics of enzyme activity was fitted to the linear equation, giving the enzyme activity in µM/min. The specific activity was calculated by the equation (2).

$$specific\ activity\ = \frac{(\frac{\mu M\ product}{min})}{mg\ protein} \qquad (2)$$

The result is given in U/mg, where 1 U = 1 µmol product / min.

PROTEIN CHARACTERIZATION BY FLUORESCENCE EMISSION SPECTROSCOPY

Fluorescence emission spectroscopy was performed in 100 mM HEPES, pH=7.0 at 20 ^{o}C using 10 µM protein. Emission spectra were collected upon excitations at 298 ($slit_{ex/em}$ = 3/3), 330 ($slit_{ex/em}$ = 5/5) and 412 nm ($slit_{ex/em}$ = 4/4). Fluorescence measurements were performed by Fluoromax (HORIBA).

2.4. SERINE ACETYLTRANSFERASE

2.4.1. PREPARATION OF EXPRESSION CONSTRUCT AND PROTEIN

GENE CLONING

The approach for preparation of a new StSAT expression system was gene-synthesis and subcloning in vector pSH21p-His_6-trxA (a kind gift from Professor Christopher S. Hayes, MCDB, University of California, Santa Barbara), replacing the insert for *E. coli* SAT. Nucleotide sequence of SAT from *S.* Typhimurium, obtained from Uniprot (entry A0A0U1JK50), was optimized for expression in *E. coli* by GeneArt and restriction sites KpnI (5' end) and AvaI (3' end) were added to the sequence. Gene was synthesized at Thermo Fisher Scientific, where it was cloned in vector pMK-T. This plasmid was transformed by electroporation in *E. coli* XL1 blue competent cells, where it was *in vivo* amplified and consequently extracted and purified (Gene Elute^{TM} Plasmid Miniprep kit, Sigma Aldrich). In the following stage, plasmids pMK-T-StSAT and pSH-21p-His_6-trxA-EcSAT were digested with restriction enzymes KpnI and AvaI in NEB buffer 2 (New England Biolabs) and after the digestion enzymes were inactivated by incubation at 80 ^oC for 20 minutes. Inserts and vectors were separated on 1 % agarose gel, from where StSAT insert and pSH21p-His_6-trxA vector were extracted using QIAquick Gel Extraction Kit (Qiagen). For the ligation, vector and insert were mixed in the molar ratio 1:7 and ligated by T4 ligase (New England Biolabs) during incubation at 16 ^oC overnight. New plasmids were electroporated in *E. coli* XL1blue cells, where they were *in vivo* amplified and consequently extracted for

further analysis. Restriction analysis of pSH-21p-StSAT was performed by PstI and buffer H (Promega Corporation). The sequence of the new construct was confirmed by sequencing reaction. New expression vector was transformed into competent *E. coli* Tuner™ BL21(DE3) cells (Novagen, Merck Biosciences, Billerica, MA, USA) by electroporation.

PROTEIN EXPRESSION AND PURIFICATION

E. coli Tuner™ BL21(DE3) cells transformed with pSH21p-His_6-trxA-STcysE were plated on LB agar with 150 μg/ml ampicillin and 1 % glucose and grown overnight at 37 °C. A single colony was inoculated in 50 mL of LB broth with 150 μg/mL ampicillin and 2 % glucose and grown overnight at 37 °C and 250 RPM. Overnight culture was diluted 1:100 in LB with 150 μg/mL ampicillin and 1 % glucose. Cells were grown at 37 °C and 250 RPM until the midlog phase (OD_{600} = 0.5 – 0.6) and induced with 1 mM IPTG. Induction was performed for 4 hours. Cells were removed from the broth by centrifugation (5000 RPM, 10 minutes), washed once with PBS and frozen at -80 °C.

Protein purification was started by resuspension of cell pellet in lysis buffer (100 mM Tris, 500 mM NaCl, 50 mM imidazole, 50 μM L-cysteine, 1 mM TCEP, pH = 7.5) in presence of 1 mg/mL lysozyme, 0.2 mM PMSF, 0.2 mM benzamidine and 1.5 μM pepstatin A. Cells were lysed by pulsed sonication to about 80 % of lysis. Cell lysis was monitored by a turbidimetric method described in chapter 2.2. Cell debris was removed by centrifugation (13000 g, 45 min). The supernatant was loaded on preequilibrated immobilized metal affinity column (IMAC) with Co^{2+} bound to the resins (Talon™, Clontech Laboratories, Inc., Mountain View,

CA, USA). Since over-expressed SAT can form a complex with OASS-A that is naturally present in *E. coli* cells, potentially present complexes were dissociated by adding OAS during a wash step (100 mM Tris, 500 mM NaCl, 50 mM imidazole, 1 mM TCEP, 10 mM OAS, pH = 7.0). Protein was eluted with 50 mM Tris, 500 mM NaCl, 800 mM imidazole, 1 mM TCEP, pH = 7.0. Eluted protein was collected in 1 mL fractions. The most concentrated fractions were combined and *in house* produced TEV protease was added to it in the ratio 1 OD_{280nm} TEV protease : 100 OD_{280nm} His_6-trxA-StSAT (this results in mass ratio ~ 1 mg TEV protease : 110 mg His_6-trxA-StSAT). The digestion was completed overnight at 4 ^oC while dialyzing into StSAT storage buffer (20 mM NaP, 85 mM NaCl, 2 mM EDTA, 10 mM β-mercaptoethanol, pH = 7.5). TEV protease and trxA-His_6 were removed by size exclusion chromatography using HiLoad 16/600 Superdex 75 prep grade column (separation range 3 – 70 kDa), on which was loaded 5 mL of enzyme solution, containing about 25 mg StSAT. Under these conditions, native StSAT eluted in the void volume and the low-molecular weight contaminants were removed. The final enzyme preparation was over 95 % pure. StSAT concentration was calculated by using extinction coefficient ε_{280}=26930 M^{-1} cm^{-1} and MW = 29320 g/mol.

2.4.2. ACTIVITY ASSAY DEVELOPMENT

DIRECT ACTIVITY ASSAY

Direct activity assay was performed as previously described [84]. Briefly, 7 nM STSAT and 1 mM L-Ser were incubated in experimental buffer (20 mM NaP, 85 mM NaCl, 1 mM EDTA, pH = 7.0) at 20 ^{o}C for about 3 min in order to equilibrate the reaction mixture at the assay temperature and reach the steady state. Reaction was initiated with 0.25 mM AcCoA and monitored at 232 nm, allowing to observe the consumption of AcCoA. OD_{232nm} was converted to AcCoA concentration by using extinction coefficient 4440 M^{-1} cm^{-1}.

INDIRECT ACTIVITY ASSAY

Indirect activity assay was adapted from a published method [83,89]. 7 nM STSAT, 1 mM DTNB and 1 mM L-Ser were incubated in the assay buffer (20 mM NaP, 85 mM NaCl, 1 mM EDTA, pH = 7.0) at 20 ^{o}C for about 3 min in order to equilibrate the reaction mixture at the assay temperature and reach the steady state. Reaction was initiated with 0.25 mM AcCoA and monitored at 412 nm, allowing to observe the production of TNB. OD_{412nm} was converted to TNB concentration by using extinction coefficient 14000 M^{-1} cm^{-1} [119].

DETERMINATION OF Km FOR L-Ser AND AcCoA

K_m of AcCoA was determined by both direct and indirect assay. All assays were performed at 20 °C. For AcCoA dependance the following conditions were used:

- 7 nM StSAT
- 1 mM L-Ser
- 0.03 - 3 mM AcCoA
- 1 mM DTNB in case of indirect assay.

When Km of AcCoA was obtained, it was used to determine the K_m of L-Ser by indirect assay. For L-Ser dependence the following conditions were used:

- 7 nM StSAT
- 0.25 mM AcCoA
- 0.1 - 15 mM L-Ser
- 1 mM DTNB

From the dependences, apparent K_m and V_{max} were calculated using the equation (3).

$$v_0 = \frac{V_{max} \cdot [S]}{K_M + [S]} \quad (3)$$

From the obtained data the k_{cat} was determined using the equation (4).

$$k_{cat} = \frac{V_{max}}{[enzyme]} \quad (4)$$

3. RESULTS AND DISCUSSION

3.1. OASS-A AND OASS-B

3.1.1. SEQUENCES OF StOASS-A AND StOASS-B FROM pET19m

Sequencing reaction of pET19m-StcysK and pET19m-StcysM were carried out to confirm the correctness of the new construct. Nucleotide sequence as the result of sequencing was aligned to the reference sequence of inserts from pET16b vectors, indicating the absence of mutations. Since the sequence was optimized for the expression of recombinant *S*. Typhimurium protein in *E. coli*, nucleotide sequences were translated to amino acid sequences and aligned to Uniprot reference sequences (for StOASS-A entry P0A1E3 and for StOASS-B entry A0A0T9W3Z0), confirming also the correctness of the amino acid sequence.

3.1.2. OPTIMIZATION OF PURIFICATION CONDITIONS

Purification of StOASS-A from both constructs was smooth and unproblematic. New expression construct allowed to complete the purification faster and resulted in higher yield of OASS-A, that is up to 70 mg of protein form 1 L of bacterial culture.

A similar yield was observed for the B isoform, where the new expression construct resulted in a good purification yield, up to about 50 mg of protein from 1 L culture. When StOASS-B was expressed both from pET16b and pET19m, it has been observed that the removal of histidine

tag is problematic, suggesting that the restriction site is in the position that is difficult to be accessed by the protease. In a pET16b construct, cleavage with factor Xa required 72 h at 37 ^{o}C. For the pET19m construct, several digestion conditions were tested (Figure 6). Incubation at 37 ^{o}C resulted in the precipitation of protein(s). Urea as chaotropic agent did not allow the digestion of a protein, likely causing denaturation of TEV protease. Panel B shows that increasing ratio between TEV protease and His_6-OASS-B results in more efficient cleavage (assay performed O/N at 5 ^{o}C). Based on these observations, it was chosen to digest the His_6-OASS-B on large scale in the ratio 1 $OD_{TEV\ protease}$: 4 $OD_{His6OASS-B}$ (in mass ratio TEV : His_6OASS-B = 1 : 5) at 5 ^{o}C for 24 h in static incubation (panel C). This resulted in about 70 % digestion of tagged protein (panel C, column (a)).

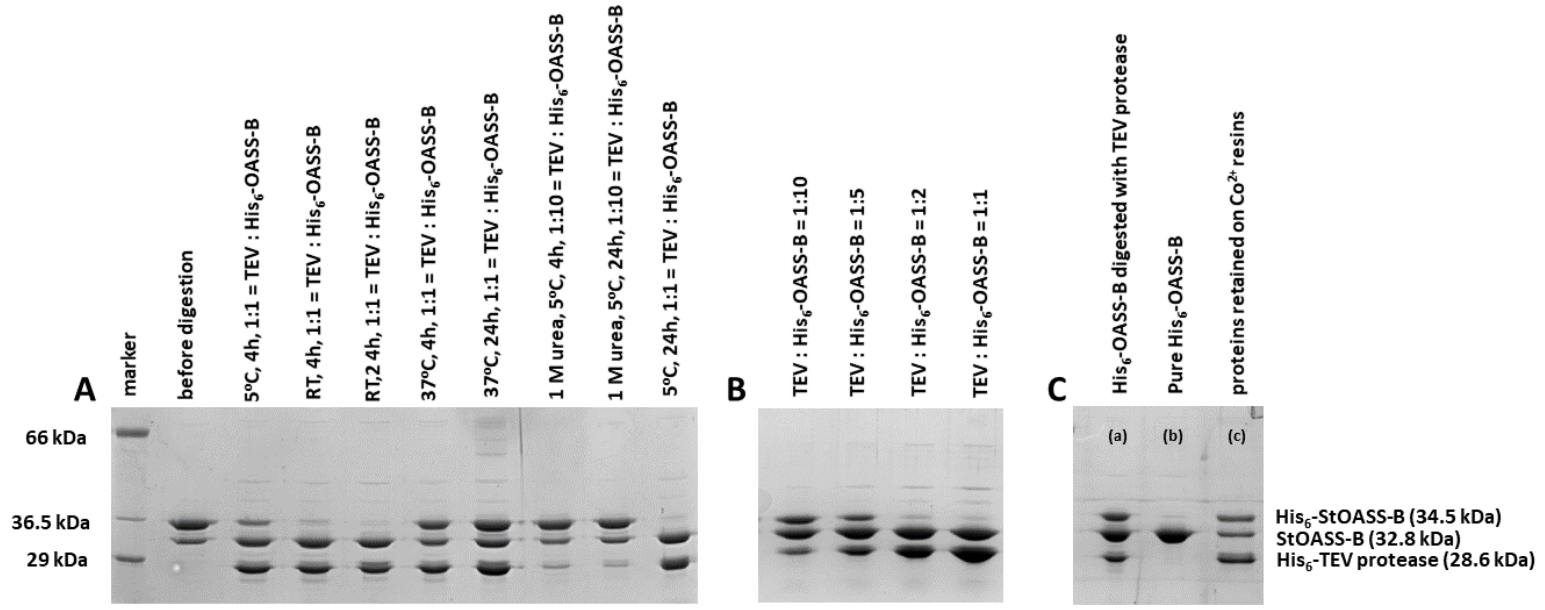

Figure 6. Conditions of His_6-OASS-B digestion with TEV protease. Panel A: effect of temperature, time, and chaothropic agent (urea) on digestion. Panel B: effect of different mass ratios between His_6-OASS-B and TEV protease on cleavage efficiency in O/N incubation at 5 °C. Panel C: Final digestion of His_6-OASS-B with TEV protease. TEV and OASS-B protease are in mass ratio 1 : 5 after 24 h digestion (a), pure OASS-B that eluted from the Co^{2+} affinity chromatography (b) and proteins that eluted from resins with imidazole (c).

Final purity of proteins was judged by the SDS PAGE gel analysis (Figure 7). Purity of the proteins was evaluated to more than 95 %.

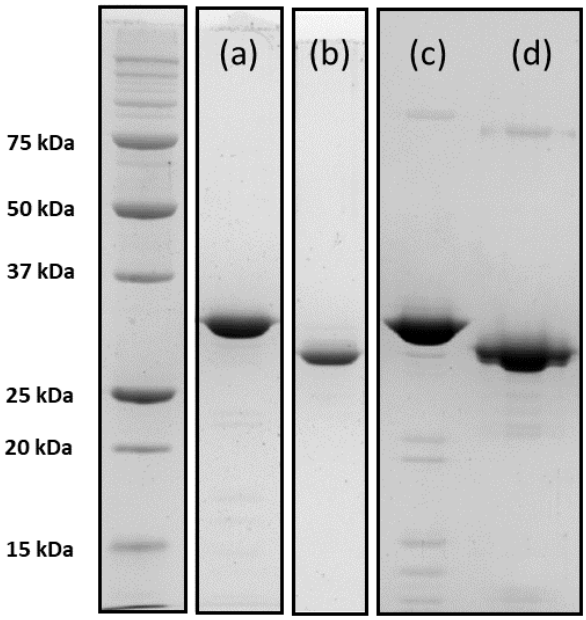

Figure 7. SDS PAGE analysis of purified proteins. (a) StOASS-A from pET16b; (b) StOASS-B from pET16b; (c) StOASS-A from pET-19m; (d) StOASS-B from pET19m.

3.1.3. CHARACTERIZATION OF PROTEINS PURIFIED FROM DIFFERENT CONSTRUCTS

Comparison of the proteins purified from different constructs was performed by activity assays and fluorescence emission spectroscopy.

Comparison of proteins' activities was evaluated by calculation of their specific activities measured under conditions, that are normally used as a control experiment when performing activity assays. In this case, 6 nM StOASS is preincubated with 1 mM OAS, that corresponds to K_m, and the reaction is started with 600 µM Na_2S, i.e. saturating conditions. StOASS-

A expressed in pET16b has a specific activity of 164 ± 2 U/mg and StOASS-A expressed in pET19m has the specific activity of 155 ± 3 U/mg, thus resulting in comparable specific activities. The same was observed for the B isoform, where StOASS-B expressed from pET16b has the specific activity of 129 ± 3 U/mg and StOASS-B expressed in pET19m 134 ± 2 U/mg.

Fluorescence emission spectrum of OASS-A upon excitation at 298 nm is characterized by a band positioned at 340 nm due to the emission of tryptophans, and a band at 500 nm that originates from an energy transfer between tryptophan emission and the excited ketoenamine tautomer of the internal Schiff's base between active site lysine and PLP (Figure 8, panel A) [120]. The overlap of the spectra from both purification procedures confirms the correctness of the distance between tryptophans and PLP, and therefore of enzyme folding. Excitation of protein at 330 nm showed differences in the tautomeric distribution of the bound PLP (panel B) [44,120]. While in the protein from pET16b, PLP is bound predominantly in the ketoenamine form, ketoenamine and enolimine tautomers are both present in the protein from pET19m. After the excitation of internal aldimine at 412 nm, both proteins exhibit emission spectrum with a peak positioned at 505 nm (panel C). Slight differences in the intensities are likely arising from differences in the abundance of tautomeric forms.

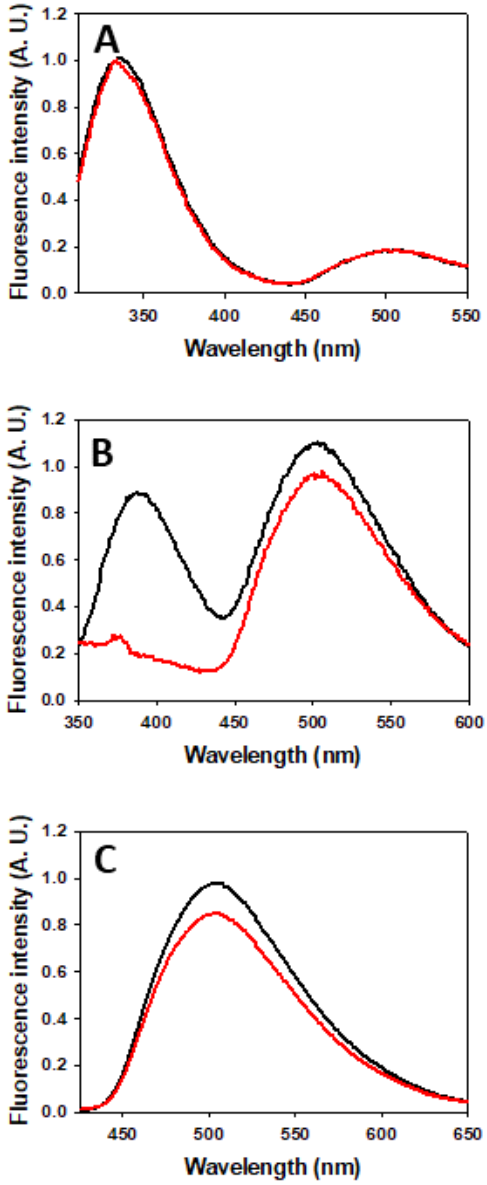

Figure 8. Characterization of StOASS-A by emission fluorescence spectroscopy. Measurements were performed in 100 mM HEPES pH=7.0 at 20 °C. Lines in black present StOASS-A expressed in pET19m and lines in red present StOASS-A expressed in pET16b. Panel A: 10.8 µM StOASS-A, excitation at 298 nm, slit ex/em = 3/3. Panel B: 10.8 µM StOASS-A, excitation at 330 nm, slit ex/em = 5/5. Panel C: 10.8 µM StOASS-A, excitation at 412 nm, slit ex/em = 4/4.

The fluorescence emission spectra of the B isoform exhibit similar behavior (Figure 9). Excitation of tryptophans shows a characteristic peak at 340 nm, although the energy transfer to PLP is lower comparing to the OASS-A (panel A) [44]. PLP is bound to active site lysine via both tautomeric forms in proteins from both constructs (panel B). The peak of PLP emission spectrum upon excitation at 412 nm is centered at 507 nm (panel C).

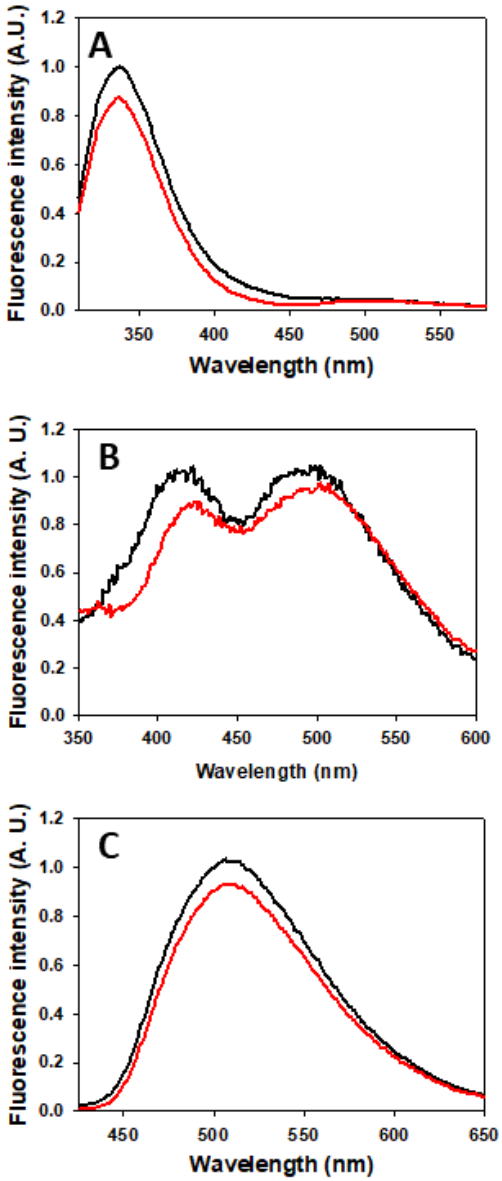

Figure 9. Characterization of StOASS-B by emission fluorescence spectroscopy. Measurements were performed in 100 mM HEPES pH=7.0 at 20 °C. Lines in black present StOASS-B expressed in pET19m and lines in red present StOASS-B expressed in pET16b. Panel A: 10 µM StOASS-B, excitation at 298 nm, slit ex/em = 3/3. Panel B: 10 µM StOASS-B, excitation at 330 nm, slit ex/em = 5/5. Panel C: 10 µM StOASS-B, excitation at 412 nm, slit ex/em = 4/4.

3.2. SERINE ACETYLTRANSFERASE

3.2.1. EXPRESSION CONSTRUCT FOR StSAT

The approach for the preparation of StSAT expression construct was gene design and its subcloning in pSH21p-His_6-trxA, replacing the insert for *E. coli* SAT. Therefore, EcSAT insert was cut from pSH21p-His_6-trxA-EcSAT and later replaced with insert for StSAT. When the ligation was completed, it was necessary to confirm that the insert inside the plasmid was coding the StSAT protein and that it was not the contamination with the plasmid coding EcSAT. For the preliminary analysis of ligation, allowing the separation between pSH-21p-His_6-trxA-EcSAT and pSH-21p-His_6-trxA-StSAT, restriction analysis with PstI was performed. This restriction enzyme was chosen based on its ability to cleave the constructs on the fragments of different sizes:

- pSH-21p-trxA-His_6-EcSAT:
    - 6575 bp

- pSH-21p-trxA-His_6-StSAT:
    - 5219 bp
    - 1008 bp
    - 150 bp
    - 135 bp
    - 63 bp

Digestion with PstI linearizes the vector for EcSAT while it cleaves the vector for StSAT into 5 fragments, allowing to see the two biggest fragments on 1 % agarose gel.

From transformed *E. coli XL1blue,* new plasmids were extracted and digested with PstI. pSH-21p-trxA-His_6-EcSAT served as a control. Figure 10 is showing the results of restriction analysis, confirming the presence of correct StSAT (columns A and B) insert in the extracted plasmids. Fragments at 150, 135 and 63 bp are not visible in the gel.

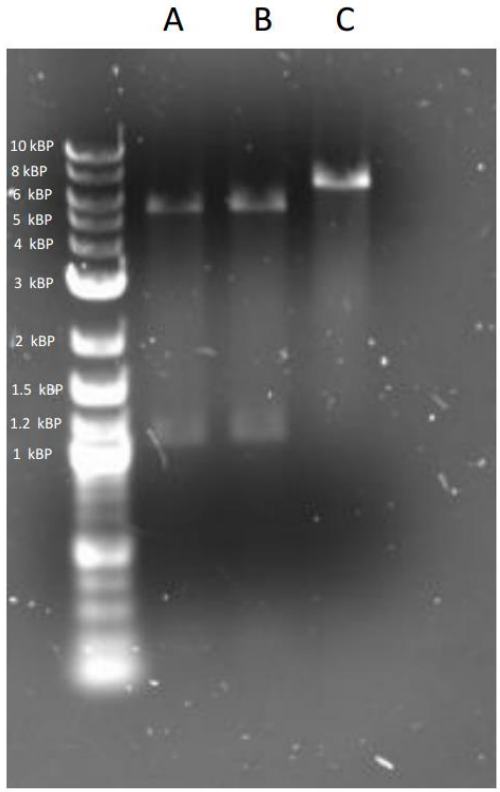

Figure 10. Digestion of pSH-21p-His_6-trxA-StSAT extracted from two transformed E. coli XL1blue colonies (A, B) and pSH-21p-His_6-trxA-EcSAT with PstI.

The total sequence was confirmed by sequencing reaction and comparison with a reference nucleotide sequence. The sequence also confirmed the presence of thioredoxin A (trxA), which was fused to the construct in order to increase its solubility, histidine tag and the recognition site for TEV protease.

3.2.2. EXPRESSION AND PURIFICATION OF STSAT

For the expression of His_6-trxA-StSAT, various *E. coli* strains, expression times and IPTG concentrations were tested and the optimized protocol is reported in Materials and Methods section. It was observed that addition of glucose in the growth medium is beneficial since it hinders cysteine operon induction by OAS production. This way we were able to prevent the SAT-OASS-A complex formation during protein expression.

Purification was started by cell lysis using sonication. Initially, we observed that about 50 % of the protein remains in the unsoluble fraction, suggesting a limited solubility. Fusion protein in the soluble fraction also showed signs of instability during steps of dialysis and concentration. Low stability of fusion protein likely arises from the fact that the N-terminal part of SAT contains trxA, that prevents the formation of native hexameric state. The stability issues were later overcomed by purification in the presence of 50 µM L-cysteine, indicating that this physiological inhibitor increases the protein stability. L-cysteine is competitive against L-serine and upon its binding SAT undergoes big conformational changes, in which normally very exposed C-terminal part of the protein moves inside the protein's active site [86]. This way,

protein is stabilized and C-terminal is protected. Cleavage with TEV protease for the removal of His_6-trxA was unproblematic and completed O/N. The most efficient way of removing the tag and low-molecular-weight contaminants was the use of size-exclusion chromatography, that produced protein of about 95% purity (Figure 11). The purification yield was up to 15 mg StSAT from 1 L of bacterial culture.

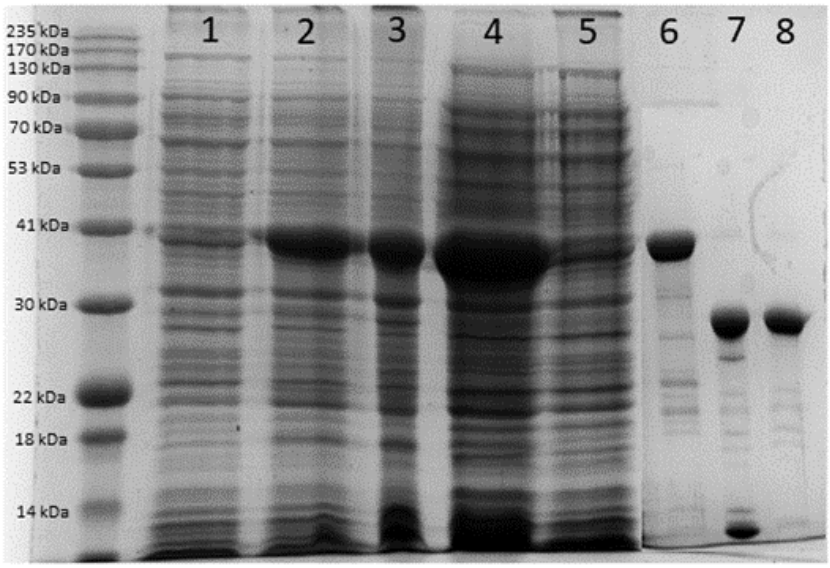

Figure 11. SDS PAGE analysis of StSAT expression and purification. Panel A: 1- not induced cells; 2-induced cells; 3-un soluble fraction; 4-soluble fraction; 5-flowthrough; 6-StSAT-trxA-His_6; 7-sample after digestion with TEV protease; 8-StSAT after SEC.

The purification in the presence of L-cysteine might inhibit enzyme's activity. However, activity of proteins purified in the absence and presence of L-cysteine were comparable, suggesting that L-cysteine dissociates during the further steps of purification (Figure 12).

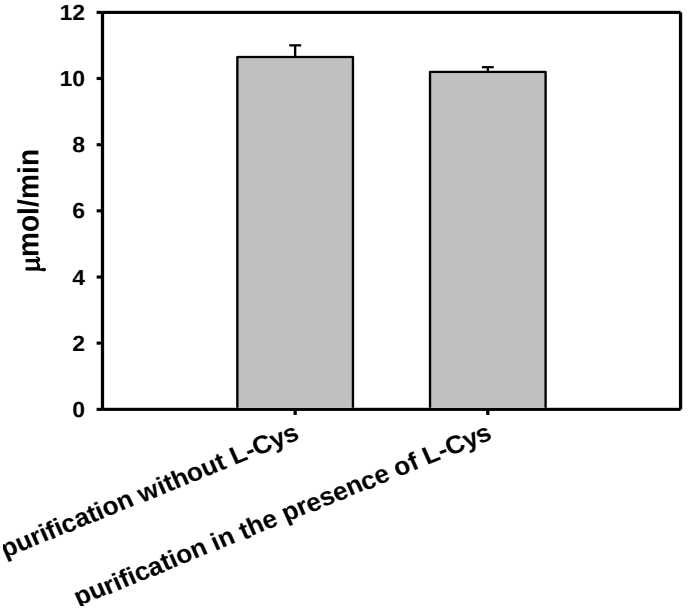

Figure 12. Comparison of StSAT activity after different purification protocols. Both samples were tested as 7 nM StSAT, 1 mM L-serine and 0.25 mM AcCoA. Enzyme activity was measured using indirect assay.

3.2.3. DEVELOPMENT AND VALIDATION OF THE INDIRECT ACTIVITY ASSAY AND COMPARISON WITH DIRECT ASSAY

Direct activity assay for SAT had already been used in our laboratory, predominantly to monitor the activity of EcSAT. However, this type of the assay is based on the measurement of AcCoA consumption at 232 nm, which is in the UV-range. For the needs of the StSAT project, we designed an indirect assay, in which we were able to follow the kinetics in the visible range. This feature allows performance of the assay on a bigger format, such as 96-well plates, that are normally not suitable for measurement in the UV-range. In a collaboration with Prof. Costantino's group (University of Parma) and Prof. Tammela's group (University of

Helsinki), the method was applied for high-throughput screening of a commercially available compound library in the search for novel StSAT inhibitors.

The indirect assay had been described previously [83] and is based on the reaction between DTNB and CoA, that is forming during the SAT reaction. CoA reacts with DTNB, releasing the chromophoric TNB that absorbs at 412 nm. The reaction is schematically shown in Figure 13.

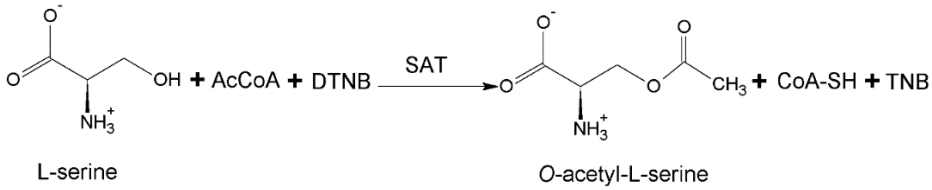

Figure 13. Schematic representation of SAT indirect activity assay.

The buffer for StSAT activity assay was the same as previously used for direct activity assay. All assays were performed at 20 °C. DTNB concentration was fixed at 1 mM, allowing to be in excess and therefore available for reaction with all CoA molecules. The time course was measured in quartz cuvettes with pathlength 1 cm, which gave the signal of TNB absorbance in the linear range of spectrophotometer. Enzyme concentration was kept constant at 7 nM.

In order to exclude any interferences of DTNB on StSAT activity, the K_m of AcCoA for the enzyme was determined by both direct and indirect assay. Dependences were determined at 1 mM L-Ser, being the apparent K_m of EcSAT at 0.25 mM AcCoA. Dependences are shown in Figure 14.

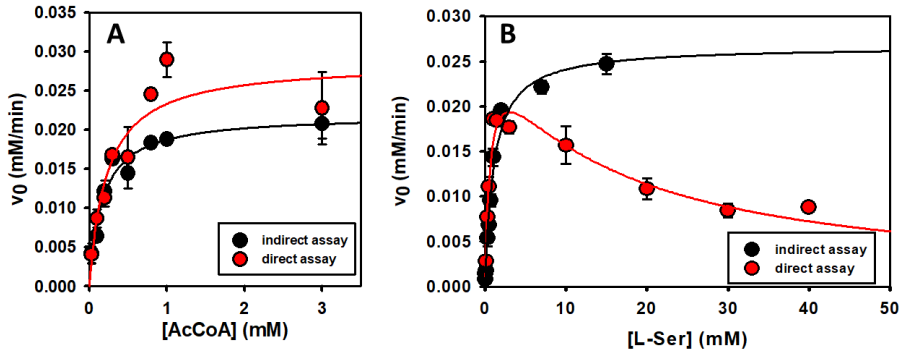

Figure 14. Panel A: StSAT activities as AcCoA dependence at 1 mM L-Ser collected with direct and indirect activity assays. Panel B: StSAT activities as L-Ser dependence at 0.25 mM AcCoA determined with indirect activity assay.

The apparent K_m of AcCoA with the direct and indirect assay was determined to be 0.17 ± 0.04 mM and 0.23 ± 0.10 mM, respectively. For the following assays we fixed AcCoA concentration at 0.25 mM. The same approach was used to calculate the K_m of L-Ser with both direct and indirect assay. Dependences are shown on Figure 14, panel B. The apparent K_m at 0.25 mM AcCoA determined with the direct and assay was 0.65 ± 0.18 mM and 1.07 ± 0.15 mM, respectively. All determined catalytic parameters are summed up in Table 4. Despite the good agreement in catalytic parameters, it should be pointed out that DTNB prevents substrate inhibition of L-serine, suggesting that DTNB is interfering with SAT reaction (Figure 14, panel B). Stabilization of EcSAT by DTNB was previously reported [83,121], although the exact mechanism of inhibition/interference is still unknown.

Table 4. Kinetic parameters of StSAT determined by direct and indirect activity assays.

	k_{cat} (min^{-1})	K_m (mM)	k_{cat}/K_m ($min^{-1}mM^{-1}$)
L-Ser dependence, direct assay	2820 ± 341	0.65 ± 0.18	4338
L-Ser dependence, indirect assay	3813 ± 196	1.07 ± 0.15	3563
AcCoA dependence, direct assay	4093 ± 483	0.23 ± 0.10	17795
AcCoA dependence, indirect assay	3128 ± 186	0.17 ± 0.04	18400

The suitability of the indirect assay for the evaluation of StSAT inhibitors was confirmed by testing glycine as a reference inhibitor. Literature reports a K_I for glycine of 13.4 mM [121] and the IC_{50} determined with the new assay was 15.1 mM. Based on the good match between our and literature values it was concluded that the assay is appropriate for identification of novel StSAT inhibitors.

BIOCHEMICAL EVALUATION OF OASS AND SAT INHIBITORS

1. INTRODUCTION

Inhibition of StOASS and StSAT are promising strategies in the development of enhancers of antibiotic therapy. Several potent StOASS inhibitors had already been identified in our laboratory [96,97,122–124] and the most potent one was crystallized in the complex with StOASS-A during the course of this project. Since identified molecules exhibited difficulties in the permeability through the complex membrane of Gram-negative bacteria, the project was focused on the design of new molecules with more beneficial characteristics for drug-likeness. Therefore, derivatives of known molecules were prepared and their structure-activity relationship was studied. Additionally, structurally different inhibitors were obtained by scaffold hopping method and biochemically evaluated. For the first time, inhibition of OASS by mechanism based inactivators was exploited. Several fluoroalanine derivatives were assayed and the chapter reports their mechanism of action and structure-activity relationship.

Despite the key role of SAT in cysteine biosynthesis, only three inhibitors of SAT have been reported in literature [114]. We focused our attention in the development of novel inhibitors by *in silico* screening of *in house* compound library and high-throughput screening of ChemDiv libraries which led to the identification of the most potent SAT inhibitor reported so far.

The aim of this project was to identify potent StOASS and StSAT inhibitors, that exhibit physico-chemical characteristics favorable for the permeability of Gram-negative membrane and should be promising candidates for microbiological evaluation.

2. MATERIALS AND METHODS

2.1. MATERIALS

All reagents, if not otherwise specified, were purchased from Sigma-Aldrich (St. Louis, MO, USA) at the highest available quality. Ninhydrin was purchased from Apollo Scientific (Stockport, UK).

For the crystallization of StOASS with automatic setup, the following screens, pre-dispensed in 96-well plates, were used:

- Classic Suite (Quiagen)
- Classic Lite Suite (Quiagen)
- JCSG+ (Molecular Dimensions)
- PH Clear I Suite (Quiagen)
- PH Clear II Suite (Quiagen)
- PEGS I Suite (Quiagen)
- PEGS II Suite (Quiagen)
- Cryo 96 Suite (Quiagen)
- $AmSO_4$ Suite (Quiagen)
- MPD Suite (Quiagen)
- Wizard I and II (Molecular Dimensions)
- Wizard III and IV (Molecular Dimensions)

2.2. StOASS CRYSTALLIZATION

2.2.1. CRYSTALLIZATION BY SITTING DROP METHOD

StOASS crystallization was initially approached during the secondment at University of Cambridge. The chosen method was sitting drop, where drops were prepared by an automatic liquid dispenser (Mosquito Crystal,

TTPLabtech Ltd). In this type of setup, 0.2 µL of protein was mixed with 0.2 µL of precipitant solution, positioned on a drop holder next to the precipitant solution container, and incubated at 19 °C. Crystallization trials were carried out using proteins in concentration 10 - 20 mg/mL in the absence and in the presence of 1 mM UPAR-415.

StOASS crystallization trials were carried out using pre-dispensed commercially available screens, stated in the chapter 2.1., as well as by customized conditions, that were chosen based on the literature reports where StOASS crystalizes [67,69–71,125] and protein behavior in the screens. In the case of customized conditions, the precipitants in a concentration gradient were dispensed in 96-well plates used for sitting drop crystallization by an automatic liquid dispenser (Dragonfly TTPLabtech).

The following customized conditions were tested for **StOASS-A**:

Condition 1, based on literature data [69,125]:

- PEG4000 (concentration gradient 26 – 40 w/v %)
- Li_2SO_4 (concentration gradient 0 - 0.9 M)
- Tris pH = 7.0

Condition 2, based on the behavior in the commercially available screens:

- PEG4000 (concentration gradient 22 – 26 w/v %)
- $MgCl_2$ (concentration gradient 0.14 - 0.18 M)
- Glycerol (concentration gradient 20 – 30 v/v %)
- Tris pH = 7.0

Condition 3, based on the behaviour in the commercially available screens:

- PEG4000 (concentration gradient 18 – 22 w/v %)
- Na_3-citrate (concentration gradient 0.08 - 0.2 M)
- Propan-2-ol (concentration gradient 18.5 – 23 v/v %)

The following customized conditions were tested for **StOASS-B**:

Condition 1, based on the literature data [67]:

- NaK-tartrate (concentration gradient 0.8 – 1.2 M)
- MES pH = 6 (concentration gradient 80 – 200 mM)

Condition 2, based on the behavior in the commercially available screens:

- PEG1000 (concentration gradient 18 – 22 w/v %)
- Glycerol (concentration gradient 0 – 10 v/v %)
- Tris pH = 7.0

Since basic sitting drop method did not give high-quality crystals, microseeding was used to obtain crystals of a higher quality. For this approach, low-quality crystals were crushed into seedstock by using Seed Bead kit (Hampton research). 10-fold dilutions of initial seedstock were prepared and following crystallization trials were carried out with different concentrations of seedstock. Seedstocks were seeded in diverse crystallization conditions, where the drops consisted of 0.2 µL of protein in the presence of 1 mM UPAR-415, 0.2 µL of chosen precipitant solution and 0.1 µL of seedstock.

For the stabilization before cryo data collection, crystals were passed in precipitant solution containing 20 % ethylene glycol as a cryoprotectant.

Crystals were then flash frozen in liquid nitrogen and data were collected at synchrotron Diamond Light Source beamline I04.
Photographs of crystals were taken by automated imaging system (Rock Imager 1000, Formulatrix Ltd).

2.2.2. CRYSTALLIZATION BY HANGING DROP METHOD

When StOASS-A crystallization was performed by a hanging drop method, 1 µL of 20 mg/mL StOASS-A expressed from pET16b was mixed with 1 µL of a precipitant solution containing 30 % PEG4000, 130 – 180 mM Li_2SO_4 (Fluka), 100 mM Tris base pH = 7.0. Crystals grew within 5 days at 25 ^oC.
For the stabilization before cryo data collection and diffusion of an inhibitor in the active site, crystals were soaked in a stabilizing solution containing 5 % glycerol, 32% PEG4000, 150 mM Li_2SO_4, 100 mM Tris pH=7 with 1 mM UPAR-415 for 2 h and then flash-frozen in liquid nitrogen. Data were collected at synchrotron Elettra Trieste. The structure reported in the thesis is preliminary. It was solved by molecular replacement using StOASS-A native structure as a model (PDB code 1OAS), while the minimization with refinement has not been performed yet.
Alignments and structure analysis were performed using PyMOL$^{(TM)}$ 2.0.6, Schrodinger, LLC.

2.3. StOASS ACTIVITY ASSAYS

2.3.1. ACTIVITY ASSAYS FOR REVERSIBLE INHIBITORS

OASS activity assays were performed by a previously described discontinuous method for the measurement of cysteine production based on ninhydrin, adjusted to 96-well plate format [84,97,118]. Assays were performed in 100 mM HEPES pH 7.0 with 1 % DMSO at room temperature. Briefly, 6 nM OASS in the presence of 10-times concentration excess of BSA (to prevent unspecific protein binding on the tube well) was incubated with 1 mM OAS for about 3 min in order allow temperature stabilization and reaching the steady state. The reaction was started by the addition of 600 µM Na_2S. 60 µL aliquotes were withdrawn from the reaction mixture at regular time intervals and reaction was stopped in 60 µL of acetic acid, dispensed in PCR strips. At least 7 time-points were measured for each kinetics. 60 µL of ninhydrin reagent was added to the strips by multichannel pipette and the reaction between cysteine and ninhydrin was completed during 10 min incubation at 100 ^{o}C. 46 µL of the reaction mixture was diluted in 156 µL of ice cold EtOH and the absorbance was measured at 550 nm. Absorbance values were corrected for the blank contribution and converted to cysteine concentration by a calibration curve. Cysteine concentration was plotted against time and kinetics of enzyme activity was fitted to the linear equation (5).

$$v_0 = \frac{[P]t - [P]0}{\Delta t} \quad (5)$$

v_0 = initial reaction rate; [P]t = cysteine concentration at time t; [P]0 = cysteine concentration at t=0h; Δt = time interval between t=0h and time= t.

IC_{50}s were calculated by the equation (6).

$$\frac{v_i}{v_0} = \frac{1}{\left(1 + \frac{[I]}{IC50}\right)} \quad (6)$$

v_0 = initial rate in the absence of inhibitor; v_i = initial rate in the presence of inhibitor at concentration [I].

Activity assays of compounds bio-2347_1F1 – bio-2412_1F1 were carried out in the presence of 5 % DMSO.

2.3.2. ACTIVITY ASSAYS FOR IRREVERSIBLE INHIBITORS

For evaluation of enzyme inactivation by irreversible inhibitors, 45 µM enzyme was incubated with inactivator and diluted 5000-times in HEPES with BSA before the assay.

Inactivation kinetics were collected at different concentrations of inactivator and k_{obs} values were determined by fitting of the data to the equation of a single exponential decay:

$$\frac{v_i}{v_0} = A + B \cdot e^{-k_{obs} \cdot t} \quad (7)$$

v_0 = initial rate in the absence of inhibitor; v_i = initial rate after incubation (for time = t) with inhibitor at concentration [I]; A = off-set; B = the amplitude; k_{obs} = the rate constant.

Potency of inhibitor was determined as the ratio k_{inact}/K_I that for OASS-A was determined from equation (8) [103].

$$k_{obs} = \frac{k_{inact} \times [I]}{K_I + [I]} \quad (8)$$

k_{obs} = observed rate constant of inactivation at inhibitor concentration [I]; k_{inact} is inactivation rate constant; K_I = concentration of inhibitor that yields k_{obs} = ½ k_{inact}.

For the OASS-B, equation (9) was used. It is derived from equation (8), when the highest [I] is << K_I and simplified to:

$$\frac{k_{obs}}{[I]} = \frac{k_{inact}}{K_I} \quad (9)$$

2.4. AFFINITY OF INHIBITORS TO StOASS DETERMINED BY DIRECT FLUORIMETRIC TITRATIONS

The affinity of compounds for OASS was measured by direct fluorimetric titrations using FluoroMax-3 fluorimeter (HORIBA). Assays were performed in 100 mM HEPES with 1 % DMSO at 20 °C. A solution containing 0.1 – 1 µM OASS (concentration depending on the K_d) was titrated with increasing concentrations of the compound. The fluorescence emission of the PLP cofactor at 500 nm upon excitation at 412 nm was collected after each compound addition, subtracted by the blank and normalized for the protein dilution. Collected fluorescence intensities were plotted against compound concentration and K_d was determined by the hyperbolic regression described by equation (10), using SigmaPlot 11.0, Systat Software, Inc.

$$I = I_0 + \frac{\Delta I \cdot [L]}{K_d + [L]} \quad (10)$$

I = measured fluorescence intensity; I_0 = flourescence intensity of OASS in the absence of inhibitor; ΔI = difference between the fluorescene intensity of the OASS-inhibitor complex and free OASS; [L] = inhibitor concentration.

In cases where K_d was similar to the enzyme concentration in the assay or lower, tight binding equation was used (11):

$$I = I_0 + \Delta I \cdot \frac{[P] + [L] + K_d - \sqrt{([P] + [L] + K_d)^2 - 4 \cdot [P] \cdot [L]}}{2} \quad (11)$$

I = measured fluorescence intensity; I_0 = flourescence intensity of OASS in the absence of inhibitor; ΔI = the amplitude between the fluorescene intensity of the OASS-inhibitor complex and free OASS; [L] = inhibitor concentration; [P] = OASS concentration.

As described elsewhere [97], the fluorimetric method allows the calculation of the intrinsic dissociation constant of a competitive inhibitor and the calculated K_d is in a very good agreement with the IC_{50} measured by the activity assays.

2.5. StOASS SPECTRAL CHANGES

Absorbance spectra were recorded with a Cary4000 spectrophotometer (Agilent Technologies) on solutions containing 5-10 µM enzyme, 1 mM inactivator, 100 mM HEPES, pH 7.0, 1 % DMSO at room temperature. Spectra were corrected for the buffer and compound contribution. The time course of band disappearance at a fixed wavelength was fitted to a single exponential decay equation (12).

$$A_t = A_0 + A_i^{-k_{obs} \cdot t} \quad (12)$$

A_t = absorbance at time t; A_0 = absorbance at infinite time; A_i = initial absorbance; k_{obs} = rate constant.

Absorbance spectra of StOASS in the presence of compounds bio-2347_1F1 – bio-2412_1F1 were monitored using TECAN SPARK 10M on 384-well plates. The final DMSO concentration in the reaction mixture was 5 %.

Fluorescence emission spectra were recorded with a FluoroMax-3 fluorimeter (HORIBA) on solutions containing 1 µM enzyme, 1 mM inactivator, 100 mM HEPES, pH 7.0, at room temperature, upon excitation at 412 nm, with $slit_{ex}$ = $slit_{em}$ = 6 nm. Spectra were corrected for buffer and compound contribution.

2.6. StSAT ACTIVITY ASSAY

A solution containing 7 nM STSAT, 1 mM DTNB, 1 mM L-Ser, inhibitor at a chosen concentration in experimental buffer 20 mM NaP, 85 mM NaCl, 1 mM EDTA, pH = 7.0 with 5 % DMSO was incubated for about 3 min at 20 ^{o}C in order to allow temperature equilibration and reaching the steady state. Reaction was initiated with 0.25 mM AcCoA and monitored at 412 nm, allowing to observe the production of TNB. Time courses were monitored using Cary4000 (Agilent Technologies). OD_{412} was converted to TNB concentration by using extinction coefficient of 14000 M^{-1} cm^{-1}. IC_{50}s were calculated using equation (6).

For the determination of inhibition mechanism of potent StSAT inhibitors, Lineweaver-Burk double reciprocal plot was used. Four inhibitor concentrations were tested at specific substrate concentration while keeping the concentration of the second substrate fixed. The mechanism of action was deduced from the double reciprocal plot. Kinetic parameters were determined by global fitting to the equation (13) for competitive inhibition.

$$v_0 = \frac{V_{max} \cdot [substrate]}{[substrate] + (K_m \cdot (1 + \frac{[inhibitor]}{K_I}))} \qquad (13)$$

v_0 = initial rate in the absence of inhibitor, v_{max} = enzyme's maximal rate; K_I = inhibition constant; K_m = apparent Michaelis constant for AcCoA at 1 mM L-Ser.

2.7. MEASURING COMPOUND SOLUBILITY

Solubility of compounds in experimental buffer was monitored by measuring scattering at 620 nm. Compounds in different concentrations were put in 200 µL of the experimental buffer while keeping DMSO concentration the same as in the assay. Samples were prepared on 96-well plate and the scattering intensity at 620 nm was measured. From the raw data, the contribution of experimental buffer was subtracted and compound concentrations yielding $OD_{620} \leq 0.05$ were considered as soluble.

3. RESULTS AND DISCUSSION

3.1. StOASS INHIBITORS

3.1.1. CRYSTALLIZATION OF StOASS BY SITTING DROP METHOD

Crystallization of both isoforms of StOASS by sitting drop method appeared to be difficult and it was unfruitful. The A isoform did not crystallize under any tested conditions, which is surprising since its structure has been published several times [69–71]. However, all of the published structures originate from hanging drop method. Even though both methods are based on the vapor diffusion principle, sitting drops are subjected to a more complex geometrical constrains, based on the crystallization chamber, microbridges and droplet holders, that can significantly alter the crystallization process [126].

In the case of StOASS-B, by using commercially available screens we identified a condition where the protein crystalizes as needles (Figure 15).

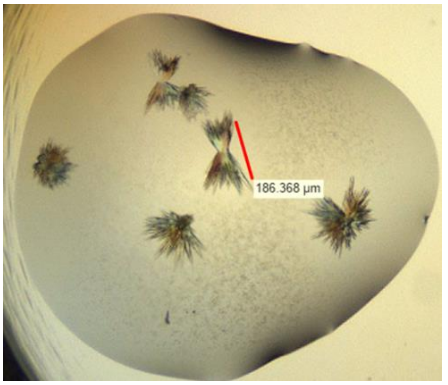

Figure 15. StOASS-B (20 mg/mL) forms crystalline structure when grown in 20 w/v % PEG1000 and 0.1 M Tris pH = 7.0

As we did not succeed in the optimization of the crystallization conditions by changing the concentration of precipitants in the mother liquid, we applied the microseeding method. The needles were crushed by seed beads to form a seedstock, that was later diluted 1000-times and used for seeding in different conditions. When microseeding was performed, 12 mg/mL StOASS-B was pre-mixed with 1 mM UPAR-415, allowing the cocrystallization of protein with inhibitor. By this approach, we obtained the crystals shown in Figure 16. Crystals were prepared for X-ray data collection, but they did not exhibit a diffraction pattern.

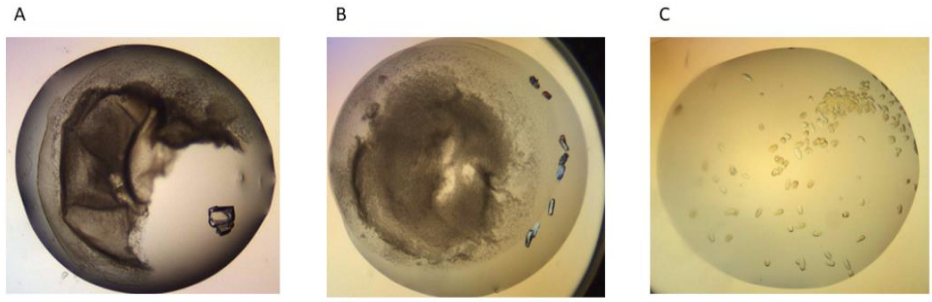

Figure 16. Cocrystals of StOASS-B and UPAR-415, obtained by microseeding technique. Panel A: 15 %v/v EtOH, 0.2 M Zn-acetate, 0.1 M MES pH = 6. Panel B: 10 %v/v isopropanol, 0.2 M Ca-acetate, 0.1 M MES pH = 6. Panel C: 1 M Na_3-citrate, 0.1 M sodium cacodylate pH=6.5.

3.1.2. CRYSTALLIZATION OF StOASS-A WITH UPAR-415 BY HANGING DROP METHOD

When crystallization was carried out by hanging drop method, StOASS-A crystallized in a rhomboid shape (Figure 17, panel A). Crystals examined with polarized absorbance spectroscopy showed a broad peak centered at 420 nm, confirming the presence of a Schiff's base linkage between

cofactor PLP and active site lysine (panel B). The crystals were birefringent when observed in cross-polarizers.

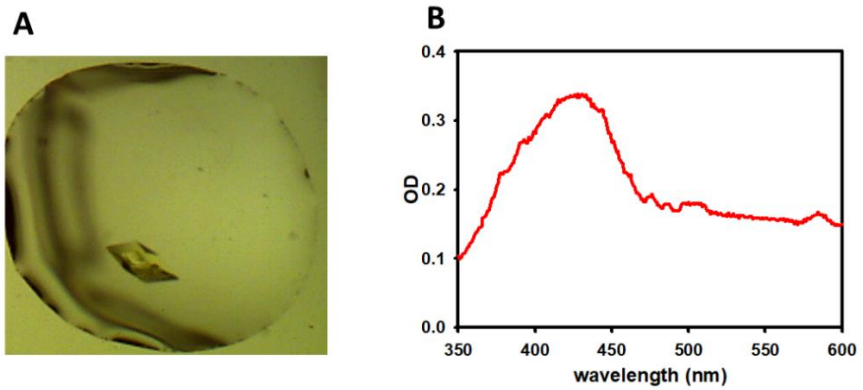

Figure 17. Panel A: StOASS-A crystal. Panel B: polarized absorption spectrum of StOASS-A crystal.

In order to observe the interactions between StOASS-A and its reversible inhibitor, we soaked crystals in 1 mM UPAR-415. UPAR-415 is the most potent inhibitor of StOASS identified so far and was designed to be a mimetic of a C-terminal part of SAT, the natural inhibitor of OASS. Its structure is shown in Figure 18.

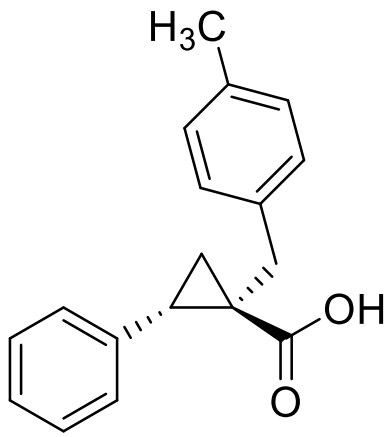

Figure 18. Structure of UPAR-415. K_d StOASS-A = 0.028 ± 0.005 µM and K_d for StOASS-B = 0.49 ± 0.05 µM [97].

Cyclopropane scaffold of UPAR-415 holds a *trans* configuration of the molecule, that is pivotal for the affinity. The carboxylic group is present in its structure to mimic the C-terminal Ile of SAT, which is essential for the binding, and the phenyl group is mimicking the side chain of Ile. To mimick the SAT backbone, a tolyl group was attached to the α-carbon. The molecule exhibits high affinity towards both isozymes of StOASS, giving K_ds of 0.029 μM and 0.49 μM towards A and B isoform, respectively. Computational and STD NMR techniques predicted its orientation in the active site of StOASS-A, that is almost superimposable with a C-terminal part of SAT with its carboxylic moiety interacting with corresponding amino acid residues in the active site [97].

In order to confirm the position of UPAR-415 in the active site of StOASS-A, we prepared their cocrystal. The inhibitor was added to the crystal by soaking. For this purpose, the crystals were transferred in a stabilizing solution with 1 mM UPAR-415. Besides inhibitor, the stabilizing solution contained also 5 % glycerol and increased concentration of PEG4000 that acted as cryoprotectants during data collection. Different soaking times were tried and the inhibitor was found in the crystals that for soaked for at least 2 h.

Protein crystallized in a space group P 2_1 2_1 2_1 with dimensions a=53.239, b=96.256, c=140.756 where α=β=γ=90.00, that is in agreement with a previously published structure (PDB code 1OAS) [69]. Crystal diffracted at 1.20 Å resolution. The structure was solved by molecular replacement

using 1OAS as a template. The structure is preliminary, as it has not been minimized yet.

Table 5. Summary of data collection.

resolution range	48.17 – 1.20
completeness (%)	92.92
number of reflections	199296
space group	$2_1\ 2_1\ 2_1$
a (Å)	53.239
b (Å)	96.256
c (Å)	140.756
α=β=γ	90.00

UPAR-415 was found in the active site close to the cofactor PLP. The structure was overlaid with *Haemophilus influenzae* OASS-A in the complex with a peptide YDI mimicking SAT (PDB code 3iqh) (Figure 19). The peptide and small reversible inhibitor are overlaying well. Their carboxylic groups, proven pivotal for the binding, are oriented in the same direction. The carboxylic group of UPAR-415 forms strong hydrogen network with StOASS-A residues Thr68, Asn71, Thr72 and Gln142, just as previously predicted by STD NMR [97]. The phenyl group of UPAR-415 is overlying the Ile side chain and the tolyl group is efficiently mimicking the SAT backbone.

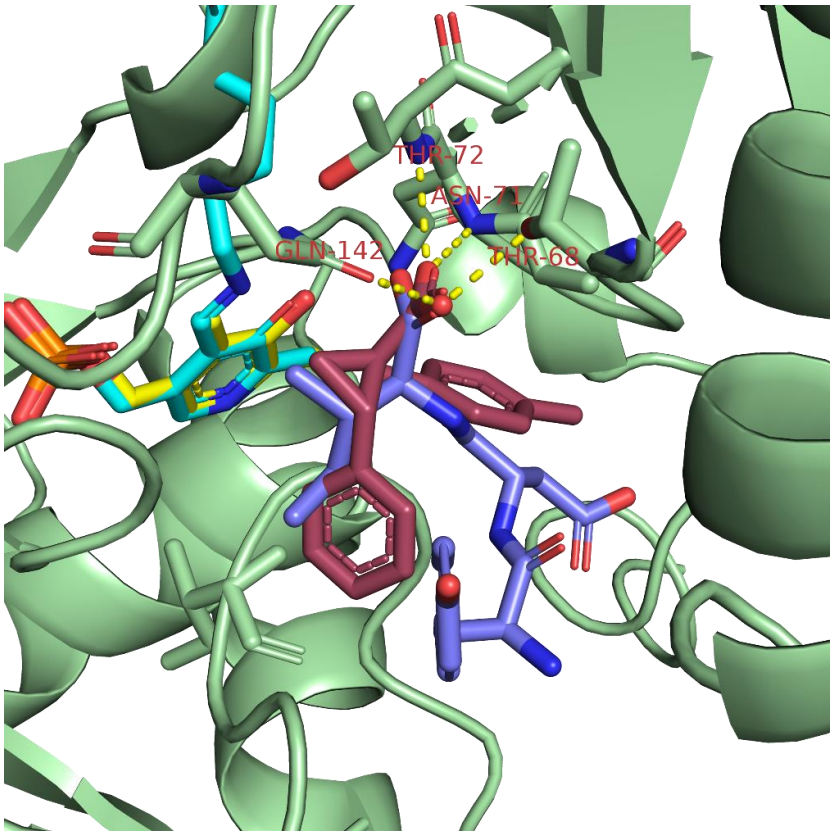

Figure 19. Close-up to the active site of the StOASS-A (pale green chain) with UPAR-415 (raspberry), overlaid with 3iqh. StOASS-A is shown as cartoon, only the interacting residues are shown as sticks for clearer presentation. From 3iqh, the HiOASS-A chain was removed, while PLP (cyan) and YDI (blue) were kept. HiOASS-A PLP is overlaying well with PLP of StOASS-A (yellow). In yellow are shown hydrogen bonds between the carboxylate of UPAR-415 and residues of StOASS-A.

Then we aligned the structure of StOASS-A in the complex with UPAR-415 with the native crystal structure of StOASS-A (PDB code 1OAS) in order to observe if ligand binding causes any conformational change of the protein. The changes in conformation of inhibited StOASS are of interest based on the existing biochemical observations:

- In direct fluorimetric titrations, where is monitored fluorescence emission of PLP upon excitation at 412 nm, ligand binding causes

an increase of fluorescence intensity. It has been proposed that this behavior originates from the differences in microenvironment around PLP, such as polarity and closure of the active site.

- When OASS-A is inhibited by SAT, it is proposed that one of two active sites is occupied by C-terminal peptide of SAT, while the other one is only partly active because of the conformational change [84,92]. Since our reversible inhibitors are mimicking SAT, the inhibited crystal structure might give insight into the behavior of OASS-A in the complex.
- When chloride is bound to StOASS-A allosteric anion binding site, the protein undergoes a large conformational change in which residues 87 – 131 are moved, resulting in the inhibition of the enzyme [71].
- Large conformational changes are also observed during a catalytic cycle of OASS. In a crystal structure of StOASS-A K41A mutant, where the enzyme is isolated as an external aldimine between PLP and free methionine, it is observed that the active site of a protein is closed. The most pronounced difference comparing to the native form originates from Asn69 that moves for about 7 Å towards the carboxylate of methionine bound. This movement induces the cascade reaction, dragging with it the residues 67-70. Following these rearrangements, also residues 82 -140 move as a rigid body and close up the entrance to the active site [70].

The alignment is shown in Figure 20. In the overall topology of the protein, no major structural difference is observed (panel A). The close-

up to the active site reveals few small changes. Asn69 moves from the native position for about 2 Å towards the inhibitor, suggesting the occurrence of the similar behavior observed in the formation of external aldimine. However, the movement is not pronounced enough to induce a cascade movement of neighboring residues. Few changes are observed, residues 93-98, 114-117, 309 and 312-315 shift slightly towards the core of the protein, but they do not move for more than 1.5 Å (panel B).

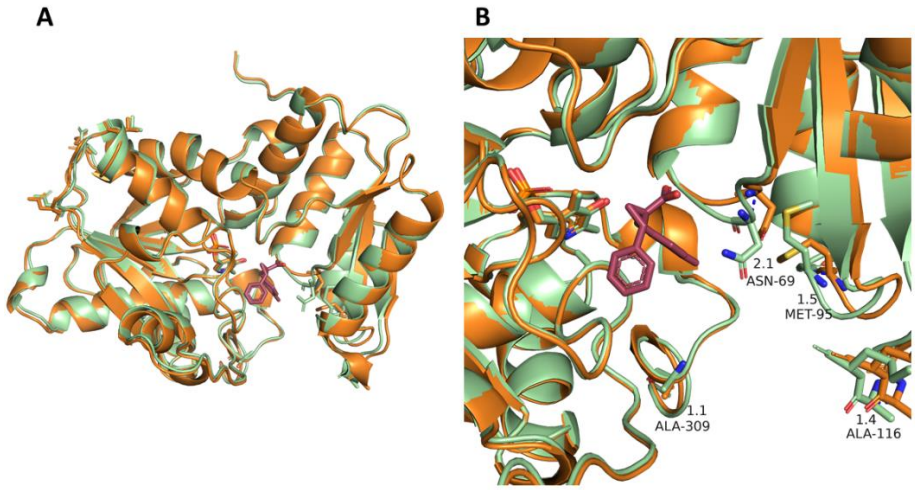

Figure 20. Alignment of StOASS-A in native (orange) and inhibited form (green) in the complex with UPAR-415 (raspberry). Panel A: general alignment of two StOASS-A crystal structures. Panel B: close-up in the active site of StOASS-A. Protein is shown as a cartoon, only residues of interest are shown as sticks for clearer presentation. Residues that were covering the active site and the residues of interest were removed.

The observed conformational changes are minor. Therefore, with the current structure we cannot justify that the binding of reversible inhibitor closes the active site of the protein. Increase in the fluorescence emission intensity of PLP during direct titrations likely originates only from differences in polarity, caused by displacement of water from the active

site by the ligand. It also should be taken into account that the obtained crystal structure is preliminary, since it has not yet been minimized and it is possible that the final structure will reveal some additional changes. Besides that, it should be considered that the ligand was added to the protein crystal by soaking. Crystals are solid forms and do not always represent the behavior of a soluble protein. Therefore, it is possible that crystals were too rigid to move upon ligand binding.

This high-resolution crystal structure confirmed the orientation of UPAR-415 in the active site of StOASS-A and demonstrated how efficiently it is mimicking the physiological inhibitor. Besides that, this structure gives an additional value to the research of OASS. The crystal structure of StOASS-A has been published before, but never in such high resolution. It is firstly reported that StOASS-A forms high quality crystals with a simple hanging drop method without microseeding. Also, it is the first structure of StOASS-A in the presence of a low-molecular weight inhibitor, which will in the future serve as an excellent model for virtual screening.

3.1.3. REVERSIBLE INHIBITORS

UPAR-415 DERIVATIVES

Results from microbiological testing of UPAR-415 (see section Effects of OASS and SAT inhibitors on bacterial growth, chapter 2.3) demonstrated that the compound is inactive towards Gram-negative bacteria. However, when assayed in the presence of a membrane permeability enhancer, UPAR-415 was able to interfere with bacterial growth, suggesting that it has difficulties in penetrating inside the bacterial cell. Permeability

through the complex Gram-negative membrane is a common problem in the development of new antibiotics and there are no clear rules that would connect the structure of the molecule with the permeability. However, literature reports favorable characteristics of antibiotic agents that have been identified by analyzing sets of permeable molecules. Generally, it has been reported that molecules with negative clogP and polar character tend to permeate more easily. Similarly it was observed for positively charged molecules, which can react with negatively charged surface of bacteria. Besides that, non sterically encumbered amines are beneficial for the permeation. Important is also the geometry of the molecule that permeates better when it is rigid and has low globularity [98–100,127].

Taking into account the structure of UPAR-415 and the guidelines, it becomes evident that the molecule does not possess many permeability-like properties. Besides its relatively high clogP it has a carboxylic group, that is negatively charged at physiological pH and is therefore likely to interfere with anionic groups present in the glucosamine backbone of lipid A [13]. In a study where a set of 100 molecules was evaluated for a permeability, it was observed that the carboxylic group prevents the permeation of all molecules which otherwise satisfy all requirements for a penetration [127].

Therefore, collaborators from Prof. Costantino's group focused their attention on a design of a permeable molecule. The phenyl and tolyl rings of UPAR-415 have been substituted with more polar groups. Carboxylic

group has been replaced with bioisosters to avoid the negative charge, or the molecule was designed to be zwitterionic.

Main results are reported in the paper *Refining the structure-activity relationships of 2-phenylcyclopropane carboxylic acids as inhibitors of O-acetylserine sulfhydrylase isoforms,* that was published in *Journal of Enzyme Inhibition and Medicinal Chemistry* [128].

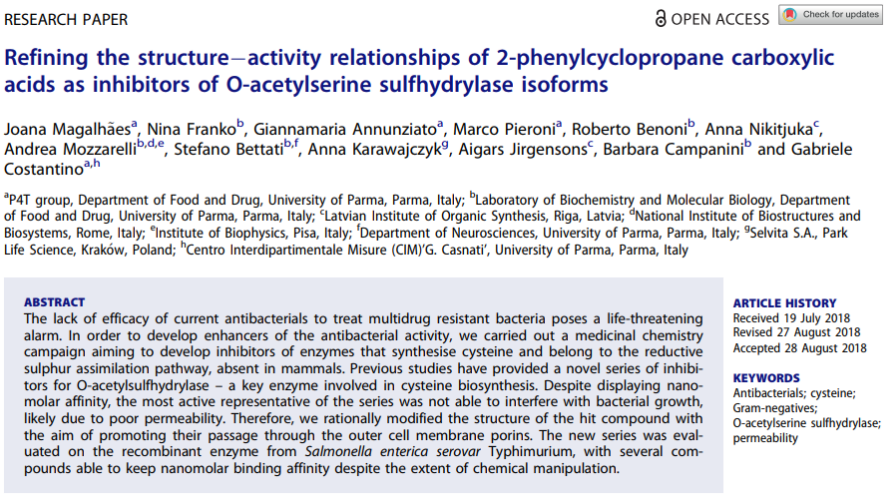

RESEARCH PAPER

OPEN ACCESS Check for updates

Refining the structure–activity relationships of 2-phenylcyclopropane carboxylic acids as inhibitors of O-acetylserine sulfhydrylase isoforms

Joana Magalhães[a], Nina Franko[b], Giannamaria Annunziato[a], Marco Pieroni[a], Roberto Benoni[b], Anna Nikitjuka[c], Andrea Mozzarelli[b,d,e], Stefano Bettati[b,f], Anna Karawajczyk[g], Aigars Jirgensons[c], Barbara Campanini[b] and Gabriele Costantino[a,h]

[a]P4T group, Department of Food and Drug, University of Parma, Parma, Italy; [b]Laboratory of Biochemistry and Molecular Biology, Department of Food and Drug, University of Parma, Parma, Italy; [c]Latvian Institute of Organic Synthesis, Riga, Latvia; [d]National Institute of Biostructures and Biosystems, Rome, Italy; [e]Institute of Biophysics, Pisa, Italy; [f]Department of Neurosciences, University of Parma, Parma, Italy; [g]Selvita S.A., Park Life Science, Kraków, Poland; [h]Centro Interdipartimentale Misure (CIM)'G. Casnati', University of Parma, Parma, Italy

ABSTRACT

The lack of efficacy of current antibacterials to treat multidrug resistant bacteria poses a life-threatening alarm. In order to develop enhancers of the antibacterial activity, we carried out a medicinal chemistry campaign aiming to develop inhibitors of enzymes that synthesise cysteine and belong to the reductive sulphur assimilation pathway, absent in mammals. Previous studies have provided a novel series of inhibitors for O-acetylsulfhydrylase – a key enzyme involved in cysteine biosynthesis. Despite displaying nanomolar affinity, the most active representative of the series was not able to interfere with bacterial growth, likely due to poor permeability. Therefore, we rationally modified the structure of the hit compound with the aim of promoting their passage through the outer cell membrane porins. The new series was evaluated on the recombinant enzyme from *Salmonella enterica serovar* Typhimurium, with several compounds able to keep nanomolar binding affinity despite the extent of chemical manipulation.

ARTICLE HISTORY
Received 19 July 2018
Revised 27 August 2018
Accepted 28 August 2018

KEYWORDS
Antibacterials; cysteine; Gram-negatives; O-acetylserine sulfhydrylase; permeability

Substitution of tolyl group.

For derivatization of UPAR-415 tolyl group, small heterocycles were chosen since they possess more polar character, that should be beneficial for crossing the bacterial membrane [100]. Good binding affinity towards StOASS-A was retained (Table 6), resulting in K_ds in low- or even sub-micromolar range (UPAR-740/758/759/760). A correlation between polarity of the heterocycle and binding affinity can be observed, in which higher polarity of compound correlates with the decrease in binding

affinity. That said, pyrrole derivative (UPAR-759, K_dOASS-A = 0.53 μM) is the most active compound of the series, while the triazole (UPAR-760, K_dOASS-A = 18.4 μM) exhibits the highest K_d. On the other hand, these compounds show high selectivity index that leads up-to 65-times lower affinity towards StOASS-B. The R^1 substituent is positioned in the small lipophilic pocket of the enzyme active site, which in the case of the B isoform cannot accept these heterocycles [128].

Interestingly, UPAR-761 has the bulkiest side group on a position R^1 and exhibits the highest affinity towards both isozymes with significantly lower selectivity index, suggesting more favorable orientation of the molecule in the active site.

Table 6. Derivatives of UPAR415 with substituents of tolyl group. Adjusted by [128].

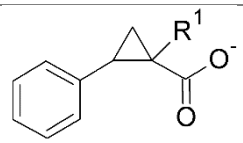

name	stereo-chemistry	R^1	K_d StOASS-A (μM)	K_d StOASS-B (μM)	S.I.[a]
UPAR-740	*trans*	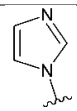	7.58 ± 0.6	397 ± 42	50.1
UPAR-758	*trans*	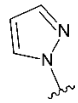	1.48 ± 0.20	96 ± 7	65.1
UPAR-759	*trans*	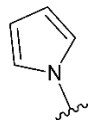	0.53 ± 0.10	22 ± 3	40.8
UPAR-760	*trans*	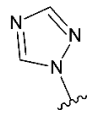	18.40 ± 4.70	250 ± 14	13.6
UPAR-761	*trans*	NA	0.21 ± 0.05	1.37 ± 0.10	6.5

[a]*selectivity index calculated as K_d StOASS-B / K_d StOASS-A. NA – not applicable – the structure is not disclosed in order to protect the intellectual property.*

***Substitution of carboxylic group*.**

The carboxylic group of substituted cyclopropanes has been proven to be essential for the ligand binding to OASS, since it is mimicking the C-terminal isoleucine of SAT [96,97]. However, its negative charge at physiological pH might be responsible for poor compound permeability

into Gram-negative bacteria [17,100,127]. To investigate whether the compound affinity towards OASS can be retained by replacing the carboxylic group with a non-charged functional group, a series of bioisosteres was assayed. Tetrazole was used as a planar bioisoster and sulfonamides as non-planar isosteres. Substituted amides were prepared due to their favorable properties towards different bacterial strains, both Gram-negative and Gram-positive [129,130]. Results are shown in Table 7.

Table 7. Derivatives of UPAR415 with substituents of carboxylic group. Adjusted by [128].

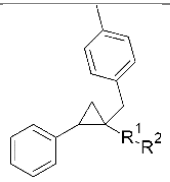

				% inhibition at 100 µM		IC_{50} / K_d (µM)	
name	**stereo-chemistry**	**R^1**	**R^2**	**OASS-A**	**OASS-B**	**OASS-A**	**OASS-B**
UPAR-426	*trans*	H	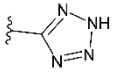	nd	nd	K_d = 90 ± 14	nd
UPAR-613	*trans*	SO_2	CH_3	~ 20*	~ 40*	K_d = 1.8 ± 1	K_d = 0.11 ± 0.0
UPAR-614	*trans*	SO_2	tolyl	~ 15*	~ 35*	K_d = 3.2 ± 2	K_d = 0.43 ± 0.4

			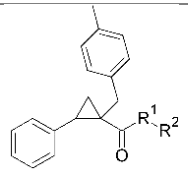				
UPAR-645	*trans*	NMe	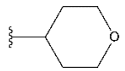	nd	nd	IC_{50}=17± 1.4	IC_{50}=137 ± 10
UPAR-646	*trans*	NH	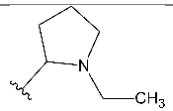	46.0 ± 5.2	37.0 ± 2.8	nd	nd
UPAR-647	*trans*	NH	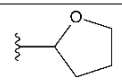	37.6 ± 2.0	10.1 ± 3.9	nd	nd
UPAR-650	*trans*	NH	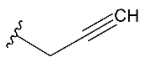	32.4 ± 0.2	26.1 ± 6.7	nd	nd
UPAR-652	*trans*	NH	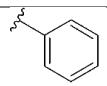	29.3 ± 2.3	33.7 ± 1.2	nd	nd

UPAR-654	*trans*	NH	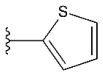	27.1 ± 4.1	28 ± 5.5	nd	nd
UPAR-656	*trans*	NH	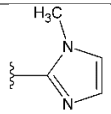	26.8 ± 3.2	12.8 ± 3.2	nd	nd

** % of inhibition evaluated under saturating conditions at 20 μM. nd – not determined.*

UPAR-426 has the carboxylic group replaced with a tetrazole, which is planar and it presents similar acidity, but it resulted in a decrease of binding affinity. When sulfonamide derivatives (UPAR-613 and UPAR-614) were assayed with direct fluorimetric titrations, they exhibited high affinity towards both isozymes of OASS. However, when peptides or other low-molecular-weight reversible inhibitors are assayed by fluorimetric titrations, ligand binding in the active site of OASS normally causes 2-5 times increase in the fluorescence emission of PLP due to the changes in the microenvironment of PLP. With sulfonamides, we observed only up to 1.6-times increase. This unusual phenomenom encouraged us to investigate their potency also with activity assays – example of reactivity between UPAR-614 and StOASS-B is shown on Figure 21, panel A. At saturation (20 μM), only up to around 35 % of inhibition was observed. By measuring the scattering of compounds solubilized in the experimental buffer, we verified that they are soluble up to 250 μM. The lack of inhibition therefore cannot originate from limited compound solubility, but it is likely a consequence of different mechanism of action, resulting in partial enzyme inhibition. Partial enzyme inhibition cannot originate from a reversible competitive inhibitor that binds in the active site of OASS, because such type of an inhibitor should reach a complete inhibition at saturation. To investigate if the observed fluorescence increase originates from sulfonaminde binding in the active site of OASS, a displacement titration was carried out. 1-ethylcyclopropane-1,2-dicarboxylic acid (1-ECP-1,2-DCA) is a weak OASS inhibitor that causes a high fluorescence increase upon binding [122]. A potent reversible inhibitor, such as UPAR-614, should displace it

from the active site and consequently decrease the fluorescence intensity. As can be seen from Figure 21, panel B, addition of 190 μM UPAR-614 does not change the emission spectrum, which is an indication that it is not able to compete for binding in the active site with 1-ECP-1,2-DCA. Therefore, it can be concluded that either the dissociation constant of UPAR-614 for OASS-B is much higher than 170 μM (the K_d of 1-ECP-1,2-DCA for OASS-B) or it does not bind to the active site of the enzyme. It is proposed that sulfonamide derivatives of UPAR-415 are allosteric inhibitors. Their binding to StOASS causes small conformational change of protein, resulting in minimal changes in the environment around PLP that are responsible for the observed fluorescence increase [128].

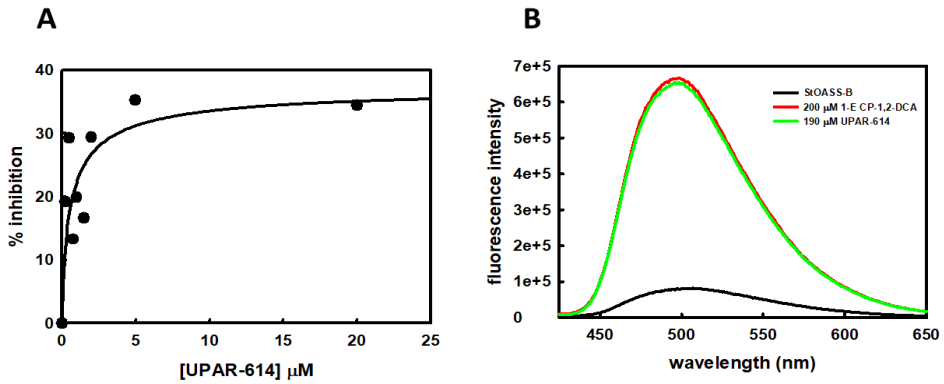

Figure 21. Panel A: Dependence of the percent inhibition of OASS-B catalytic activity on UPAR-614 concentration. Line through data points is the fitting to a hyperbolic function and was drawn to guide the eye. Panel B: competitive binding assay between 1-ECP-1,2-DCA and UPAR-614 suggests that the latter inhibitor does not bind in the active site of the StOASS-B. Adapted by [128].

When amide derivatives (UPAR-645 – UPAR-656) were assayed by fluorimetric titrations, it was observed that they are not able to cause any increase in the fluorescence emission spectrum of PLP, suggesting that they do not enter the active site. Consequently, they were assayed with

activity assays. UPAR-645 was the most potent inhibitor of the series, showing IC_{50} = 17 μM for OASS-A and 137 μM for OASS-B. Other compounds were screened at 100 μM concentration, where they showed modest inhibition of both isozymes.

Analysis of UPAR-415 derivatives with substituted carboxylic group showed that inhibition of StOASS-A is still possible, while these molecules exhibit different mechanism of action. Our observations confirm the importance of carboxylic group for the competitive mode of inhibition of OASS [92,96].

Substitution of phenyl group.

UPAR-610 and UPAR-611 were designed to make the molecules zwitterionic at physiological pH, which could compensate towards negatively charged carboxylic group. Small electron donor groups on a *para* position of a benzyl group, such as the amino moiety, allowed to maintain good binding properties (UPAR-611). On the other hand, bulkier groups such as the nitro and a substituted alkylamine (UPAR-610 and 612) weakened the interaction of the molecule with the active pocket, thus decreasing the affinity. It is possible to conclude that substitution on the *para* position of the phenyl ring, unless carried out with small groups, is detrimental for the activity of the compounds. To increase the polarity of the molecule, substitution of the β carbon of cyclopropane with a pyridine resulted to be a more fruitful strategy, with high affinity towards both the isoforms (UPAR-609) [128].

When a bulkier sidegroups were attached to the β carbon of cyclopropane (UPAR-791-795), compounds exhibited high affinity

towards both isozymes. These moieties likely fit in a newly identified pocket in the OASS active site and therefore change the orientation of the whole molecule [124]. These inhibitors are showing an excellent selectivity index towards both isozymes and are exhibiting polar character, making them very interesting candidates for the microbiological testing.

Table 8. Derivatives of UPAR415 with substituents of phenyl group. Adjusted by [128].

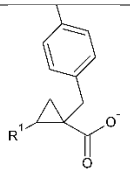

name	stereo-chemistry	R^1	K_d StOASS-A (μM)	K_d StOASS-B (μM)	S.I.[a]
UPAR -609	*trans*	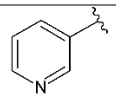	0.41 ± 0.02	6.1 ± 0.5	14.9
UPAR -610	*trans*	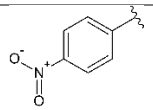	61.3 ± 6.5	145.2 ± 2.3	2.4
UPAR -611	*trans*	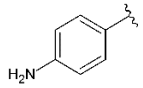	1.4 ± 0.26	5.7 ± 0.7	4.1
UPAR -612	*trans*	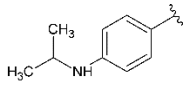	155.6 ± 5.1	7.1 ± 2.2	0.05
UPAR -791	*trans*	NA	0.57 ± 0.2	1.29 ± 0.1	2.3
UPAR -792	*trans*	NA	1.86 ± 0.8	2.63 ± 0.0	1.4

UPAR -793	*trans*	NA	2.51 ± 0.6	6.8 ± 1	2.7
UPAR -794	*trans*	NA	1.01 ± 0.4	3.05 ± 0.2	3.0
UPAR -795	*trans*	NA	0.163 ± 0.10	3.86 ± 0.3	23.7

[a]selectivity index calculated as K_d StOASS-B / K_d StOASS-A. NA – not applicable – the structure is not disclosed in order to protect the intellectual property.

Biochemical evaluation of novel reversible StOASS inhibitors does not only identify suitable molecules for microbiological testing of potential antibiotic adjuvants, but it also contributes to the biochemical knowledge of the enzyme. Substituted cyclopropanes were designed based on our knowledge of interaction between OASS-A and SAT. Even though the structure of this protein complex is unknown, it has been extensively biochemically assayed [84,92,131]. The crystal structure between a peptide, mimicking the C-terminal part of SAT, as well as modifications of these peptides, give an important insight to an inhibition of OASS-A, identifying reactive residues essential for binding [96]. Taking into account these findings, development of inhibitors for the A isoform of OASS is much easier than for the B isoform, for which no physiological inhibitors are known. Since SAT and its mimicking peptides are competitive against OAS, that is a substrate for both OASS isozymes, it was proposed that the peptides could also inhibit OASS-B. However, assays have shown that they bind to the B isoform weakly, leading to a high selectivity index in favour of the A isoform [131]. The selectivity index was lowered to some extent with a design of low-molecular-weight inhibitors [97,122]. In this study, we saw that the majority of new

molecules still preferentially bind to the StOASS-A, while we also identified several molecules with the best selectivity index so far (UPAR-761, UPAR-610/611, UPAR-791 – UPAR-794). It seems that addition of bulky polar group on Cβ results in good affinity towards both isozymes of StOASS, giving a great predisposition for a further development and added value to the OASS-B characterization. For antibiotic development this finding is also of a great importance. Even though the role of OASS-B *in vivo* remains uncharacterized and controversial, it is possible that in the absence or complete inhibition of OASS-A, OASS-B can contribute to a sufficient cysteine biosynthesis for bacterial viability and resistance to oxidative stress. This hypothesis is further supported by the fact that bacteria, living in harsh oxidizing conditions, have at least two enzymes that catalyze the last step in cysteine biosynthesis (*S*. Typhimurium and *E. coli* have 2, and *M. tuberculosis* has 3). Therefore, inhibition of all OASS isozymes is pivotal and it can only be reached with molecules with high affinity towards all of them.

PYRAZOLES

Taking into account the discrepancy between the characteristics of substituted cyclopropanes and generally favorable characteristics of permeable molecules, Prof. Costantino's group focused its attention towards the design and synthesis of new, structurally different molecules that would retain the affinity against OASS while being of a smaller size and having lower clogP. The chosen approach for design of these structurally different molecules was scaffold hopping and results of the study are published in paper *Discovery of novel fragments inhibiting O-acetylserine sulphhydrylase by combining scaffold hopping and ligand–based drug design* in *Journal of Enzyme Inhibition and Medicinal Chemistry* [132].

JOURNAL OF ENZYME INHIBITION AND MEDICINAL CHEMISTRY
2018, VOL. 33, NO. 1, 1444–1452
https://doi.org/10.1080/14756366.2018.1512596

Taylor & Francis
Taylor & Francis Group

RESEARCH PAPER

OPEN ACCESS Check for updates

Discovery of novel fragments inhibiting O-acetylserine sulphhydrylase by combining scaffold hopping and ligand–based drug design

Joana Magalhães[a], Nina Franko[b], Giannamaria Annunziato[a], Martin Welch[c], Stephen K. Dolan[c], Agostino Bruno[d], Andrea Mozzarelli[b,e,f], Stefano Armao[g], Aigars Jirgensons[h], Marco Pieroni[a], Gabriele Costantino[a,i] and Barbara Campanini[b]

[a]P4T group, Department of Food and Drug, University of Parma, Parma, Italy; [b]Laboratory of Biochemistry and Molecular Biology, Department of Food and Drug, University of Parma, Parma, Italy; [c]Department of Biochemistry, Cambridge University, Cambridge, United Kingdom; [d]Experimental Therapeutics Program, IFOM – The FIRC Institute for Molecular Oncology Foundation, Milano, Italy; [e]National Institute of Biostructures and Biosystems, Rome, Italy; [f]Institute of Biophysics, CNR, Pisa, Italy; [g]Centro Interdipartimentale "Biopharmanet-tec", Università degli Studi di Parma, Parma, Italy; [h]Latvian Institute of Organic Synthesis, Riga, Latvia; [i]Centro Interdipartimentale Misure (CIM)'G. Casnati', University of Parma, Parma, Italy

ABSTRACT

Several bacteria rely on the reductive sulphur assimilation pathway, absent in mammals, to synthesise cysteine. Reduction of virulence and decrease in antibiotic resistance have already been associated with mutations on the genes that codify cysteine biosynthetic enzymes. Therefore, inhibition of cysteine biosynthesis has emerged as a promising strategy to find new potential agents for the treatment of bacterial infection. Following our previous efforts to explore OASS inhibition and to expand and diversify our library, a scaffold hopping approach was carried out, with the aim of identifying a novel fragment for further development. This novel chemical tool, endowed with favourable pharmacological characteristics, was successfully developed, and a preliminary Structure–Activity Relationship investigation was carried out.

ARTICLE HISTORY
Received 18 July 2018
Revised 10 August 2018
Accepted 10 August 2018

KEYWORDS
Scaffold hopping; fragments; O-acetylserine sulphhydrylase; medicinal chemistry; pyrazoles; ligand-based drug design

During the inhibitors design, carboxylic group, mimicking the C-terminal part of SAT, was decided to be kept in the molecule since it has been shown in our previous research that is pivotal for molecular binding [96,131]. For a scaffold hopping process (performed by Prof. Costantino's

group), UPAR-415 was docked in the structure of StOASS-A (PDB code 1OAS) using LeadIt software, where Asn70, Gln143 and Thr73 were chosen as pharmacophores. Scaffold hopping of UPAR-415 was performed by ReCore tool of LeadIt, resulting in the identification of several hit compounds. Between them, now named UPAR-693 was considered as an appropriate molecule for further investigation. Comparing to the UPAR-415, it exhibited similar interactions with protein backbone, while it had higher total polar surface area (TPSA) and comparable clogP, making it an interesting candidate for further optimization. In the initial screening of its inhibitory potency, UPAR-693 showed around 50% inhibition of OASS activity at 1 mM concentration. [132].

In order to improve the fragment's potency, a series of 1-arylpyrazole-3-carboxylic acid and 1-arylpyrazole-5-carboxylic acid molecules was prepared, where the phenyl ring was either unsubstituted or adorned. Their inhibitory potency of StOASS was screened with activity assays in 1 μM and 1 mM concentration. Results are reported in Table 9.

Table 9. Inhibitory potency of substituted pyrazoles for StOASS. Adjusted by [132].

		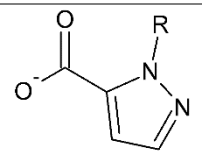				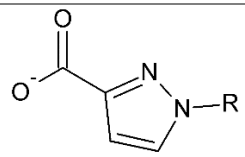			
		% inhibition OASS-A		**% inhibition OASS-B**		**% inhibition OASS-A**		**% inhibition OASS-B**	
name	**R**	**1 µM**	**1 mM**	**1 µM**	**1 mM**	**1 µM**	**1 mM**	**1 µM**	**1 mM**
UPAR-693	tolyl	ns	45 ± 3	ns	65 ± 2	nd	nd	nd	nd
UPAR-699	Ph	ns	66 ± 0	11 ± 3	65 ± 0	nd	nd	nd	nd
UPAR-689	H	ns	94 ± 1	ns	82 ± 0	nd	nd	nd	nd
UPAR-701/687	4-ClPh	ns	60 ± 2	ns	56 ± 0	ns	68 ± 0	15 ± 2	63 ± 1

UPAR-690/691	4-BrPh	ns	84 ± 0	ns	58 ± 2	ns	62 ± 0	ns	35 ± 2
UPAR-695/698	4-C(CH_3)$_3$Ph	ns	47 ± 0	ns	52 ± 5	ns	81 ± 0	11 ± 6	82 ± 1
UPAR-686/688	4-FPh	ns	95 ± 1	14 ± 2	62 ± 1	ns	73 ± 0	ns	36 ± 3
UPAR-697/696	Cyclohexyl	ns	57 ± 1	ns	30 ± 1	ns	79 ± 1	ns	43 ± 3

nd – *not determined*; ns – inhibition under 10 % was considered as *not significant*.

In the case of electron donating group (EDG) attached to the phenyl ring, it has been observed that a bulky group such as tert-butyl results in 2-fold higher inhibition in the case of 1,3-isomer over 1,5 isomer (UPAR-695 vs UPAR-698). The same trend is observed in the case of cyclohexane substituent. Attachment of the phenyl group on 1,5-position managed to retain the inhibitory potency of the scaffold hopping hit. Substitution of phenyl ring with small electron withdrawing group (EWD), such as fluorine, chlorine and bromine improved inhibitory potency for StOASS-A comparing to scaffold hopping hit UPAR-693, while no significant differences between 1,3 and 1,5-isomers were observed. On the other hand, attachment of EWD on 1,5-isomer does not contribute to the inhibition of the B isoform, and 1,3-isomer can even hider its potency (UPAR-691 and and UPAR-688) [132].

Interestingly, UPAR-689, which is the least decorated molecule, exhibited the highest inhibitory potency of the series, showing more than 90 % inhibition for StOASS-A and more than 80 % for the B isoform at 1 mM concentration. Based on these observations, other heterocycles functionalized with a carboxylic group were examined. Their affinities towards StOASS are reported in Table 10.

Table 10. Affinities of UPAR-415 and heterocycles, functionalized with carboxylic group, for StOASS and their ligand efficiencies (LE). Adapted from [127].

name	structure	MW (g/mol)	K_d OASS-A (μM)	K_d OASS-B (μM)	LE (OASS-A)* kcal/mol/HA	LE (OASS-B)* kcal/mol/HA	ClogP¥	TPSA¥
UPAR-415	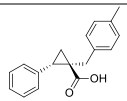	266.33	0.028±0.005	0.49±0.05	0.52	0.50	3.60	37.3
UPAR-689	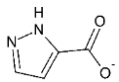	112.09	121.8±5.5	272±10.4	0.67	0.61	0.13	66.0
UPAR-733	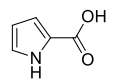	111.1	59.0±11.0	465.0±50.1	0.72	0.60	0.66	53.1
UPAR-734	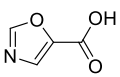	113.07	120.2±11.9	548.5±59.8	0.67	0.60	0.04	63.3
UPAR-735	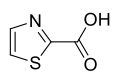	129.14	51.5±5.6	338.4±13.9	0.74	0.60	0.17	50.2

**LE= (1.37/HA). pIC_{50} where HA refers to heavy (non-hydrogen) atoms; ¥ ClogP and TPSA were calculated using molinspiration software. LE, clogP and TPSA values data provided by Prof. Costantino's group.*

These compounds (UPAR-733/734/735) exhibited K_ds against OASS in the same range as UPAR-689, while their affinity towards the enzyme is significantly lower comparing to the UPAR-415. However, it must be considered that the new molecules have a similar value of Ligand Efficiency (LE) as UPAR-415 [132]. This is a calculated parameter of a binding energy per non-hydrogen atom to a target and it is used in medicinal chemistry to assess the viability of a fragment as a starting point for optimization [133,134].

The project of designing new inhibitors of StOASS with enhanced permeability-like properties followed by scaffold hopping approach resulted in the identification of weakly binding molecules. However, UPAR-733 and UPAR-735 were identified as the most potent molecules and comparing to UPAR-415 they have improved physicochemical properties (ligand efficiency, clogP and TPSA), favouring *in vivo* efficacy. Based on their drug-like properties, they present an attractive starting point for identification of novel StOASS inhibitors and microbiological testing [132].

3.1.4. IRREVERSIBLE INHIBITORS

In a collaboration with Latvian institute of organic synthesis (Prof. Jirgensons group), inactivation of StOASS by fluoroalanine derivatives as mechanism based inactivators was assessed for the first time. The majority of results are reported in research paper *Inhibition of O-acetylserine sulfhydrylase by fluoroalanine derivatives* published in *Journal of Enzyme Inhibition and Medicinal Chemistry* [65].

JOURNAL OF ENZYME INHIBITION AND MEDICINAL CHEMISTRY
2018, VOL. 33, NO. 1, 1343–1351
https://doi.org/10.1080/14756366.2018.1504040

Taylor & Francis
Taylor & Francis Group

RESEARCH PAPER

OPEN ACCESS Check for updates

Inhibition of *O*-acetylserine sulfhydrylase by fluoroalanine derivatives

Nina Franko[a]*, Konstantinos Grammatoglou[b]*, Barbara Campanini[a], Gabriele Costantino[a], Aigars Jirgensons[b] and Andrea Mozzarelli[a,c]

[a]Food and Drug Department, University of Parma, Parma, Italy; [b]Latvian Institute of Organic Synthesis, Riga, Latvia; [c]National Research Council, Institute of Biophysics, Pisa, Italy

ABSTRACT

O-acetylserine sulfhydrylase (OASS) is the pyridoxal 5′-phosphate dependent enzyme that catalyses the formation of L-cysteine in bacteria and plants. Its inactivation is pursued as a strategy for the identification of novel antibiotics that, targeting dispensable proteins, holds a great promise for circumventing resistance development. In the present study, we have investigated the reactivity of *Salmonella enterica* serovar Typhimurium OASS-A and OASS-B isozymes with fluoroalanine derivatives. Monofluoroalanine reacts with OASS-A and OASS-B forming either a stable or a metastable α-aminoacrylate Schiff's base, respectively, as proved by spectral changes. This finding indicates that monofluoroalanine is a substrate analogue, as previously found for other beta-halogenalanine derivatives. Trifluoroalanine caused different and time-dependent absorbance and fluorescence spectral changes for the two isozymes and is associated with irreversible inhibition. The time course of enzyme inactivation was found to be characterised by a biphasic behaviour. Partially distinct inactivation mechanisms for OASS-A and OASS-B are proposed.

ARTICLE HISTORY
Received 31 May 2018
Revised 16 July 2018
Accepted 19 July 2018

KEYWORDS
Fluoroalanine; cysteine biosynthesis; enzyme inhibition; pyridoxal 5′-phosphate

Several PLP-dependent enzymes have already been studied for their inactivation by mono-, di- and trihalogenated alanines that can be either chloro- or fluoro-based. Examples of these enzymes are alanine racemase [105], aspartate aminotransferase [106], γ-cystathionase [107,108], tryptophan synthase and tryptophanase [109,110], ornithine decarboxylase [111], 8-amino 7-oxononanotote synthase [135] and kynurenine transaminase [136]. These studies revealed that the mechanism of inactivation is dependent on the number of halogen substituents on the inactivator [112,113] as well as the enzyme and its natural catalytic cycle [135].

Two major inactivation mechanisms of PLP dependent enzymes can be observed (Scheme 1). The inactivation starts by the binding of halogenated alanine to the cofactor PLP and formation of external aldimine (transaldimination), after which the α-proton is abstracted and HF of HCl is eliminated. This mechanism results in the formation of an unsaturated Schiff's base, the α-aminoacrylate-PLP complex (Scheme 1, path B). Another way of inactivation is the fluorodecarboxylation mechanism, in which HF elimination is accompanied by the elimination of the carboxylic group (Scheme 1, path A) [135,137]. Also this mechanism results in the production of unsaturated Schiff's base. In both paths, the unsaturated Schiff's base is a reactive intermediate that undergoes the Michael attack by the enzyme nucleophile, likely the active site lysine. The efficiency of the nucleophilic attack is strongly dependent on the active site environment and electronegativity of the halogenated alanine. After the Michael attack, further chemical rearrangements take place, causing further halogen ions elimination and formation of stable covalent adduct.

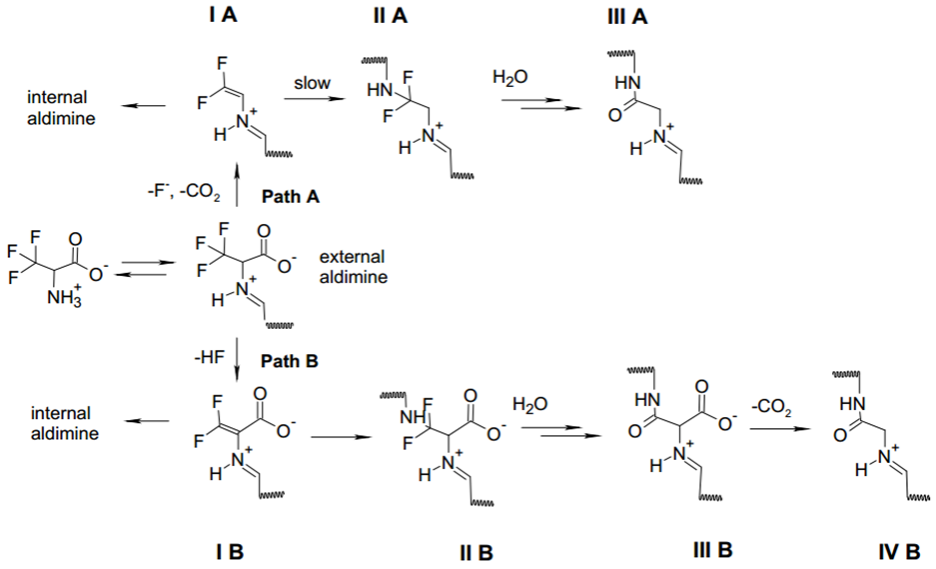

Scheme 1. Possible inactivation pathways of PLP-dependent enzymes by β,β,β-trifluoroalanine. Adapted by [65].

In order to identify StOASS inactivators, we firstly investigated its reactivity with β-monofluoroalanine and β,β,β-trifluoroalanine to get an insight into their mechanism of action. Then, we investigated their derivatives in order to determine SAR and identify more potent inactivators [65].

REACTIVITY BETWEEN StOASS AND MONO- AND TRIFLUOROALANINE

Reactivity of monofluoro- and trifluoroalanine with OASS-A and OASS-B monitored by absorbance and fluorescence spectroscopy.

The cofactor PLP is bound to the catalytic lysine of OASS-A and OASS-B via ketoenamine tautomer of the internal aldimine, which exhibits a band in the absorption spectrum centred at 412 nm (Figure 22). Addition of 1 mM monofluoroalanine (F-Ala) to OASS-A shifted the band to 470 nm,

indicating the formation of α-aminoacrylate Schiff's base (Figure 22, panel A) [66,138,139]. This species was stable for at least 21 hours and is formed by the β-elimination reaction of HF. The behaviour resembles the β-elimination reaction observed for the acetoxy moiety of the natural substrate OAS. When the reaction was monitored on the B isoform, similar spectral changes were observed. However, after a rapid formation of the α-aminoacrylate, the band at 412 nm slowly reappeared (Figure 22, panel B) concomitantly with the appearance of a broad absorbance between 300 and 350 nm, attributed to the pyruvate elimination. These observations indicate that the α-aminoacrylate Schiff's base of OASS-B decomposes to pyruvate and ammonia faster than comparing to the one of OASS-A [65]. The same behaviour had been previously observed in the formation of aminoacrylate with *O*-acetylserine [67].

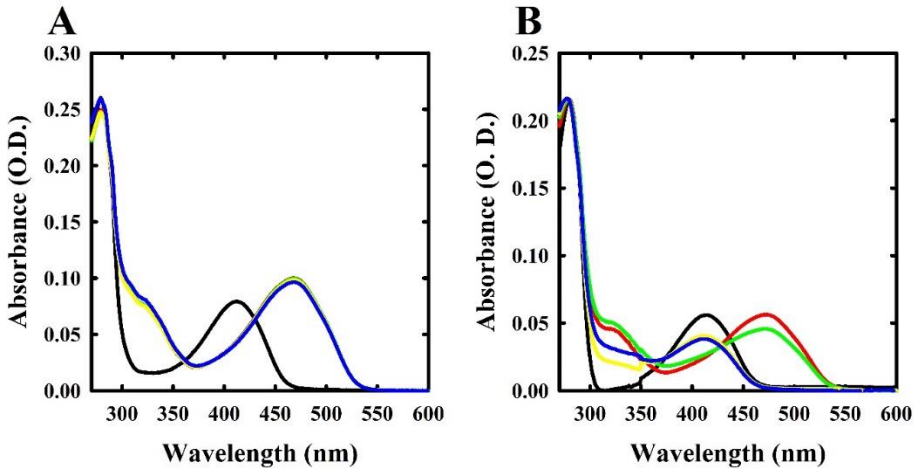

Figure 22. Spectral changes of OASS in the presence of F-Ala. Panel A: OASS-A in the absence of reagent (black line), 1 min (red line), 1 h (green line), 5 h (yellow line), and 21 h (blue line) after addition of 1 mM F-Ala. Panel B: OASS-B in the absence of reagent (black line), 1 min (red line), 1 h (green line), 3 h (yellow line), and 7 h (blue line) after addition of 1 mM F-Ala. Adapted from [65].

Reactivity between F-Ala and OASS was also monitored by fluorescence spectroscopy. Excitation of internal aldimine of OASS-A upon 412 nm gives a characteristic peak centred at 505 nm [73,120]. When F-Ala was added to the protein, the emission peak disappeared (Figure 23, panel A). This observation is in agreement with previous studies indicating that the α-aminoacrylate has lower fluorescence quantum yield than the internal aldimine [73]. Monitoring the reaction of F-Ala with OASS-B (Figure 23, panel B) revealed a shift of emission peak to 550 nm, that is in agreement with our previous work [74]. It is proposed that different emission spectra for OASS-A and OASS-B isozymes are arising from different conformations and microenvironments of the active site [65].

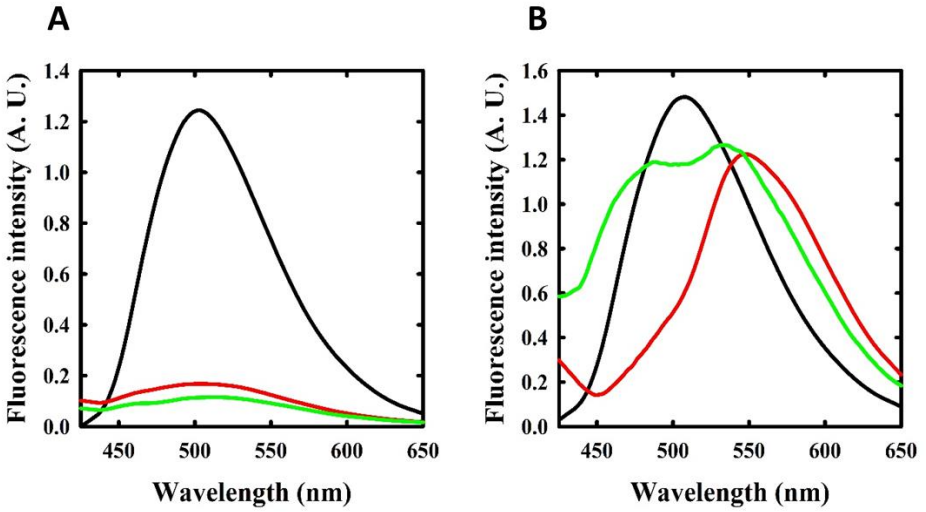

Figure 23. Fluorescence emission spectra of OASS upon excitation at 412 nm in the absence and presence of F-Ala. Panel A: OASS-A in the absence of reagent (black line), 1 min (red line), and 4 h (green line) after addition of 1 mM F-Ala. Panel B: OASS-B in the absence of reagent (black line), 1 min (red line), and 3 h (green line) after addition of 1 mM F-Ala. Adapted from [65].

Based on the observed spectral changes, it can be concluded that F-Ala is a substrate analog of OASS, just as previously observed for β-chloroalanine [113], and that it forms the α-aminoacrylate intermediate. This species is oriented within the active site in such mode that it disfavors any reaction with active site residues. Since α-aminoacrylate intermediate is normally formed during the catalytic cycle, it is not surprising that it has been evolved as a stable species, ready to react with the incoming nucleophilic sulfide [65]. When the same type of reaction was monitored on alanine racemase, partition ratio between α-aminoacrylate hydrolysis and Michael addition on the adduct formed by the F-Ala was found to be 820:1, confirming the poor reactivity of this species [112,140].

Then we investigated the reactivity of OASS-A and OASS-B with 1 mM β,β,β-trifluoroalanine (triF-Ala), which is a well-known suicide substrate of other PLP-dependent enzymes [107,109–113,135]. When the reactivity between OASS-A and triF-Ala was monitored by absorbance spectroscopy as a function of time, a complex behavior was observed (Figure 24, panel A). Addition of the reagent to OASS-A immediately resulted in the appearance of two major peaks, positioned at 440 and 466 nm, in a parallel with two minor peaks at 360 and 380 nm. This type of behavior indicates a presence of a species with extended conjugation and it has been already observed between triF-Ala and alanine racemase [113]. When the triF-Ala concentration was increased to 10 mM, no significant change in the absorbance intensity was observed (data not shown). The fact that the behavior is independent of the reagent

concentration, indicates that all enzyme sites are saturated and have reacted with it by forming a metastable species. The absorbance intensity at 466 nm slowly decreased (k_{obs} = 0.43 h^{-1}) with a reappearance of a band centered at 412 nm (Figure 24, panel C). Reaction between OASS-B and triF-Ala resulted in similar, but less intense spectral changes in the range 400-500 nm (Figure 24, panel B). Also for this isoform the behavior was independent of reagent concentration (data not shown). The time course of peak decay positioned at 470 nm was similar to OASS-A (k_{obs}=0.48 h^{-1}), while it was accompanied by the increase in the absorbance in the range 300 – 350 nm. This indicates the elimination of a keto-acid, possibly difluoropyruvate [65].

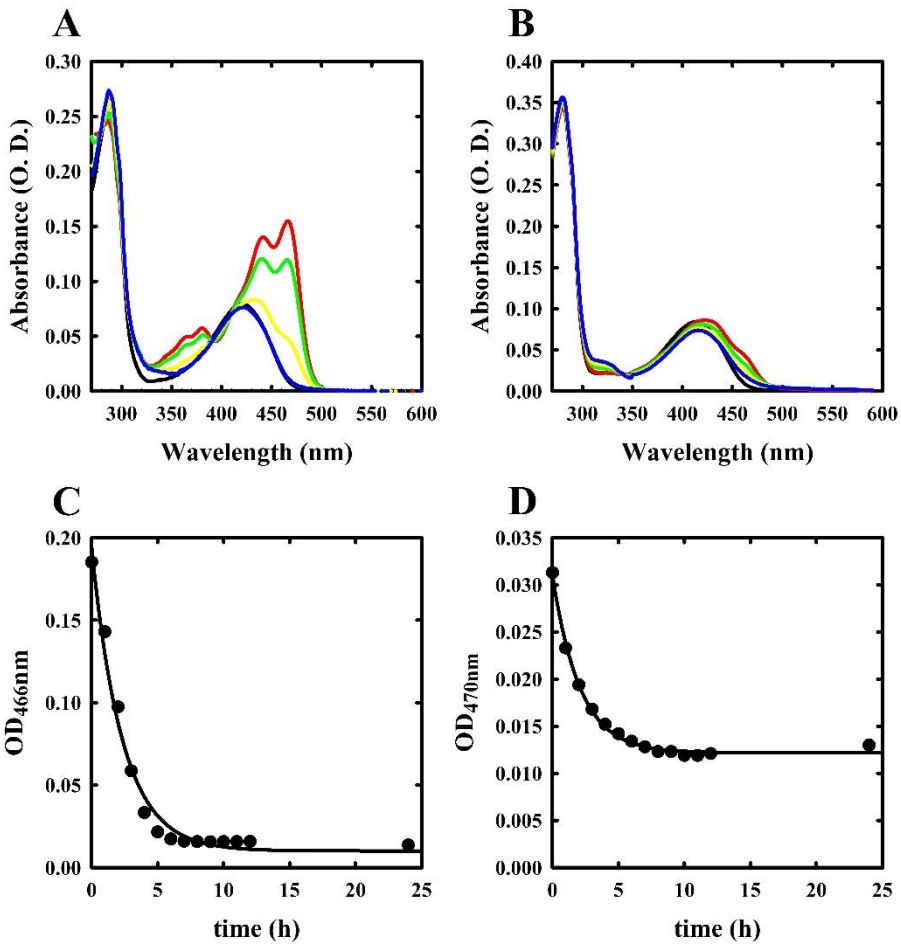

Figure 24. Absorbance spectra of OASS in the absence and presence of 1mM triF-Ala. Panel A: absorbance spectrum of OASS-A in the absence of reagent (black line), 1 min (red line), 1 h (green line), 3 h (yellow line), and 7 h (blue line) after addition of the reagent. Panel B: absorbance spectrum of OASS-B in the absence of reagent (black line), 1 min (red line), 1 h (green line), 3 h (yellow line), and 7 h (blue line) after addition of the reagent. Panel C: time course of spectral changes of OASS-A, monitored at 466 nm. Panel D: time course of spectral changes of OASS-B, monitored at 470nm starting 1 min after the addition of triF-Ala. Data were fitted to a monoexponential decay. Adapted from [65].

The reactivity of triF-Ala with OASS was also monitored by fluorescence emission spectroscopy by excitation of cofactor at 412 nm (Figure 25). Addition of triF-Ala to OASS-A immediately resulted in a small blue shift of the peak to 495 nm, accompanied by only a small decrease in emission intensity (panel A). This observation confirms that the reaction between PLP and triF-Ala does not form an α-aminoacrylate and is in agreement with absorbance spectra. The intensity of emission band was slowly decreasing in parallel with the disappearance of the absorption bands at 440 and 466 nm. However, with fluorescence emission assay we did not observe the reappearance of the original spectrum. This finding suggests that the species, that forms and absorbs at 412 nm, is not the internal aldimine [65].

Monitoring the reaction between triF-Ala and OASS-B by fluorescence emission spectroscopy (Figure 25, panel B) reveals a different behavior comparing to the A isoform. When triF-Ala is added to the protein, intensity of emission band immediately increases, then slowly decreases. Concomitantly a small blue shift to 501 nm takes place, which that re-centers to 505 nm after 7 h. The intense increase in emission intensity is a characteristic of the external aldimine [73,74], while a blue shift indicates the presence of a transient species [65].

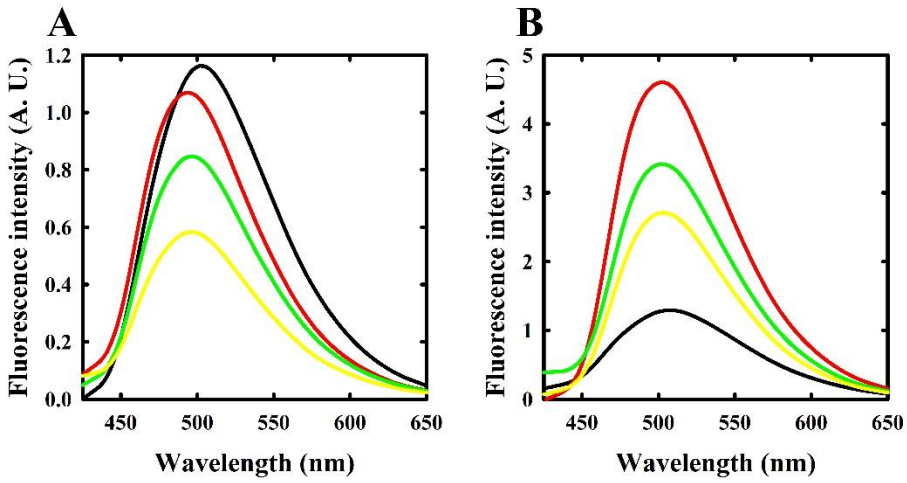

Figure 25. Fluorescence emission spectrum of OASS in the absence and presence of 1 mM triF-Ala. Emission spectra were recorded upon excitation at 412 nm. Panel A: OASS-A in the absence of reagent (black line), 1 min (red line), 4 h (green line), and 6 h (yellow line) after addition of the reagent. Panel B: OASS-B in the absence of reagent (black line), 1 min (red line), 3 h (green line), and 7 h (yellow line) after addition of the reagent. Adapted from [65].

Reaction of F-Ala and triF-Ala with OASS-A and OASS-B monitored by activity assays.

To evaluate the inhibitory and inactivation potency of F-Ala and triF-Ala on OASS-A and OASS-B, two distinct types of activity assays were carried out. Firstly, inhibitory potency of both F-Ala and triF-Ala was evaluated by IC_{50} measurement, where enzymes were exposed to increasing concentrations of reagent for a short amount of time. F-Ala exhibits IC_{50} values of 480 ± 50 µM for A and 1290 ± 230 µM for B isoform (Figure 26, panels A and B). For triF-Ala, determined IC_{50} values were 130 ±10 µM for A and 940 ± 60 µM for B isoform (Figure 26, panels C and D) [65].

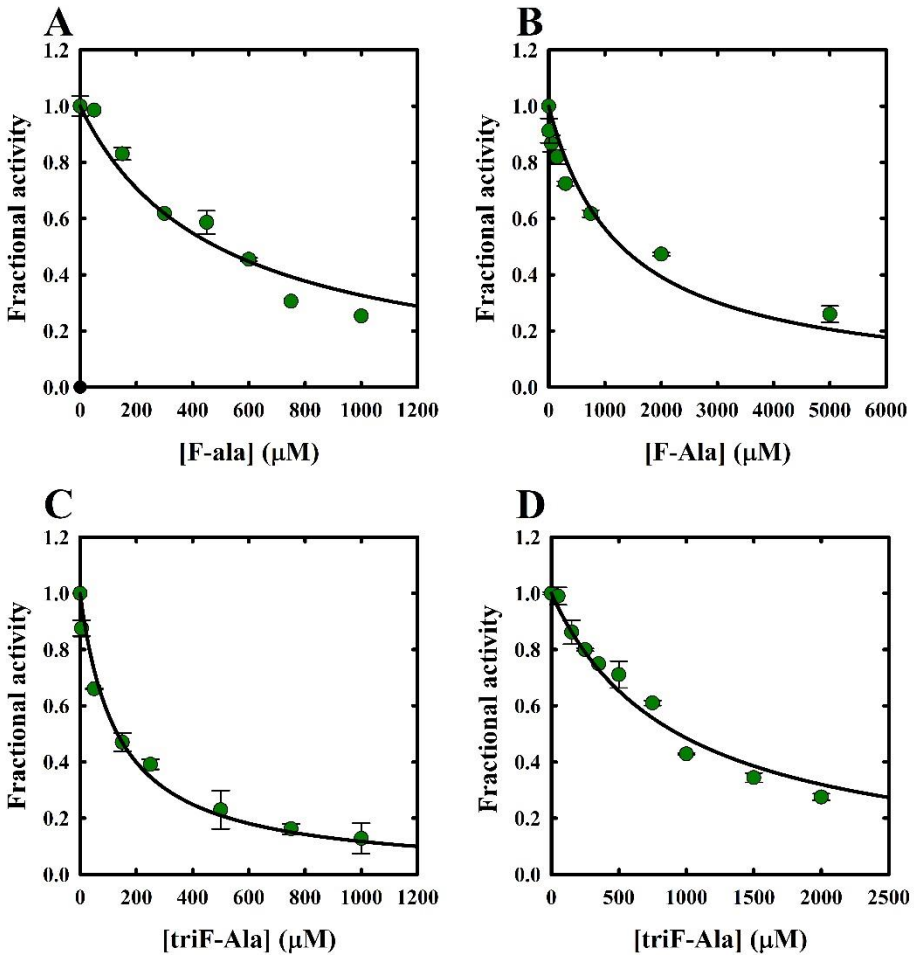

Figure 26. Dependence of OASS fractional activity on the concentration of fluoroalanine derivatives. (A) OASS-A and F-Ala; (B) OASS-B and F-Ala; (C) OASS-A and triF-Ala; (D) OASS-B and triF-Ala. The IC_{50} was obtained by fitting data points to Equation (2). The calculated IC_{50} values for F-Ala were 480 ± 50 mM and 1290 ± 230mM for OASS-A and OASS-B, respectively, and for triF-Ala 130 ± 10 mM and 940 ± 60 mM, for OASS-A and OASS-B, respectively. Adapted from [65].

Whereas F-Ala was found to be a substrate analogue of OASS, triF-Ala might inhibit it by irreversible inactivation. To detect if irreversible inactivation takes place, we exposed OASS-A to 1, 2.5, 10, 30, 50 mM triF-Ala and monitored its inactivation kinetics (Figure 27). At each time point,

the enzyme activity was measured upon a 5000-fold dilution of the reaction mixture in order to separate reversible inhibition from the inactivation.

Inactivation kinetics revealed a biphasic behavior. Immediately upon the addition of triF-Ala to the OASS-A, a very fast phase takes place of which rate constant cannot be measured. The result of this first phase is partial inactivation of the enzyme, that is proportional to the reagent concentration and is approaching a saturation (Figure 27, panel B). After that, the slow phase takes place where enzyme gets further inactivated with a k_{obs} proportional to the reagent concentration, just as expected for mechanism based inactivators.

By determination of a second-order rate constant k_{inact}/K_I, that is 3.95×10^{-5} min^{-1} mM^{-1}, it can be concluded that triF-Ala is a poor and inefficient inactivator of OASS-A [65].

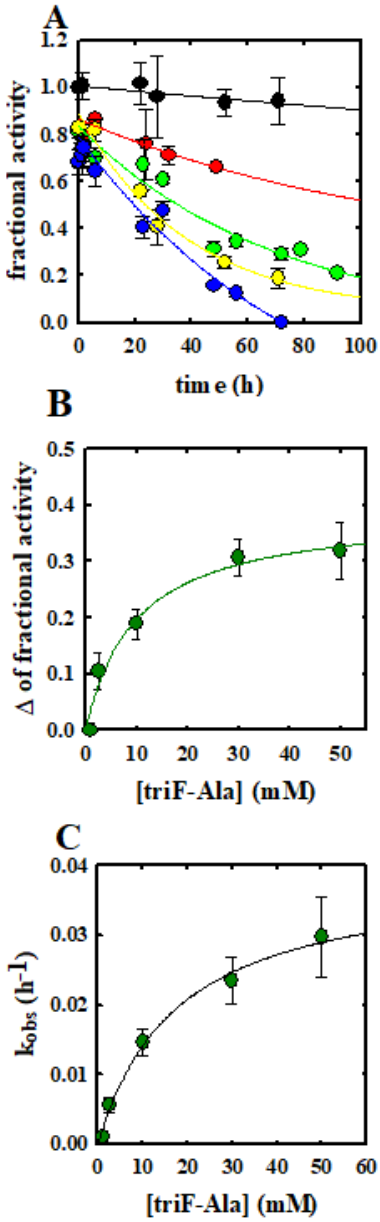

Figure 27. Panel A: Inactivation kinetics of OASS-A upon prolonged incubation time with 1 (black), 2.5 (red), 10 (green), 30 (yellow) and 50 mM (blue) triF-Ala. Panel B: Extent of OASS-A inactivation determined upon completion of the fast phase. Panel C: dependence of k_{obs} on the concentration of triF-Ala [65].

By comparing absorbance spectra as a function of time (Figure 24, panels A and C) with a kinetic data of enzyme inactivation (Figure 27), three phases of reaction between triF-Ala and the enzyme are identified:

- Phase I takes place immediately upon addition of triF-Ala to OASS. It results in a formation of species absorbing at 440-470 nm and decrease of enzyme activity, that is proportional to the reagent concentration;
- Phase II is completed in about 10 hours of incubation. In this time, species absorbing at 440-470 disappears with the concomitant appearance of a species at 412. In enzyme activity only minor progress in inhibition is observed.
- Phase III is a very slow phase where most of enzyme inactivation takes place without any changes in the absorption spectrum of OASS-A (Figure 24, panel A).

Since 1 mM triF-Ala does not cause any significant inactivation in first 8 h of incubation (Figure 27, panel A), it can be concluded that any decrease in the enzyme activity up to 1 mM concentration is completely dependent on reversible inhibition during short term exposure. Therefore, the IC_{50}s (Figure 26) are a good estimate of relative affinity of F-Ala and triF-Ala for the enzyme.

Emerging is the observation that absorbance spectra and inactivation kinetics are exhibiting different phases of reactivity. These discrepancies are likely arising from the different ratio between enzyme concentration

(10 μM in the absorbance spectra and 45 μM in the activity assays) and inactivator concentration.

Verification of enzyme inactivation after 85-hour incubation with 10 mM triF-Ala was carried out using activity assays. After the incubation, enzyme retained about 25 % of activity comparing to the non-treated control. The ligand was completely removed by extensive ultrafiltration, after which the enzyme was incubated with PLP in saturating concentration and assayed. Ligand removal and incubation with cofactor did not restore the enzyme activity, indicating that triF-Ala does not displace PLP from the active site, but it causes irreversible covalent modification of active site residue(s).

When kinetics of enzyme inactivation by triF-Ala were measured on OASS-B (Figure 28), a biphasic enzyme inactivation was observed again. In the fast phase decrease in the enzyme activity is proportional to the inactivator concentration, although the amplitude is smaller comparing to the A isoform. On the other hand, the fast phase is about 10 fold faster on the B isoform, being again proportional to the concentration of triF-Ala (Figure 28, panel B). The relationship between k_{obs} and [I] appears to be linear, which is not expected for suicide substrates. However, it is likely that this behaviour is observed because the saturation conditions were not reached. k_{inact}/K_I was therefore estimated by the equation (9) that describes single step inactivation, and is 10.3×10^{-5} min^{-1} mM^{-1} [65].

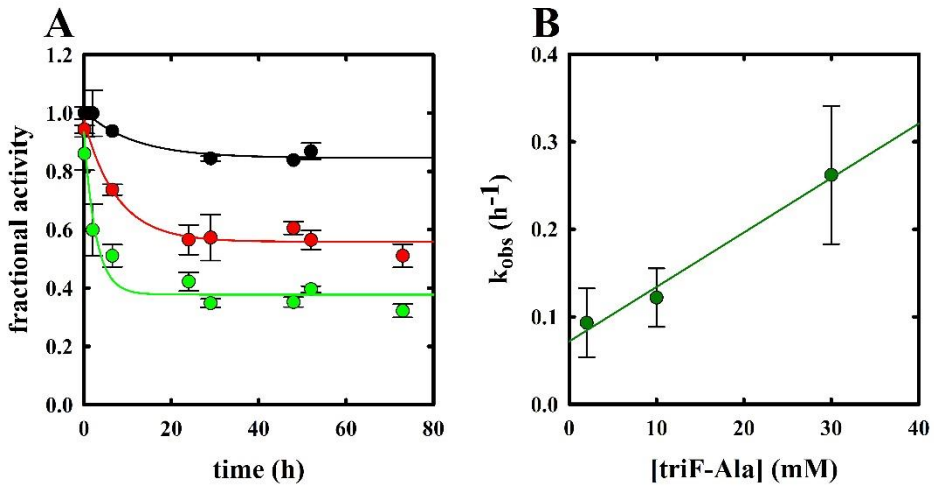

Figure 28. Panel A: Inactivation kinetics of OASS-B upon prolonged incubation time with 2 (black), 10 (red) and 30mM (green) triF-Ala. Panel B: dependence of k_{obs} to the concentration of triF-Ala. Adapted from [65].

By comparing the reactivity between OASS-B and triF-Ala using absorbance spectroscopy and inactivation kinetics, two phases of reaction observed:

- Phase I takes place immediately upon addition of triF-Ala to OASS-B and results in absorbance changes at 470 nm, accompanied by a fast decrease in enzyme activity;
- In Phase II a shoulder at 470 nm is disappearing in parallel with a slow phase of enzyme inactivation.

These findings suggest different mechanisms of enzyme inactivation for OASS-A and OASS-B [65].

Proposed mechanism of StOASS inactivation by triF-Ala.

Based on our experimental data and reaction schemes previously proposed in the reaction of triF-Ala with other PLP-dependent enzymes [105,107,110,112,113,135,140], we propose the following inactivation mechanism for OASS-A. The behavior is similar to the mechanism proposed for alanine racemase [113] reported in Scheme 1, path B. As the decarboxylation does not occur in the catalytic cycle of OASS, it is unlikely that the inactivation follows path A.

The reaction starts by binding of triF-Ala to the cofactor PLP, forming the external aldimine. This is followed by the elimination of HF, resulting in a reactive species β,β-difluoro-α,β-unsaturated imine (intermediate **I B,** Scheme 1). This intermediate contains delocalized electrons and is responsible for the spectrum with bands at 440 and 466 nm. The stability of this species is questionable, since it can be hydrolyzed, leading to the recovery of an internal aldimine before undergoing the Michael attack by enzyme nucleophile. Hydrolysis and Michael attack will both lead to the decrease in intensity of peaks in 450-470 nm and cannot be distinguished by the absorbance spectroscopy. Wheather hydrolysis or nucleophilic attack will take place, is dictated by the concentration of inhibitor, geometry of active site residues and water accessibility. If the covalent modification takes place, the species **I B** undergoes the Michael attack by the enzyme nucleophile, likely the active site lysine, leading to intermediate **II B**. This is a species which absorbs at a similar wavelength as an internal aldimine, but it exhibits different behavior in fluorescence emission spectroscopy (Figure 25, panel A). Based on the literature data

[135], we propose that this species is unstable and it undergoes the addition of water on β-carbon, followed by the elimination of two fluoride ions, resulting in the intermediate **III B**. As this step has been observed on alanine racemase only after a partial denaturation with sodium borohydrate, it is proposed that at this point the active site of OASS is open and accessible to the water. Conformational changes in the active site and associated water accessibility also control the slow fluoride elimination. Literature data suggest that the final step might be the loss of the carboxylic moiety with formation of intermediate **IV B.**

Inactivation of OASS-B by triF-Ala follows the reaction scheme of the A isozyme, although the distribution of intermediates and their interconversion rates are different. In the case of OASS-B, external aldimine is the predominant species. HF elimination leads to the formation of β,β-difluoro-α,β-unsaturated imine (**I B**), but unlike on the A isoform, this reactive species does not accumulate to a significant extent and consequently the fraction of inactivated enzyme is small. When Michael attack by the catalytic lysine takes place, ammonia and difluoropyruvate are released and the latter is responsible for the broad absorption around 320 nm. This reaction is more efficient for the OASS-B isozyme with respect to the OASS-A isozyme and consequently the accumulation of the **I B** intermediate is prevented. Inactivation follows the mechanism proposed for OASS-A, that is by an attack of an active site nucleophile, likely the catalytic lysine, on the β-carbon [65].

REACTIVITY BETWEEN StOASS AND FLUOROALANINE DERIVATIVES

Several fluoroalanine derivatives were tested in the search of more potent inactivators. Firstly, we exploited the effect of chain extension, branching and fluorine substitution (Table 11). None of these modifications resulted in an improvement in inactivation for both isozymes [65].

Table 11. Reactivity between StOASS and alanine derivatives. Adapted from [65].

		reactivity against StOASS-A		reactivity against StOASS-B	
name	**structure**	**% inactivation***	**spectral changes**	**% inactivation***	**spectral changes**
INT-3	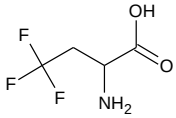	ns	no	18 ± 2	no
INT-4	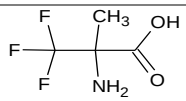	ns	no	ns	no
INT-5	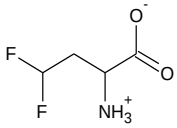	12 ± 1	no	16 ± 5	no
KG-008**	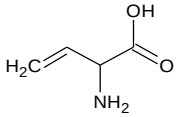	14 ± 1	no	ns	no

** % inhibition was evaluated after 6 h incubation of the enzyme with 1 mM inhibitor, following 5000-times dilution for the assay (0.2 µM inhibitor in the assay) in 2 replicates. **In a form of TFA salt. ns – inhibition ≤ 10 % was considered as not significant. nd - not determined.*

In a further effort, series of trifluoroalanine derivatives where the carboxylic moiety was substituted with bioisosters was tested (Table 12). These analogs were aimed to identify a scaffold with options to tune activity and selectivity of the inhibitor which is not possible for trifluoroalanine. A set of amides and sulfonamides with different *N*- and *S*- substitution patterns was prepared and assayed. Compounds were initially screened for reactivity with PLP using absorbance spectroscopy.

Table 12. Reactivity between StOASS and trifluoroalanine derivatives with isosters of carboxylic group. Adjusted from [65].

		reactivity against StOASS-A			reactivity against StOASS-B		
name**	**structure**	**% inacti-vation***	**IC_{50} (µM)**	**spectral changes**	**% inacti-vation***	**IC_{50} (µM)**	**spectral changes**
KG-INT-110	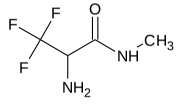	ns	nd	no	ns	nd	no
KG-INT-108	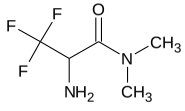	ns	nd	no	ns	nd	no
KG-INT-111	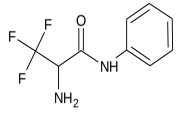	ns	nd	no	ns	nd	no
KG-INT -109	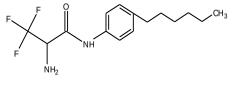	10 ± 2	nd	no	ns	nd	no

KG-INT-114	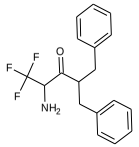	ns	nd	no	12 ± 7	nd	no
INT-107	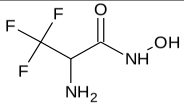	15 ± 5	nd	yes	ns	nd	no
INT-007	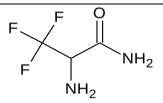	ns	nd	no	ns	nd	no
INT-100	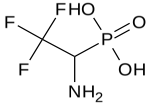	ns	nd	no	ns	nd	no
bio-2347_1F1	NA	nd	nd	no	ns	nd	no
bio-2348_1F1	NA	ns	542 ± 43	yes	ns	> 1000	no
bio-2352_1F1	NA	nd	nd	no	nd	nd	no
bio-2356_1F1	NA	nd	nd	no	nd	nd	no
bio-2357_1F2	NA	nd	nd	no	nd	nd	no
bio-2359_1F1	NA	nd	nd	no	nd	nd	no

bio-2360_1F1	NA	nd	nd	no	nd	nd	no
bio-2362_1F1	NA	nd	nd	no	nd	nd	no
bio-2363_1F1	NA	nd	nd	no	nd	nd	no
bio-2365_1F1	NA	nd	nd	no	nd	nd	no
bio-2368_1F1	NA	nd	nd	no	nd	nd	no
bio-2369_1F1	NA	nd	nd	no	nd	nd	no
bio-2389_1F1	NA	ns	179 ± 22	yes	ns	583 ± 84	yes
bio-2390_1F1	NA	nd	nd	no	nd	nd	no
bio-2391_1F1	NA	nd	nd	no	nd	nd	no
bio-2392_1F1	NA	nd	nd	no	nd	nd	no
bio-2393_1F1	NA	nd	nd	no	nd	nd	no
bio-2394_1F3	NA	ns	570 ± 151	yes	ns	762 ± 53	yes
bio-2395_1F1	NA	nd	nd	no	nd	nd	no
bio-2396_1F1	NA	nd	nd	no	nd	nd	no
bio-2397_1F1	NA	nd	nd	no	nd	nd	no

bio-2398_1F1	NA	nd	nd	yes	nd	nd	no
bio-2399_1F1	NA	nd	nd	no	nd	nd	no
bio-2400_1F1	NA	nd	nd	no	nd	nd	no
bio-2401_1F1	NA	nd	nd	yes	nd	no	no
bio-2402_1F1	NA	nd	nd	no	nd	nd	no
bio-2403_1F1	NA	ns	167 ± 16	yes	ns	650 ± 78	yes
bio-2404_1F1	NA	nd	nd	no	nd	nd	no
bio-2405_1F1	NA	nd	nd	no	nd	nd	no
bio-2409_1F1	NA	nd	nd	no	nd	nd	no
bio-2410_1F1	NA	nd	nd	no	nd	nd	no
bio-2411_1F1	NA	nd	nd	no	nd	nd	no
bio-2412_2F1	NA	ns	177 ± 29	yes	ns	> 1000	no
bio-2418_1F1	NA	nd	nd	no	nd	nd	no
bio-2421_1F1	NA	nd	nd	no	nd	nd	no

** % inhibition was evaluated after 6 h incubation of the enzyme with 1 mM inhibitor, following 5000-times dilution for the assay (0.2 µM inhibitor in the assay) in 2 replicates. NA – not applicable – structures are not disclosed in order to protect the intellectual property. **In a form of TFA salt. ns – inhibition ≤ 10 % was considered as not significant. nd - not determined.*

We identified few reactive compounds and those that caused the most pronounced spectral changes were selected for further testing with activity assays to evaluate binding and inactivation potency (bio2348_1F1, bio2389_1F1, bio2394_1F3, bio2403_1F1, and bio2412_2F1).

As it can be seen in Figure 29, all compounds that react with StOASS-A exhibit the same spectral behaviour as triF-Ala, suggesting the formation of identical intermediates, that disappear with different velocities. Bio2348_1F1 and bio2412_2F1 (*N*-substituted) do not react with StOASS-B, while bio2389_1F1, bio2394_1F3 and bio2403_1F1 (*S*-substituted) are reactive with both isozymes. Also for the B isoform the reaction mechanism seems to be similar to triF-Ala. Bio2394_1F3 is the most reactive towards the B isoform, causing the most pronounced spectral changes and is likely the most promising inhibitor.

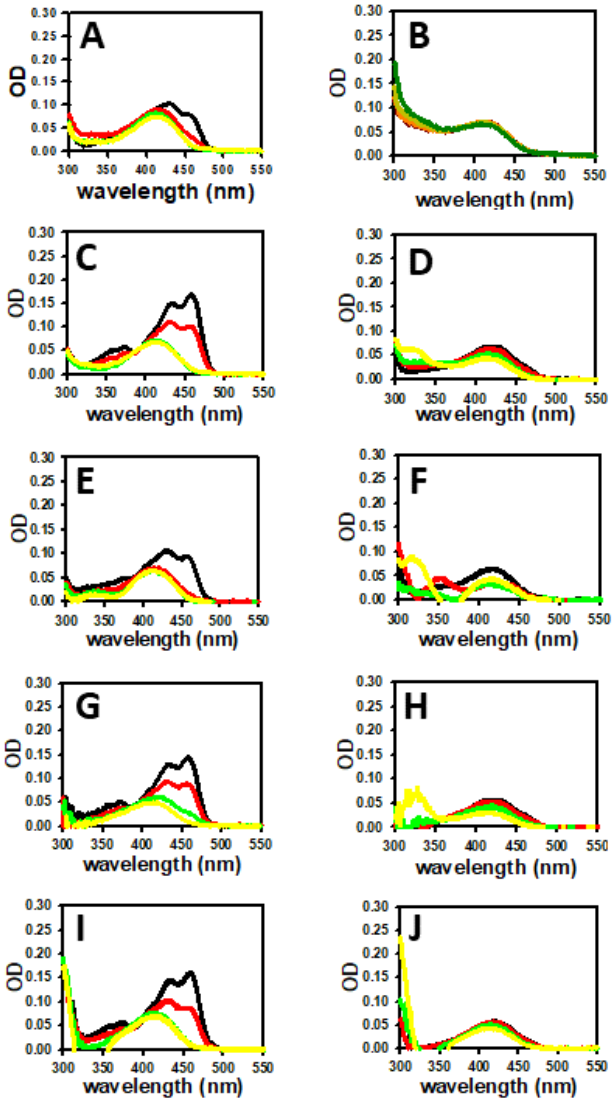

Figure 29. Absorbance spectra of OASS in the presence of 1mM triF-Ala derivatives. Absorbance spectra were measured 5 min (black line), 1 h (red line), 6 h (green line) and 24 h (yellow line) after the addition of the reagent. Panel A: OASS-A + bio2348_1F1; Panel B: OASS-B + bio2348_1F1; Panel C: OASS-A + bio2389_1F1; Panel D: OASS-B + bio2389_1F1; Panel E: OASS-A + bio2394_1F3; Panel F: OASS-B + bio2394_1F3; Panel G: OASS-A + bio2403_1F1; Panel H: OASS-B + bio2403_1F1; Panel I: OASS-A + bio2412_2F1; Panel J: OASS-B + bio2412_2F1.

Then we measured their IC_{50}s to have an insight which substituents have more favourable affinity (Table 12). *N*- and *S*-substituted derivatives both react with OASS-A, where bio2389_1F1, bio2403_1F1, and bio2412_2F1 have comparable inhibitory efficiency as triF-Ala. These three molecules also cause the slowest disappearing spectral changes in the absorption spectrum of the A isoform, with observed kinetics that are comparable to the triF-Ala. Even though the number of selected compounds is small, it can be proposed that *S*- substituted derivatives with more hydrophobic groups react better with OASS-A, while *N*- substitution favours hydrophilic groups.

For the B-isoform, *S*-substituted derivatives (bio2389_1F1, bio2394_1F3, bio2403_1F1) exhibit IC_{50}s comparable or better than triF-Ala, as well as reactivity with cofactor PLP. On the other hand, *N*-substituted derivatives do not react with StOASS-B.

Inactivation assays at 1 mM concentration of inhibitors (Figure 30) did not reveal any significant enzyme inactivation within 48 h incubation. On StOASS-A it was observed that compounds with better IC_{50}s (reported in Table 12) cause about 20 % of inhibition at 5 min incubation, that does not proceed to further inactivation. This phenomenon is attributed to the formation of reactive intermediate that hydrolyses before the nucleophilic attack takes place. At 1 mM concentration, the molecule is consumed before it could cause any inactivation. Also for the B isoform no significant inactivation was observed. At 48 h, bio2348_1F1 and bio23403_1F1 show a decrease in the enzyme activity. However, since at

previous time points no inactivation was observed, these phenomena cannot be attributed to the inactivation mechanism, but it is rather caused by enzyme spontaneous denaturation due to the prolonged incubation times.

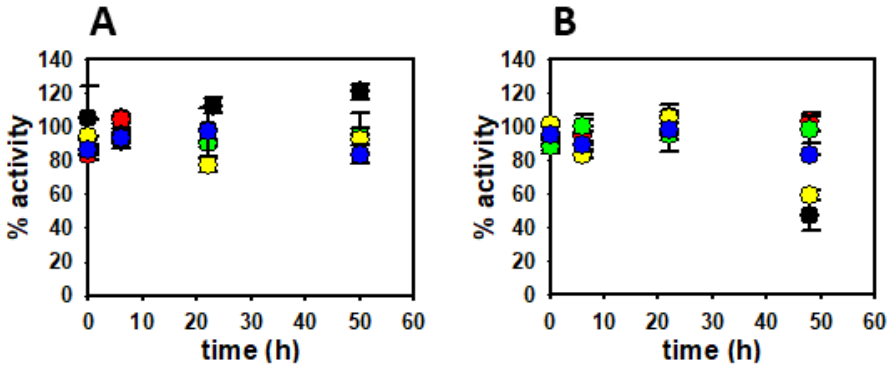

Figure 30. Inactivation of OASS in the presence of 1 mM triF-Ala derivatives. The colour marks identifies an inhibitor: bio2348_1F1 (black), bio2389_1F1 (red), bio2394_1F3 (green), bio2403_1F1 (yellow), bio2412_2F1 (blue). Panel A: inactivation of StOASS-A. Panel B: inactivation of StOASS-B.

Even though in biochemical and medicinal chemistry research 1 mM inhibitor concentration is normally considered as high, in the case of StOASS inactivation by fluoroalanine derivatives is not enough to observe any measurable inactivation. This finding is not surprising since literature reports inactivation of other PLP dependent enzymes with fluoroalanines at even higher concentrations, up to 80 mM [110,112,113]. However, their low potency is raising concerns regarding their use as drugs. High drug concentration required for target inhibition *in vivo* could lead to off-target effects, presumably with other abundant PLP-dependent enzymes in human body and nucleophilic residues. Additionally, it is proposed that fluoroalanines will have difficulties in the permeation through the Gram-negative membrane. The pKa of the triF-Ala α-amino group is 5.8, thus

not making it zwitterionic at physiological pH and consequently difficult to internalize [140].

From the biochemical point of view, it is interesting to notice how inhibition of StOASS by reversible inhibitors can be efficient while it is unsuccessful when mechanism-based inactivators are used. Poor inactivation likely arises from the fact that the reactive intermediate is in a position that only with difficulty can be reached by the enzyme nucleophilic residues. In this way, OASS is somehow protected by unspecific reactions that could take place during the catalytic cycle, leading to inactivation or undesired reactivity with substrate analogues.
This study failed to identify potent mechanism based inactivators of StOASS. We found that monofluoroalanine is a weak substrate analog for both isozymes, whereas trifluoroalanine acts as irreversible, although inefficient, inhibitor. In an effort to improve enzyme inactivation, we identified triF-Ala derivatives with substituted carboxylic group that react with StOASS in a similar manner, making them interesting candidates for further enzyme inactivation assays.

3.2. StSAT INHIBITORS

3.2.1. INHIBITORS DESIGNED BASED ON *IN SILICO* SCREENING OF *IN HOUSE* COMPOUND LIBRARY

1st series.

The first series of StSAT inhibitors was a collection of structurally heterogeneous molecules that were chosen based on the *in silico* screening of *in house* library by Prof. Costantino's group. In order to separate between efficient and non-efficient molecules, they were screened at 1 mM concentration and percentage of inhibition is shown in Table 13.

Table 13. 1st series of StSAT inhibitors, derived from in silico screening of in house compound library.

INHIBITOR NAME	STRUCTURE	% INHIBITION AT 1 mM	IC_{50} [mM]
UPAR-101	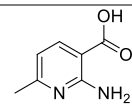	19 ± 1	
UPAR-238	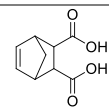	35 ± 6	
UPAR-191	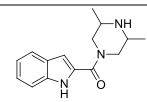	31 ± 5	
UPAR-328	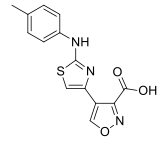	99 ± 1	0.12 ± 0.02

UPAR-136	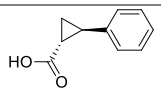	42 ± 5	> 2
UPAR-167	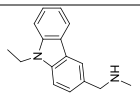	24 ± 1	

UPAR-328 was identified as far the most potent inhibitor of the series and was further assayed. We determined that its IC_{50} was 116 ± 16 µM. For the evaluation of its mechanism of action, kinetics at constant L-Ser and variable AcCoA and inhibitor concentrations were carried out. Double reciprocal plot showed K_I = 64 ± 12 µM and competitive mode of inhibition against AcCoA (Figure 31).

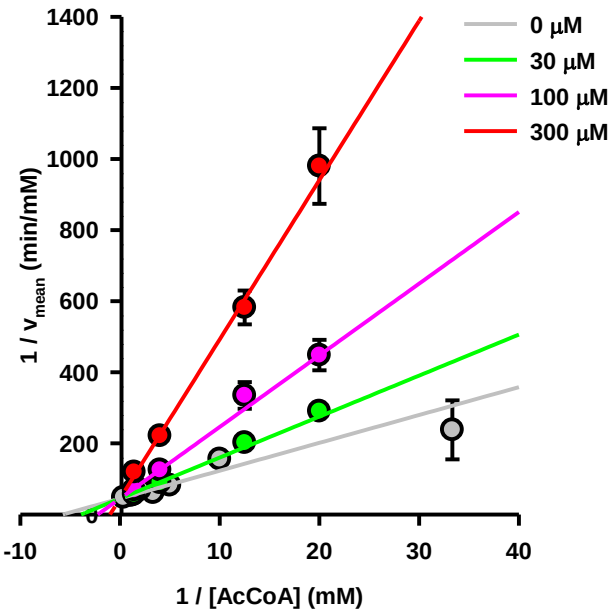

Figure 31. Double-reciprocal plot of StSAT at constant L-Ser and variable AcCoA and UPAR-328 concentrations is showing that the inhibitor is competitive against AcCoA.

2nd series.

The second series of StSAT inhibitors was a collection of molecules, structurally similar to UPAR-328. They were designed in order to investigate their structure-activity relationship (SAR) and identification of potent molecules. Structures and IC_{50}s are presented in Table 14.

Table 14. 2nd series of StSAT inhibitors, based on the structure of UPAR-328.

INHIBITOR NAME	STRUCTURE	IC_{50} (μM)
UPAR-325	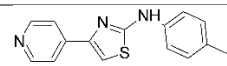	>400
UPAR-337	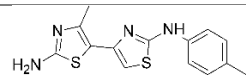	337 ± 88
UPAR-456	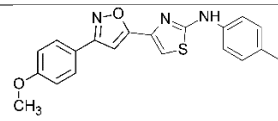	~13
UPAR-330	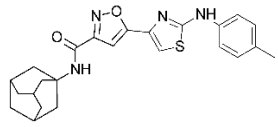	9.3 ± 2.6
UPAR-451	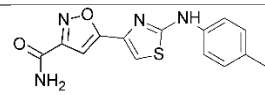	26 ± 4
UPAR-465	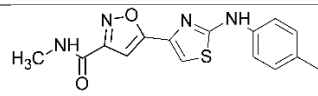	~ 60
UPAR-452	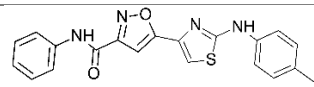	~16
UPAR-326	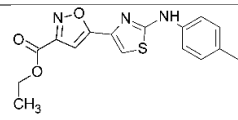	~ 10
UPAR-329	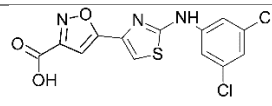	11 ± 1

UPAR-327	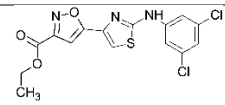	18 ± 4
UPAR-460	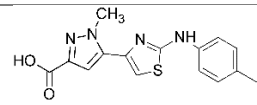	184 ± 13
UPAR-463	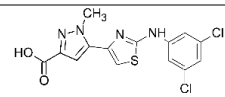	21 ± 5
UPAR-750	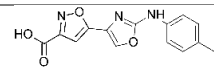	1.0 ± 0.2
UPAR-751	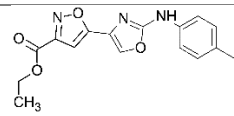	7.3 ± 1.8
UPAR-768	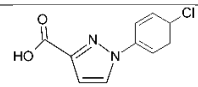	204 ± 21
UPAR-701	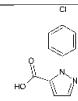	336 ± 87

The majority of molecules had a common general structure, based on two substituted heterocycles. Molecules with an isoxazole-thiazole (UPAR-456/330/451/456/452/326/329/327) show a very flat structure-activity relationship with IC_{50} in micromolar range. This finding suggests that the binding interactions are arising from the heterocycles and the side groups do not significantly contribute to the inhibition. UPAR-329, with IC_{50} = 11 µM, was later tested in microbiological assays.

Potency of compounds was improved when the core of the molecule was substituted with isoxazole-oxazole heterocycles. UPAR-750 and UPAR-751 exhibit IC_{50}s in low micromolar range. Even though only two molecules with this type of core were tested, the effect of side groups in

this type of molecules seems to be more pronounced. Surprisingly, esterification of the carboxylic group leads to 7-fold decrease in affinity, suggesting the imporance of the carboxylic moiety for the binding. UPAR-750 has IC_{50} of 1.0 ± 0.2 μM and is the most potent SAT inhibitor identified so far [114].

3.2.2. INHIBITORS DESIGNED BASED ON HIGH-THROUGHPUT SCREENING

In the search of StSAT inhibitors, a high-throughput screening (HTS) of a commercially available library (collaboration between Prof. Costantino's group (University of Parma) and Prof. Tammela group (University of Helsinki) was also carried out in order to identify structurally different inhibitors with hopefully bacterial membrane-permeable characteristics. For HTS, antibacterial, antiinfective and antimicrobial compound libraries were chosen from ChemDiv (ChemDiv Inc). ~ 92000 compounds were initially screened *in silico* and the most potent hits were chosen for *in vitro* screening with indirect SAT activity assay, adjusted for 96-well-plate format.

UPAR-803 was recognized as the most potent SAT inhibitor from the library. Later it was synthesized *in house* and its derivatives were prepared in order improve the potency and investigate preliminary SAR. *In house* produced molecules were assayed in our laboratory (Table 15).

Table 15. Inhibitory potency of StSAT inhibitors, derived from hits of high-throughput screening.

			% activity		
Compound	**structure**	**IC_{50} (μM)**	**1 μM**	**10 μM**	**50 μM**
UPAR-799	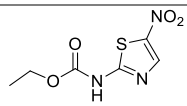	22.0 ± 2.0			
UPAR-800	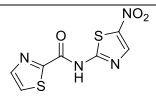	> 50	80 ± 2	76 ± 4	68 ± 5
UPAR-801	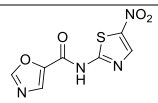	> 50	88 ± 7	81 ± 4	81 ± 2
UPAR-802	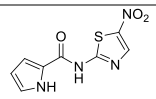	> 50	95 ± 2	90 ± 8	77 ± 1
UPAR-803 (commercial)	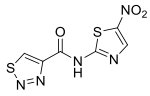	31.0 ± 2.3			
UPAR-804 (*in house*)		10.8 ± 1.5			

Structurally, the molecules are 5-nitrothiazoles, substituted with a side group at position 2 via amide linkage. The hit from HTS, UPAR-803 and its *in house* synthesized analog UPAR-804 exhibit IC_{50} in low micromolar range. Similar potency was reached with UPAR-799, having an alkylether as a side group. UPAR-800/801/802 are substituted with heterocycles and are less potent. Although the library of assayed compounds is small, the observed trend suggests that the increased polarity of the substituents improves inhibitor binding.

EFFECTS OF OASS AND SAT INHIBITORS ON BACTERIAL GROWTH

1. INTRODUCTION

High affinity of reversible inhibitors against OASS and SAT is a promising step towards inhibition of cysteine biosynthesis in Gram-negative bacteria. However, the question remains if these molecules will also be active *in vivo*. Penetration through the complex membrane of Gram-negative bacteria is one of the most challenging problems in the development of new antibiotics and there is no clear relationship between the structure of a molecule and its permeability properties [13,17,98–100,127]. Therefore, microbiological assays were carried out to evaluate the *in vivo* efficacy of selected OASS and SAT inhibitors. Additionally, a method for measurement of intracellular amount of reduced thiols was developed in order to detect changes in the cysteine biosynthesis upon exposure to inhibitors [49,63,141].

ABBREVIATIONS USED:
LB – Luria Bertani broth; PMBN – polymyxin nonapeptide; RSH – intracellular reduced thiols; MIC – minimal inhibitory concentration

2. MATERIALS AND METHODS

2.1. MATERIALS

All reagents, if not otherwise specified, were obtained from Sigma Aldrich (St. Louis, MO, USA) at the best commercial quality available.

M9 minimal broth contained:

- 1x M9 salts (12.8 g/L $Na_2HPO_4x7H_2O$, 3 g/L KH_2PO_4, 0.5 g/L NaCl, 1 g/L NH_4Cl)
- 11 mg/L $CaCl_2$
- 240 mg/L $MgSO_4$
- For addition of carbon source, M9 was supplemented with 0.4% glucose

LB broth contained:

- 10 g/L tryptone
- 10 g/L NaCl
- 5 g/L yeast extract

LB agar plates were prepared from LB with the addition of 15 g/L agar.

20 % LB was prepared by LB dilution in sterile H_2O directly before use.

2.2. STANDARD MICROBIOLOGICAL METHODS

2.2.1. GROWING E. coli BACTERIAL CULTURE

E. coli cultures were grown at 37^oC and 150 RPM. Overnight cultures were grown in LB and diluted 1:100 in experimental broth for initiation of bacterial growth curve.

2.2.2. COUNTING COLONY FORMING UNITS

Aliquots of bacterial cultures were serially diluted in PBS. For each dilution, 40 µL were plated on LB agar and incubated O/N at 37°C. The following day colonies were counted and CFU/mL in the original sample was calculated.

2.3. MINIMAL INHIBITORY CONCENTRATION

Compounds for testing were serially diluted in DMSO, where they were 100-times more concentrated than in the assay. 1 µL of each dilution was transferred in a 96-well plate with U-bottom. Bacteria were grown O/N on LB agar at 37 °C. Colonies were scraped from the plate and diluted to 0.5 McFarland (corresponding to ~ $3x10^8$ CFU/mL) in saline solution. This solution was diluted 1:200 in an experimental broth (containing PMBN if assayed). 100 µL of bacteria in experimental broth were added to 96-well plate containing 1 µL of compound. Covered plates were incubated for 24 h at 37 °C. Bacterial growth and MIC were judged by unaided eyes. Each experimental plate contained a negative control with 1 % DMSO and sterility control of broth with compound without bacteria. Compounds were tested in concentrations up to their limit of solubility.

2.4. COLONY FORMING UNITS COUNT IN MIC ASSAY

Bacteria were exposed to the testing compounds following the protocol described in chapter 2.3. UPAR415 was serially diluted in DMSO from 51.2 mg/mL to 0.4 mg/mL and 1 µL of each dilution was placed on 96-well plate. *E. coli* ATCC 35218 was suspended in saline solution to 0.5 McFarland and then diluted 1:200 in M9 + 0.4 % glucose with 3 µg/mL

PMNB. 100 µL of bacteria were added to the compound on the plate. Covered plates were incubated at 37 ^{o}C.

For each time point, one 96-well-plate was prepared. The plate was taken out of the incubator at a time point and bacteria from each assay condition were serially diluted and plated for CFU counting.

2.5. MEASUREMENT OF INTRACELLULAR REDUCED THIOLS

RSH measurement was based on a previously published method [141]. Overnight culture was diluted 1:100 in a chosen experimental broth and grown further for the time of the assay at 37 ^{o}C at 150 RPM. At each experimental point, about 1 x 10^{9} CFU were taken from the culture and cells were pelleted by centrifugation at 7000 RPM for 20 min at 5 ^{o}C. Supernatant was removed and the pellet was stored at -20 ^{o}C until analysis. If the bacterial culture was grown in 20 % LB, cells were washed once with PBS before storage.

The pellet was suspended in 500 µL of lysis buffer (50mM Tris, 5mM EDTA, 0.1% SDS, 0.1 mM DTNB, pH = 8) and incubated at 37 ^{o}C for 30 min. Suspension was centrifuged at 13000 RPM for 20 min at 5 ^{o}C and supernatant was removed from the pellet. 200 µL of supernatant were transferred on a 96-well plate and the absorbance was measured at 405 nm. Molar concentration of RSH was calculated from the calibration curve, obtained using cysteine solubilized in deoxygenated buffer. Protein concentration in the supernatant was determined by BCA

method. The amount of thiols was given as nM of RSH per µg of cellular proteins.

2.6. STATISTICAL ANALYSIS

Statistical significance was determined by 2way Anova using GraphPad Prism 6.

3. RESULTS AND DISCUSSION

3.1. EVALUATION OF UPAR INHIBITORS ON BACTERIAL GROWTH WITH MIC

To evaluate the *in vivo* efficacy of compounds, three inhibitors were selected for microbiological testing (Figure 32):

- UPAR-415: the compound was chosen because is the most potent inhibitor of both OASS isozymes. However, its carboxylic group is likely to interfere with the permeability through the bacterial membrane, since it is negatively charged at physiological pH.
- UPAR-613: the compound is an analog of UPAR-415 and it has a good affinity against both isozymes of OASS. Since it does not have a carboxylic group it might show different behaviour in bacterial cell penetration.
- UPAR-329: the compound was chosen for microbiological testing because is one of the most potent SAT inhibitors.

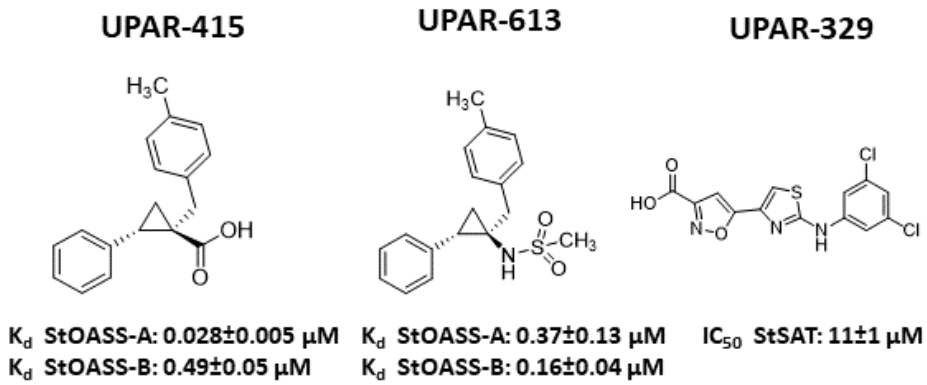

Figure 32. Compounds for microbiological testing.

Selected compounds were designed to inhibit enzymes of *S.* Typhimurium. However, it was decided to perform initial microbiological assays on *E. coli* ATCC 35218. Both *S*. Typhimurium and *E. coli* are enteric bacteria that possess identical pathway for biosynthesis of cysteine. Sequence identity between *E. coli* and *S*. Typhimurium isozymes is 97 % for OASS-A, 94 % for OASS-B and 96 % for SAT. Therefore, *E. coli* is a good model for microbiological testing of the inhibitors.

Initially, the effect of the compounds was tested by determination of minimal inhibitory concentration in minimal (M9 + 0.4 % glucose) and rich broth (CAMHB). Since it was expected, based on preliminary observations, that compounds might have issues in the penetration through bacterial cell wall, assays were carried out also in the presence of 3 µg/mL PMBN (PMBN3). This low, sub-MIC concentration of antibiotic makes bacterial membranes more permeable, while it does not affect bacterial viability. MICs are reported in Table 16.

Table 16. MICs of UPAR compounds. All units in µg/mL.

	***E. coli* ATCC 35218**			***E. coli* ATCC 35218 + PMBN3**		
	UPAR -415	**UPAR -613**	**UPAR -329**	**UPAR -415**	**UPAR -613**	**UPAR -329**
CAMHB	> 256*	> 128	> 64	nd**	nd**	nd**
M9 + 0.4 % glucose	> 512	> 128	> 64	**512-256**	> 128	**32**

**512 µg/mL not assayed; **nd – not determined.*

None of the compounds showed any effect on the growth of *E. coli* when tested in rich medium. This result is expected because bacteria can obtain sufficient amount of cysteine for their viability from the environment, even if their *in vivo* cysteine biosynthesis is inhibited. However, also no effect was observed in the minimal medium, suggesting that the compounds might not enter bacterial cell.

When the assay was performed in minimal medium in the presence of PMBN, an interesting behaviour was observed. UPAR415 showed MIC between 512 – 256 μg/mL, depending on the replicate. UPAR613 changed the visual aspect of bacterial growth. Instead of classical, round-shaped colony on the bottom of the well, bacteria grew in several small colonies dispersed on the wells (pinpoint growth). Judged by the eye, the number of bacteria was decreased above 64 μg/mL, although their growth was never completely inhibited. UPAR329 showed MIC of 32 μg/mL.

These results indicate that compounds have issues in the permeability in Gram-negative bacteria, but can interfere with bacterial growth once they enter. However, MIC assay does not allow to observe bacterial behaviour during 24 h incubation with the compound and cannot distinguish between bacteriostatic and bactericidal effects. To obtain a deeper insight in the mechanism of action of UPAR415, we performed an assay where bacteria were exposed to the same conditions as for MIC determination, while the number of CFU was counted as a function of time. Results are shown in Figure 33.

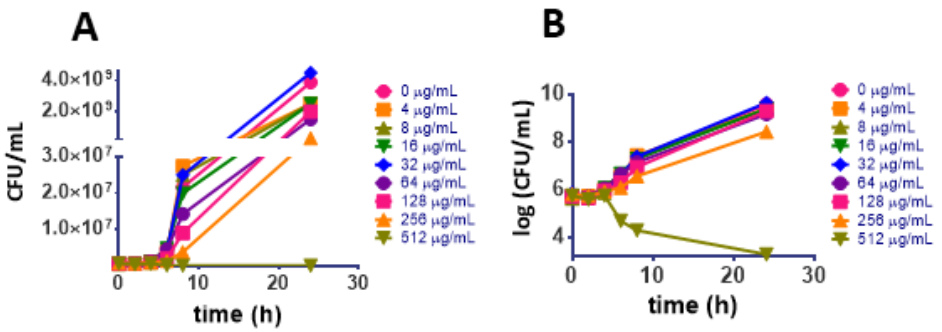

Figure 33. UPAR415 effect on E. coli ATCC 35218 growth in minimal medium in the presence of 3 µg/mL PMBN as a function of time. Results of the same experiment are shown with two different scales. Panel A: CFU/mL vs time (h). Panel B: log (CFU/mL) vs time (h).

Panel A shows that increasing concentrations of UPAR-415 from 64 to 256 µg/mL are causing small dose-response in bacterial growth. However, the difference between 256 µg/mL and untreated control is not high and after 24 h UPAR415 at this concentration inhibits the growth of bacteria for only about ½ log value. Up to 256 µg/mL, UPAR415 acts as a bacteriostatic compound.

When its concentration was doubled (512 µg/mL), UPAR415 unexpectedly acted as a bactericidal compound (panel B). Interestingly, it did not show any effect on bacterial viability in the first 4 h when bacteria were in the lag phase and started to show the effect only when bacteria entered in the exponential phase. It has to be noted that concentration 512 µg/mL is higher than those routinely used in microbiological assays. Therefore, unspecific effects under these conditions are likely to take place.

Based on these results, it was concluded that UPAR inhibitors exhibit issues in the permeability through the Gram-negative bacteria, but are able to interfere with bacterial growth once they enter the cell. However, it is not yet known whether they bind to OASS and SAT inside the cells or do they target any other macromolecules. To evaluate if compounds are reaching the theoretical target, we measured the amount of intracellular reduced thiols (RSH) as a marker of cysteine biosynthesis.

3.2. PRODUCTION OF INTRACELLULAR REDUCED THIOLS IN *E. coli* AND ASSAY VALIDATION

First, to understand the basal behaviour of RSH, we measured the kinetics of thiols production in *E. coli* ATCC 35218 when grown in two types of minimal medium – M9 supplemented with 0.4 % glucose and 20 % LB. The latter broth contains significantly less amino acids than rich medium and it represents the infection environment better than M9, although it has to be noted that it contains some cysteine which could be consumed by bacteria. To evaluate if the method is suitable to monitor changes in cysteine production, we used 1,2,4-triazole as a control. Triazole is a known substrate analog for OASS that replaces H_2S. In its presence OASS, instead of cysteine, catalyses the production of 1,2,4-triazole-alanine, that does not contain a thiol group. OASS reaction with triazole is shown in figure Figure 34. Since in the presence of triazole bacteria are not producing cysteine, the culture cannot grow in the minimal medium [39].

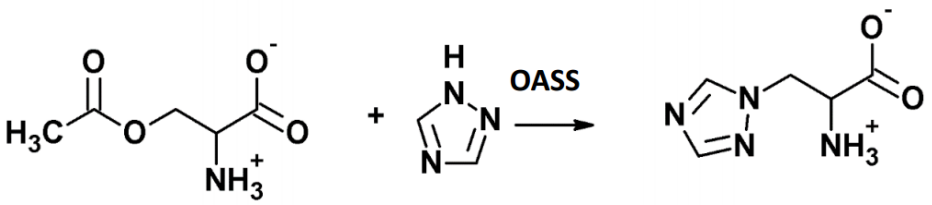

Figure 34. Reaction between O-acetlyserine and 1,2,4-triazole catalysed by OASS forming 1,2,4-triazole-alanine.

When *E. coli* behaviour was monitored in M9 (Figure 35), we observed that triazole inhibits its growth (panel A). When all triazole is consumed, bacteria start to grow and catch the untreated control 24 h after the culture preparation. The dependence of thiols with time (panel B) shows that at time 0 h, when O/N culture grown in LB is diluted in M9, the amount of thiols is the lowest in the course of the whole assay. However, when bacteria are growing, the concentration of thiols increases, reaching its peak in the early stationary phase. This observation suggests that the expression of the enzymes involved in the biosynthesis is changing at different stages of bacterial growth. It is proposed that the number of thiols in O/N culture, grown in LB, is higher and suddenly decreases upon dilution in M9 due to the overall stress. When triazole is present in M9, it acts as a preferential substrate for OASS over bisulfide. Since bacteria are not producing cysteine under these conditions, the number of thiols is constant until all the triazole is consumed. Therefore, we proved that the amount of RSH correlates with cysteine biosynthesis and bacterial growth in M9 broth.

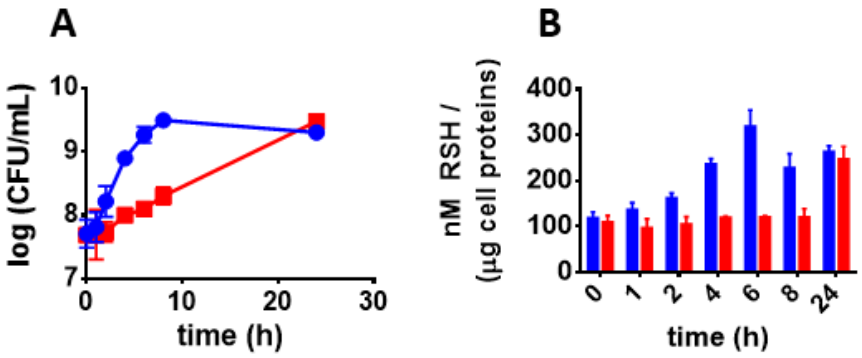

Figure 35. Legend: blue – cells in M9; red – cells in M9 + 5 mM triazole. Panel A: E. coli ATCC 35218 growth curve in M9 + 0.4 % glucose in the absence and presence of triazole. Panel B: RSH production in E. coli ATCC 35218, grown in M9 + 0.4 % glucose in the absence and presence of triazole. Assays were performed in 2 biological replicates.

Different behaviour was observed in 20 % LB (Figure 36). In bacterial growth (panel A), the effect of triazole is lost, likely due to cysteine present in the broth that can compensate for inhibition of cysteine biosynthesis. At time 0 h, the amount of RSH is higher than in M9, suggesting lower intracellular stress because of the dilution in the broth that still contains nutrients (panel B). A constant concentration of RSH is observed at all stages of bacterial growth, suggesting that the upregulation of expression of cysteine producing enzymes is not necessary, since bacteria can obtain enough cysteine from the environmental broth. Cysteine uptake is energetically favourable comparing to its biosynthesis, where for each mole of cysteine synthesized 1 mole of GTP, 2 moles of ATP and 1 mole of NADH are required [40,142]. The hypothesis of cysteine uptake from the broth is further confirmed by literature data stating that addition of cysteine in M9 prevents defects in the growth of *ΔcysJIH* mutant and *ΔcysE* auxotroph strains of *S.* Typhimurium [49,143]. Because the effect of

triazole in 20 % LB medium cannot be observed, it was concluded that this broth is not appropriate for evaluation of reactivity between UPAR inhibitors and target enzymes.

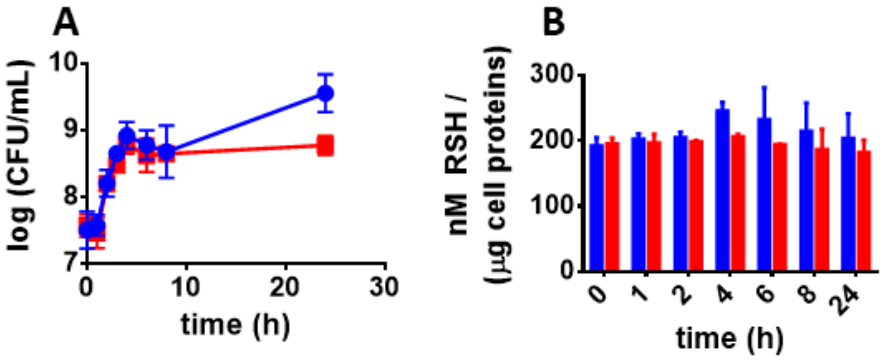

Figure 36. Legend: blue – cells in 20 % LB; red – cells in 20 % LB + 5 mM triazole. Panel A: E. coli ATCC 35218 growth in 20 % LB in the absence and presence of triazole. Panel B: RSH production in E. coli ATCC 35218, grown in 20 % LB in the absence and presence of triazole. Assays were performed in 2 biological replicates.

By comparing the RSH behaviour in M9 and 20 % LB it can be hypothesized that *E. coli* tends to maintain RSH concentrations around 200 nM / µg cellular proteins, likely being an optimal concentration for maintenance of intracellular redox balance. When concentrations of RSH are lower, bacteria are more vulnerable to reactive oxygen species, as they possess fewer molecules with antioxidant properties. Higher concentrations are potentially toxic for the cell [144,145]. Maintenance of physiological RSH pool is a complex interplay between regulation of cysteine biosynthesis, such as induction of cysteine regulon by CysB and *N*-acetylserine, its repression by interaction between CysB, H_2S and cysteine [90,143,144,146,147], SAT and OASS feedback inhibition by cysteine [86,89,114] and cysteine synthase complex [84].

Cysteine itself possesses antioxidant activity and is a precursor of other important antioxidants, such as glutathione and mycothiol [40,148]. Inhibition of its biosynthesis has been linked to increased intracellular oxidative stress [49]. To validate that the RSH method is also appropriate to observe changes in the intracellular redox state, *E. coli* was grown until the mid-exponential phase in M9 and exposed to H_2O_2, a known inducer of oxidative stress. Cells were exposed to increasing concentrations of H_2O_2 for 10 minutes and RSH were measured in samples, where cell viability was not affected (Figure 37). Low concentration of H_2O_2 slightly increase levels of RSH. This is likely due to the induction of *oxyR* and *soxR* operons, leading to the expression of defence mechanisms, such as catalase, that effectively scavenge toxic oxygen species [49,149,150]. Concentrations above 5 mM decrease the number of thiols to the levels that are measured in cells when they are diluted from O/N culture in M9 (Figure 35).

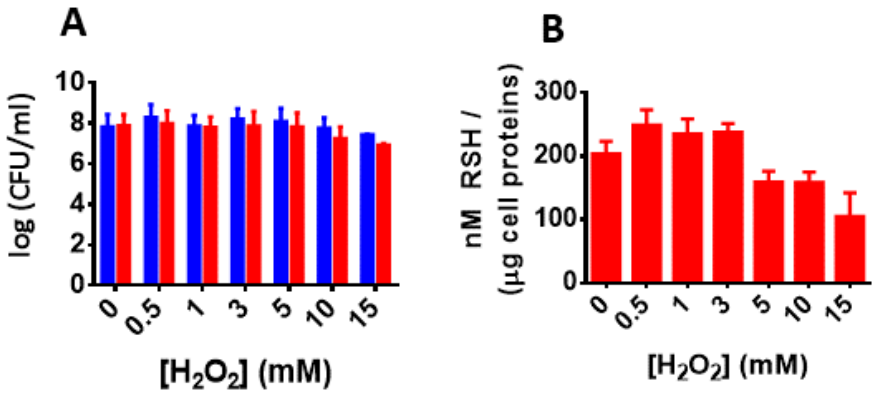

Figure 37. Effect of H_2O_2 on E. coli ATCC 35218. Legend: blue – cells before exposure to H_2O_2; red – cells after exposure to H_2O_2. Panel A: CFU before and after 10 min exposure to H_2O_2. Panel B: RSH after 10 min exposure to H_2O_2. Data are the average of two replicates.

3.3. EFFECT OF UPAR INHIBITORS ON INTRACELLULAR THIOLS

UPAR415 and UPAR329 were chosen to evaluate the effect of inhibitors on cysteine biosynthesis by RSH measurement. *E. coli* ATCC 35218 was grown in M9 + 0.4 % glucose in the presence of 3 μg/mL PMBN until the mid-exponential phase and then exposed to UPAR inhibitor at MIC concentration. For UPAR415, 256 μg/mL was chosen in order to exclude any unspecific effects originating from higher concentrations.

Cells were grown until the mid-exponential phase before the exposure to the compounds because of the sensitivity limitations of RSH measurements. In order to have a TNB signal strong enough to be in the linear range of the spectrophotometer, measurements need to be performed with at least 5 x 10^8 CFU. To have this number of CFU when cells are in the lag phase, roughly 15 mL of the culture has to be withdrawn and pelleted. Consequently, for measurement of RSH at several time points, the volume of the culture should be high enough. Large culture volume also requires an increased amount of inhibitors used in order to maintain the same concentration. The estimated quantity of compounds, needed for RSH measurement throughout the complete growth curve, was not feasible to produce. For this reason, bacteria were grown until the mid-exponential phase and inhibitor was added to the 10 mL of the culture. Under these conditions we were able to withdraw culture aliquots of volumes between 1 and 2 mL. Figure 38, panel A shows that compounds do not cause any inhibition of bacterial growth under assay conditions. Also triazole is not able to significantly

interfere with bacterial growth. This is expected since in the exponential phase the internal pool of cysteine is high enough to support the bacterial growth even if its biosynthesis is inhibited [39]. In terms of RSH (panel B), UPAR inhibitors are causing a small, not significant decrease in the RSH concentrations comparing to the untreated control. Triazole is able to prevent the synthesis of thiols, but it cannot lower their concentration enough to prevent the bacterial growth.

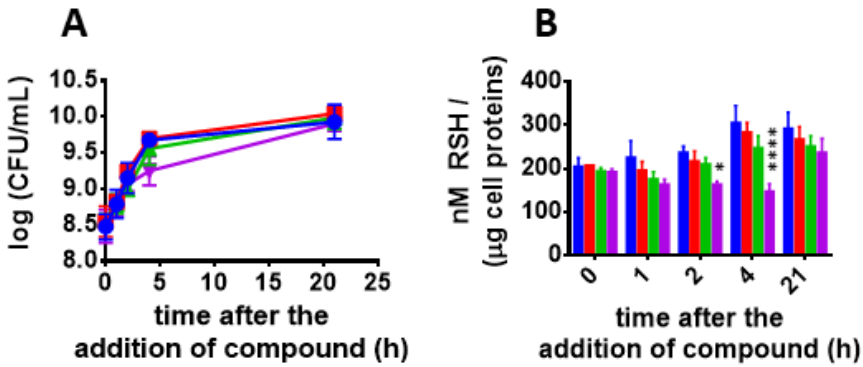

*Figure 38. Effect of UPAR compounds on E. coli ATCC35218. Legend of broth conditions – all M9 + 0.4 % glucose with the addition of: blue – 1 % DMSO; red – 32 µg/mL UPAR-329; green – 256 µg/mL UPAR-415; purple – 5 mM triazole, 1 % DMSO. Panel A: effect of compounds on bacterial growth. Panel B: effect of compounds on RSH concentration. Data are showing the average of 2 biological replicates. Statistical significance was performed by 2way Anova and values are shown in a comparison with a DMSO control at a specific time point. * - p< 0.05; **** - p<0.0001.*

These observations are raising questions of data discrepancy between different experiments. In MIC assays compounds clearly inhibited bacterial growth, while they did not cause any significant effect in thiols concentration. The important difference arises from the assay structure – in MIC assay, bacteria are exposed to the inhibitor in the lag phase and

in the RSH assay in the exponential phase. We have demonstrated that the amount of thiols (and likely, the internal pool of cysteine) is higher in the exponential than in the lag phase (Figure 35). Presumably, the amount of RSH correlates with the amount of OASS and SAT present in the cell. Therefore, the effect of cysteine biosynthesis inhibition on cell viability/thiol content is more evident in the lag phase than in the exponential phase. It is proposed that for the inhibition of cysteine biosynthesis in exponential phase a higher concentration of the compound is needed. This theory is further supported by the literature stating that in the case of the natural antimicrobial compound, allicin, inhibition of bacterial growth in the exponential phase can be reached by compound in concentration 6-times higher than the MIC. Under these conditions, allicin also causes a significant decrease in the amount of RSH [151]. Taking into account the high MIC of UPAR inhibitors, increasing their concentrations in microbiological assays is not feasible and meaningful. Another possibility for the loss of the effect of inhibitors on RSH and bacterial growth in the exponential phase is the bacterial adaptation that is more efficient in the exponential phase when cells are more active. Inhibition of OASS leads to the accumulation of OAS, that is converted to NAS which induces transcription of whole cysteine operon (see section General introduction, Figure 1) [90]. In this way, more OASS is produced and the amount of compound inside bacteria is not sufficient anymore. The mechanism of bacterial adaptation after inhibition of SAT is unknown. For confirmation of OASS and SAT inhibition inside the bacteria, ideally RSH would be measured in the lag phase. With the existing method, this approach is not feasible due to its limited sensitivity.

A new, more sensitive method, that requires less chemical material and cells should be applied to address this issue, such as labelling thiol groups with N-ethylmaleimide or fluorescence probes and chromatographic analysis [152].

CONCLUSIONS

The project started with the preparation of proteins and the development of activity assays necessary for testing of OASS and SAT inhibitors. We optimized the expression constructs and purification conditions for both isozymes of StOASS and StSAT and we were able to obtain pure proteins in high yields. We designed and validated an indirect continuous activity assay for StSAT, which was later used for identification and characterization of inhibitors. This assay was applied in a cuvette based assays in our laboratory as well as for high-throughput screening on 96-well-plates in partner laboratories.

The design of StOASS reversible inhibitors is a good example of a successful medicinal chemistry approach by mimicking nature. The crystal structure of StOASS-A in the complex with UPAR-415 revealed how efficiently the low-molecular-weight (LMW) inhibitor is mimicking the C-terminal part of SAT, leading to inhibition of StOASS. Additionally, the high-resolution crystal structure allowed to observe small changes in the conformation of StOASS-A in the presence of inhibitor and it will in future serve as an excellent model for *in silico* screening of new inhibitors.

The permeability of LMW molecules through the complex outer membrane of Gram-negative bacteria is one of the main pitfalls in the development of new antibiotics. Relatively high logP and negatively charged carboxylic group of the existing StOASS reversible inhibitors are unfavourable characteristics regarding the membrane permeability. In order to increase the drug-likeness and penetration, several derivatives of UPAR-415 were prepared for increasing the compound polarity and

diminishing the negative charge. When the carboxylic group was substituted by the biosiosters, partial inhibition was observed, suggesting a different mechanism of action with respect to carboxylic compounds. Substitution of the tolyl group on Cα by polar heterocycles managed to retain good affinity towards the StOASS-A, while they were less potent inhibitors of the B isoform. The issue of the selectivity towards one of the isozymes was overcomed when the substitution was performed on Cβ. Derivatives with bulky polar side groups exhibited good K_ds for the both isozymes and are promising candidates for microbiological testing, promising complete inhibition of cysteine biosynthesis *in vivo*.

Considering the discrepancy between the characteristics of existing reversible inhibitors, that are substituted cyclopropanes, and generally favourable characteristics of antibiotics, identification of novel fragments for structurally different inhibitors was carried out by a scaffold hopping approach. The identified fragment was a carboxylated pyrazole. This fragment and its derivatives are weak StOASS inhibitors, while they possess similar ligand efficiency as UPAR-415. Even though their affinities against the target are not high, their physicochemical characteristics are favourable in terms of antibiotic design and permeability and therefore are attractive candidates for microbiological screening.

We also approached the inactivation of StOASS by fluoroalanine derivatives. Monofluoroalanine was found to behave as substrate analog and trifluoroalanine as weak mechanism based inactivator. Covalent modification of StOASS by fluoroalanines seem to be inefficient, likely due

to the formation of reactive intermediate that is in geometrically unfavourable position to undergo the Michael attack by enzyme nucleophile. Therefore, covalent modification is a slow process and the intermediate hydrolyzes before it could cause inactivation. Consequently, high concentrations of inactivator are needed to observe any measurable effects. In order to expand the knowledge of enzyme inactivation and improve the potency of fluoroalanines, several *N*- and *S*-substituted derivatives with replaced carboxylic group were tested and inhibitors with a similar mechanism of action as trifluoroalanine were identified. These are the first reported derivatives of modified amino acid that can react with a PLP dependent enzyme and since they exhibit similar affinity towards StOASS as trifluoroalanine, they present a promising path towards a more efficient enzyme inactivation.

In this project, the first medicinal chemistry campaign for the identification of StSAT inhibitors was carried out. First, *in silico* screening of in house compound library was carried out to identify an active fragment that was later optimized in terms of higher affinity. We found that substituted heterocycles are able to inhibit StSAT in micromolar range and that they are competitive against AcCoA. By high-throughput screening of commercially available library, structurally different SAT inhibitors were identified. Their physicochemical properties make them favourable for the bacterial membrane permeability. While some of StSAT inhibitors are very potent (IC_{50} ~ 1 μM), during the following steps of drug design, special attention should be carried out to identify any possible cross-reactivity with other AcCoA-dependent enzymes.

Microbiological evaluation of potent protein inhibitors failed to identify a molecule that is able to penetrate in Gram-negative bacteria. In the presence of membrane permeability enhancer, assayed compounds showed *in vivo* activity only at high concentrations and consequently their use in further steps of antibiotics development does not seem very promising. A strategy might be to carry out growth inhibition assays with other inhibitors, even if they are less potent *in vitro*, to identify whether they possess any structural characteristics that are more favourable for the permeation through the complex Gram-negative bacteria and higher potency *in vivo*.

ACKNOWLEDGEMENTS

When I applied for the position of ESR within Marie Curie INTEGRATE ITN project in 2015, I had big expectations for exciting international experience, I hoped to learn from the best scientists and to become a successful researcher. In three years of INTEGRATE project I gained lots of knowledge and experience and I will always be grateful for this opportunity. Soon after my arrival to Parma, I realized how lucky I was to be chosen for a particular position in Prof. Mozzarelli's group.

I would like to express sincere gratitude to my advisors, Prof. Andrea Mozzarelli and Assoc. Prof. Barbara Campanini for constant support, guidance and teaching. You were always available for discussions and provided me with advices. I could not wish for better supervisors and I will keep you in a fond memory.

My performance in the lab would not be the same withouth my colleagues. My deepest acknowledgements go to my tutor and friend Roberto Benoni for helping me start in the lab and introducing me to the proteins and laboratory techniques. I would like to thank to Omar de Bei for all his help and to Stefano Armao for carrying out experiments with SAT. I am grateful that every single person in Mozzarelli's group made me feel welome and a part of the team, you guys are the reason I am already missing Parma.

The scientific work could not be performed without the collabolators. My sincere thanks go to Gabriele Costantino, Marco Pieroni, Joana Magalhães, Aigars Jirgensons and Konstantinos Grammatoglou for all the hard work they had put in the design and synthesis of inhibitors, to Paola Storici and Nicola Dimitri for collecting the data of protein crystals, and to Martin Welch and Antonio Felici for hosting me on secondments in their laboratories.

I would like to acknowledge my family for accepting my decision to move abroad and supporting me every step of the way. And finally to Jernej, whom I need to thank for continuous encouragement.

REFERENCES

[1] WHO. Antibiotic resistance [Internet]. [cited 2018 Aug 28]. Available from: http://www.who.int/news-room/fact-sheets/detail/antibiotic-resistance.

[2] Ventola CL. The Antibiotic Resistance Crisis Part 1 : Causes and Threats. P&T. 2015;40:277–283.

[3] Gould IM, Bal AM. New antibiotic agents in the pipeline and how hey can help overcome microbial resistance. Virulence. 2013;4:185–191.

[4] Levy SB, Marshall B. Antibacterial resistance worldwide : causes , challenges and responses. Nat. Med. 2004;10:122–129.

[5] Tackling drug-resistant infections globally [Internet]. [cited 2019 Jan 15]. Available from: https://amr-review.org.

[6] Bush K, Page MGP. What we may expect from novel antibacterial agents in the pipeline with respect to resistance and pharmacodynamic principles. J. Pharmacokinet. Pharmacodyn. 2017;44:113–132.

[7] Higgins PG, Dammhayn C, Hackel M, et al. Global spread of carbapenem-resistant Acinetobacter baumannii. J. Antimicrob. Chemother. 2010;65:233–238.

[8] Lewis K. Platforms for antibiotic discovery. Nat. Rev. Drug Discov. 2013;12:371–387.

[9] European Centre for Disease Prevention and Control. Antimicrobial Resistance and Healthcare-associated Infections Programme [Internet]. [cited 2018 Sep 3]. Available from: https://ecdc.europa.eu/en/about-us/who-we-are/disease-

programmes/antimicrobial-resistance-and-healthcare-associated.

[10] WHO. Global priority list of antibiotic-resistant bacteria to guide research, discovery, and development of new antibiotics. [Internet]. [cited 2018 Aug 28]. Available from: http://www.who.int/medicines/publications/global-priority-list-antibiotic-resistant-bacteria/en/.

[11] Lewis K. Antibiotics: Recover the lost art of drug discovery. Nature. 2012;485:439–440.

[12] Smith PA, Koehler MFT, Girgis HS, et al. Optimized arylomycins are a new class of Gram-negative antibiotics. Nature. 2018;561:189–194.

[13] Delcour AH. Outer membrane permeability and antibiotic resistance. Biochim. Biophys. Acta - Proteins Proteomics. 2009;1794:808–816.

[14] Brown DG. Drug discovery strategies to outer membrane targets in Gram-negative pathogens. Bioorg. Med. Chem. 2016;24:6320–6331.

[15] Miller SI, Salama NR. The gram-negative bacterial periplasm: Size matters. PLoS Biol. 2018;16:1–7.

[16] Bellio P, Luzi C, Mancini A, et al. Cerium oxide nanoparticles as potential antibiotic adjuvant. Effects of CeO2 nanoparticles on bacterial outer membrane permeability. BBA - Biomembr. 2018;1860:2428–2435.

[17] Zgurskaya HI, López CA, Gnanakaran S. Permeability Barrier of Gram-Negative Cell Envelopes and Approaches to Bypass It. ACS Infect. Dis. 2016;1:512–522.

[18] Nicolaou KC, Rigol S. A brief history of antibiotics and select advances in their synthesis. J. Antibiot. (Tokyo). 2018;71:153–184.

[19] Spellberg B, Powers JH, Brass EP, et al. Trends in Antimicrobial Drug Development: Implications for the Future. Clin. Infect. Dis. 2004;38:1279–1286.

[20] Andries K, Verhasselt P, Guillemont J, et al. A Diarylquinoline Drug Active on the ATP Synthase of Mycobacterium tuberculosis. Science (80-.). 2005;307:223–227.

[21] González-Bello C. Antibiotic adjuvants – A strategy to unlock bacterial resistance to antibiotics. Bioorg. Med. Chem. Lett. 2017;27:4221–4228.

[22] Rampioni G, Pillai CR, Longo F, et al. Effect of efflux pump inhibition on Pseudomonas aeruginosa transcriptome and virulence. Sci. Rep. 2017;7:1–14.

[23] Y. Mahmood H, Jamshidi S, Mark Sutton J, et al. Current Advances in Developing Inhibitors of Bacterial Multidrug Efflux Pumps. Curr. Med. Chem. 2016;23:1062–1081.

[24] Lomovskaya O, Zgurskaya HI, Totrov M, et al. Waltzing transporters and “the dance macabre” between humans and bacteria. Nat. Rev. Drug Discov. 2007;6:56–65.

[25] Vaara M. Agents that increase the permeability of the outer membrane. Microbiol. Rev. 1992;56:395–411.

[26] Rishi P, Vij S, Maurya IK, et al. Peptides as adjuvants for ampicillin and oxacillin against methicillin-resistant Staphylococcus aureus (MRSA). Microb. Pathog. 2018;124:11–20.

[27] Milton ME, Minrovic BM, Harris DL, et al. Re-sensitizing Multidrug

Resistant Bacteria to Antibiotics by Targeting Bacterial Response Regulators: Characterization and Comparison of Interactions between 2-Aminoimidazoles and the Response Regulators BfmR from Acinetobacter baumannii and QseB from Fr. Front. Mol. Biosci. 2018;5:1–12.

[28] Clinical trials. [Internet]. [cited 2018 Sep 10]. Available from: https://clinicaltrials.gov/.

[29] Martin-Loeches I, Dale GE, Torres A. Murepavadin: a new antibiotic class in the pipeline. Expert Rev. Anti. Infect. Ther. 2018;16:259–268.

[30] Pantel L, Florin T, Dobosz-Bartoszek M, et al. Odilorhabdins, Antibacterial Agents that Cause Miscoding by Binding at a New Ribosomal Site. Mol. Cell. 2018;70:83–94.e7.

[31] Nichols D, Cahoon N, Trakhtenberg EM, et al. Use of ichip for high-throughput in situ cultivation of “uncultivable” microbial species. Appl. Environ. Microbiol. 2010;76:2445–2450.

[32] Ling LL, Schneider T, Peoples AJ, et al. A new antibiotic kills pathogens without detectable resistance. Nature. 2015;517:455–459.

[33] Centers for Disease Control and Prevention. Salmonella [Internet]. [cited 2018 Oct 3]. Available from: https://www.cdc.gov/salmonella/general/index.html.

[34] Broz P, Ohlson MB, Monack DM. Innate immune response to Salmonella typhimurium, a model enteric pathogen. Gut Microbes. 2012;3:62–70.

[35] Fàbrega A, Vila J. Salmonella enterica serovar Typhimurium skills

to succeed in the host: Virulence and regulation. Clin. Microbiol. Rev. 2013;26:308–341.

[36] Eng SK, Pusparajah P, Ab Mutalib NS, et al. Salmonella: A review on pathogenesis, epidemiology and antibiotic resistance. Front. Life Sci. 2015;8:284–293.

[37] Almeida F, Seribelli AA, In M, et al. Phylogenetic and antimicrobial resistance gene analysis of Salmonella Typhimurium strains isolated in Brazil by whole genome sequencing. PLoS One. 2018;1–16.

[38] Feasey NA, Dougan G, Kingsley RA, et al. Invasive non-typhoidal salmonella disease : an emerging and neglected tropical disease in Africa. Lancet. 2012;379:2489–2499.

[39] Hulanicka D, Klopotowski S, Smith DA. The Effect of Triazole on Cysteine Biosynthesis in Salmonella typhimurium. J. Gen. Microbiol. 1972;72:291–301.

[40] Sekowska A, Kung H, Danchin A. Sulfur Metabolism in Escherichia coli and Related Bacteria : Facts and Fiction. 2000;2:145–177.

[41] Beinert H. A tribute to sulfur. Eur. J. Biochem. 2000;267:5657–5664.

[42] Mihara H, Esaki N. Bacterial cysteine desulfurases : their function and mechanisms. Appl Microbiol Biotechno. 2002;60:12–23.

[43] Kessler D. Enzymatic activation of sulfur for incorporation into biomolecules in prokaryotes. FEMS Microbiol Rev. 2006;30:825–840.

[44] Mozzarelli A, Bettati S, Campanini B, et al. The multifaceted pyridoxal 5’-phosphate-dependent O-acetylserine sulfhydrylase.

Biochim. Biophys. Acta - Proteins Proteomics. 2011;1814:1497–1510.

[45] Jothivasan VK, Hamilton CJ. Mycothiol: Synthesis, biosynthesis and biological functions of the major low molecular weight thiol in actinomycetes. Nat. Prod. Rep. 2008;25:1091–1117.

[46] Shelly CL. Glutathione synthesis. Biochim. Biophys. Acta - Gen. Subj. 2013;1830:3143–3153.

[47] Senaratne RH, De Silva AD, Williams SJ, et al. 5'-Adenosinephosphosulphate reductase (CysH) protects Mycobacterium tuberculosis against free radicals during chronic infection phase in mice. Mol. Microbiol. 2006;59:1744–1753.

[48] Lestrate P, Delrue RM, Danese I, et al. Identification and characterization of in vivo attenuated mutants of Brucella melitensis. Mol. Microbiol. 2000;38:543–551.

[49] Turnbull AL, Surette MG. Cysteine biosynthesis, oxidative stress and antibiotic resistance in Salmonella typhimurium. Res. Microbiol. 2010;161:643–650.

[50] Turnbull AL, Surette MG. L-Cysteine is required for induced antibiotic resistance in actively swarming Salmonella enterica serovar Typhimurium. Microbiology. 2008;154:3410–3419.

[51] Kohanski MA, Dwyer DJ, Hayete B, et al. A Common Mechanism of Cellular Death Induced by Bactericidal Antibiotics. Cell. 2007;130:797–810.

[52] Campanini B, Pieroni M, Raboni S, et al. Inhibitors of the sulfur assimilation pathway in bacterial pathogens as enhancers of antibiotic therapy. Curr. Med. Chem. 2015;22:187–213.

[53] Hatzios SK, Bertozzi CR. The regulation of sulfur metabolism in mycobacterium tuberculosis. PLoS Pathog. 2011;7:1–9.

[54] Steiner EM, Böth D, Lössl P, et al. CysK2 from Mycobacterium tuberculosis is an O-phospho-L-serine-dependent S-sulfocysteine synthase. J. Bacteriol. 2014;196:3410–3420.

[55] Westrop GD, Goodall G, Mottram JC, et al. Cysteine Biosynthesis in Trichomonas vaginalis Involves Cysteine Synthase Utilizing O -Phosphoserine. J. Biol. Chem. 2006;281:25062–25075.

[56] Nakamura T, Kawai Y, Kunimoto K, et al. Structural Analysis of the Substrate Recognition Mechanism in O-Phosphoserine Sulfhydrylase from the Hyperthermophilic Archaeon Aeropyrum pernix K1. J. Mol. Biol. 2012;422:33–44.

[57] Mino K, Ishikawa K. A novel O-phospho-L-serine sulfhydrylation reaction catalyzed by O-acetylserine sulfhydrylase from Aeropyrum pernix K1. FEBS Lett. 2003;551:133–138.

[58] Nakamura T, Kon Y, Iwahashi H, et al. Evidence that thiosulfate assimilation by Salmonella typhimurium is catalyzed by cysteine synthase B. J. Bacteriol. 1983;156:656–662.

[59] Zhao C, Kumada Y, Imanaka H, et al. Cloning, overexpression, purification, and characterization of O-acetylserine sulfhydrylase-B from Escherichia coli. Protein Expr. Purif. 2006;47:607–613.

[60] Nakatani T, Ohtsu I, Nonaka G, et al. Enhancement of thioredoxin/glutaredoxin-mediated L-cysteine synthesis from S-sulfocysteine increases L-cysteine production in Escherichia coli. Microb. Cell Fact. 2012;11.

[61] Schnell R, Oehlmann W, Singh M, et al. Structural Insights into

Catalysis and Inhibition of O -Acetylserine Sulfhydrylase from Mycobacterium tuberculosis. J. Biol. Chem. 2007;282:23473–23481.

[62] O'Leary SE, Jurgenson CT, Ealick SE, et al. O -Phospho- L -serine and the Thiocarboxylated Sulfur Carrier Protein CysO-COSH Are Substrates for CysM , a Cysteine Synthase from Mycobacterium tuberculosis. Biochemistry. 2008;47:11606–11615.

[63] Palde PB, Bhaskar A, Pedró Rosa LE, et al. First-In-Class Inhibitors of Sulfur Metabolism with Bactericidal Activity against Non-Replicating M. tuberculosis. ACS Chem. Biol. 2015;acschembio.5b00517.

[64] Brunner K, Maric S, Reshma RS, et al. Inhibitors of the cysteine synthase CysM with antibacterial potency against dormant mycobacterium tuberculosis. J. Med. Chem. 2016;59:6848–6859.

[65] Franko N, Grammatoglou K, Campanini B, et al. Inhibition of *O* -acetylserine sulfhydrylase by fluoroalanine derivatives. J. Enzyme Inhib. Med. Chem. 2018;33:1343–1351.

[66] Cook PF, Wedding RT. A reaction mechanism from steady state kinetic studies for O-acetylserine sulfhydrylase from Salmonella typhimurium LT-2. J. Biol. Chem. 1976;251:2023–2029.

[67] Chattopadhyay A, Meier M, Ivaninskii S, et al. Structure, mechanism, and conformational dynamics of O-acetylserine sulfhydrylase from Salmonella typhimurium: Comparison of A and B isozymes. Biochemistry. 2007;46:8315–8330.

[68] Tai CH, Nalabolu SR, Jacobsen TM, et al. Kinetic Mechanisms of the A and B Isozymes of O-Acetylserine Sulfhydrylase from

Salmonella typhimurium LT-2 Using the Natural and Alternative Reactants. Biochemistry. 1993;6433–6442.

[69] Burkhard P, Jagannatha Rao G., Hohenester E, et al. Three-dimensional structure of O-acetylserine sulfhydrylase from Salmonella typhimurium. J. Mol. Biol. 1998;283:121–133.

[70] Burkhard P, Tai CH, Ristroph CM, et al. Ligand binding induces a large conformational change in O-acetylserine sulfhydrylase from Salmonella typhimurium. J. Mol. Biol. 1999;291:941–953.

[71] Burkhard P, Tai CH, Jansonius JN, et al. Identification of an allosteric anion-binding site on O-acetylserine sulfhydrylase: structure of the enzyme with chloride bound. J. Mol. Biol. 2000;303:279–286.

[72] Benci S, Vaccari S, Mozzarelli A, et al. Time-resolved fluorescence of O-acetylserine sulfhydrylase. Biochim. Biophys. Acta - Protein Struct. Mol. Enzymol. 1999;1429:317–330.

[73] Benci S, Vaccari S, Mozzarelli A, et al. Time-Resolved Fluorescence of O -Acetylserine Sulfhydrylase Catalytic Intermediates. Biochemistry. 1997;36:15419–15427.

[74] Salsi E, Guan R, Campanini B, et al. Exploring O-acetylserine sulfhydrylase-B isoenzyme from Salmonella typhimurium by fluorescence spectroscopy. Arch. Biochem. Biophys. 2011;505:178–185.

[75] Tanous C, Soutourina O, Raynal B, et al. The CymR Regulator in Complex with the Enzyme CysK Controls Cysteine Metabolism in Bacillus subtilis. J. Biol. Chem. 2008;283:35551–35560.

[76] Benoni R, Beck CM, Garza-sánchez F, et al. Activation of an anti-

bacterial toxin by the biosynthetic enzyme CysK : mechanism of binding , interaction specificity and competition with cysteine synthase. Sci. Rep. 2017;7:1–16.

[77] Singh P, Brooks II JF, Ray VA, et al. CysK Plays a Role in Biofilm Formation and Colonization by Vibrio fischeri. Appl. Environ. Microbiol. 2015;81:5223–5234.

[78] Filutowicz M, Wiater A, Hulanicka D. Delayed Inducibility of Sulphite Reductase in cysM Mutants of Salmonella typhimurium Under Anaerobic Conditions. J. Gen. Microbiol. 1982;128:1791–1794.

[79] Hulanicka MD, Hallquist SG, Kredich NM, et al. Regulation of O-acetylserine sulfhydrylase B by L-cysteine in Salmonella typhimurium. J. Bacteriol. 1979;140:141–146.

[80] Kröger C, Colgan A, Srikumar S, et al. An Infection-Relevant Transcriptomic Compendium for Salmonella enterica Serovar Typhimurium. Cell Host Microbe. 2013;14:683–695.

[81] Kredich NM, Tomkins GM. The Enzymic Synthesis of L-Cysteine in Escherichia coli nad Salmonella typhimurium. J. Biol. Chem. 1966;241:4955–4966.

[82] Wiebers JL, Garner HR. Acyl derivatives of homoserine as substrates for homocysteine synthesis in Neurospora crassa, yeast, and Escherichia coli. J. Biol. Chem. 1967;242:5644–5649.

[83] Hindson VJ, Shaw W V. Random-order ternary complex reaction mechanism of serine acetyltransferase from Escherichia coli. Biochemistry. 2003;42:3113–3119.

[84] Benoni R, De Bei O, Paredi G, et al. Modulation of *Escherichia coli*

serine acetyltransferase catalytic activity in the cysteine synthase complex. FEBS Lett. 2017;591:1212–1224.

[85] Pye VE, Tingey AP, Robson RL, et al. The structure and mechanism of serine acetyltransferase from Escherichia coli. J. Biol. Chem. 2004;279:40729–40736.

[86] Olsen LR, Huang B, Vetting MW, et al. Structure of serine acetyltransferase in complexes with CoA and its cysteine feedback inhibitor. Biochemistry. 2004;43:6013–6019.

[87] Hindson VJ, Moody PCE, Rowe AJ, et al. Serine acetyltransferase from Escherichia coli is a dimer of trimers. J. Biol. Chem. 2000;275:461–466.

[88] Gorman J, Saphiro L. Structure of serine acetyltransferase from Haemophilus influenzae Rd. Acta Crystallogr. D-Biological Crystallogr. 2004;60:1600–1605.

[89] Hindson VJ. Serine acetyltransferase of Escherichia coli: substrate specificity and feedback control by cysteine. Biochem. J. 2003;375:745–752.

[90] Lynch AS, Tyrrell R, Smerdon SJ, et al. Characterization of the CysB protein of Klebsiella aerogenes: direct evidence that N-acetylserine rather than O-acetylserine serves as the inducer of the cysteine regulon. Biochem. J. 1994;299:129–136.

[91] Mino K, Hiraoka K, Imamura K, et al. Characteristics of Serine Acetyltransferase from Escherichia coli Deleting Different Lengths of Amino Acid Residues from the C-Terminus. Biosci. Biotechnol. Biochem. 2000;64:1874–1880.

[92] Campanini B, Speroni F, Salsi E, et al. Interaction of serine

acetyltransferase with O-acetylserine sulfhydrylase active site: evidence from fluorescence spectroscopy. Protein Sci. 2005;14:2115–2124.

[93] Huang B, Vetting MW, Roderick SL. The Active Site of O-Acetylserine Sulfhydrylase Is the Anchor Point for Bienzyme Complex Formation with Serine Acetyltransferase. J. Bacteriol. 2005;187:3201–3205.

[94] Zhao C, Moriga Y, Feng B, et al. On the interaction site of serine acetyltransferase in the cysteine synthase complex from Escherichia coli. Biochem. Biophys. Res. Commun. 2006;341:911–916.

[95] Kredich NM, Becker MA, Tomkins GM. Purification and Characterization a Bifunctional Protein Complex , Salmonella typhimurium of Cysteine from. J. Biol. Chem. 1969;244.

[96] Salsi E, Bayden AS, Spyrakis F, et al. Design of O-acetylserine sulfhydrylase inhibitors by mimicking nature. J. Med. Chem. 2010;53:345–356.

[97] Pieroni M, Annunziato G, Beato C, et al. Rational Design, Synthesis, and Preliminary Structure-Activity Relationships of α-Substituted-2-Phenylcyclopropane Carboxylic Acids as Inhibitors of Salmonella typhimurium O-Acetylserine Sulfhydrylase. J. Med. Chem. 2016;59:2567–2578.

[98] Shea RO, Moser HE. Physicochemical Properties of Antibacterial Compounds : Implications for Drug Discovery Perspective Physicochemical Properties of Antibacterial Compounds : Implications for Drug Discovery. J. Med. Chem. 2008;51:2871–

2878.

[99] Brown ED, Wright GD. Antibacterial drug discovery in the resistance era. Nature. 2016;529:336–343.

[100] Brown DG, May-Dracka TL, Gagnon MM, et al. Trends and exceptions of physical properties on antibacterial activity for gram-positive and gram-negative pathogens. J. Med. Chem. 2014;57:10144–10161.

[101] Singh J, Petter RC, Baillie TA, et al. The resurgence of covalent drugs. Nat. Rev. Drug Discov. 2011;10:307–317.

[102] Baillie TA. Targeted Covalent Inhibitors for Drug Design. Angew. Chemie - Int. Ed. 2016;55:13408–13421.

[103] Copeland RA. Evaluation of Enzyme Inhibitors in Drug Discovery. John Wiley Sons, Inc. 2005.

[104] Silverman RB. Mechanism-based enzyme inactivators. Methods Enzymol. 1995;249:240–283.

[105] Azam MA, Jayaram U. Inhibitors of alanine racemase enzyme: A review. J. Enzyme Inhib. Med. Chem. 2016;31:517–526.

[106] John RA, Tudball N. Evidence for Induced Fit of a Pseudo-Substrate of Aspartate Aminotransferase. Eur. J. Biochem. 1972;138:135–138.

[107] Silverman RB, Abeles RH. Mechanism of Inactivation of γ-Cystathionase by β,β,β-Trifluoroalanine. Biochemistry. 1977;16:5515–5520.

[108] Alston A, Mumats H, Uedat T, et al. Inactivation of λ-cystathionase by λ-fluorinated amino acids. FEBS Lett. 1981;128:293–297.

[109] Phillips RS, Dua RK. Indole protects tryptophan indole-lyase, but not tryptophan synthase, from inactivation by trifluoroalanine. Arch. Biochem. Biophys. 1992;296:489–496.

[110] Silverman RB, Abeles RH. Inactivation of Pyridoxal Phosphate Dependent Enzymes by Mono- and Polyhaloalanines. Biochemistry. 1976;15:4718–4723.

[111] Withers SG, Tysoe C. Fluorinated Mechanism-Based Inhibitors: Common Themes and Recent Developments. Curr. Top. Med. Chem. 2014. p. 865–874.

[112] Wang EA, Walsh C. Characteristics of β,β-difluoroalanine and β,β,β-trifluoroalanine as suicide substrates for Escherichia coli B alanine racemase. Biochemistry. 1981;20:7539–7546.

[113] Faraci WS, Walsh CT. Mechanism of Inactivation of Alanine Racemase by β,β,β-Trifluoroalanine. Biochemistry. 1989;28:431–437.

[114] Agarwal SM, Jain R, Bhattacharya A, et al. Inhibitors of Escherichia coli serine acetyltransferase block proliferation of Entamoeba histolytica trophozoites. Int. J. Parasitol. 2008;38:137–141.

[115] Kapust RB, Tözsér J, Fox JD, et al. Tobacco etch virus protease: mechanism of autolysis and rational design of stable mutants with wild-type catalytic proficiency. Protein Eng. Des. Sel. 2001;14:993–1000.

[116] Dolan SK, Bock T, Hering V, et al. Structural, mechanistic and functional insight into gliotoxin bis-thiomethylation in Aspergillus fumigatus. Open Biol. 2017;7.

[117] Shastry RP, Dolan SK, Abdelhamid Y, et al. Purification and

characterisation of a quorum quenching AHL-lactonase from the endophytic bacterium Enterobacter sp. CS66. FEMS Microbiol. Lett. 2018;365:1–7.

[118] Gaitonde MK. A spectrophotometric method for the direct determination of cysteine in the presence of other naturally occurring amino acids. Biochem. J. 1967;104:627–633.

[119] Eyer P, Worek F, Kiderlen D, et al. Molar absorption coefficients for the reduced ellman reagent: Reassessment. Anal. Biochem. 2003;312:224–227.

[120] Benci S, Bettati S, Vaccari S, et al. Conformational probes of O-acetylserine sulfhydrylase: fluorescence of tryptophans 50 and 161. J. Photochem. Photobiol. B Biol. 1999;48:17–26.

[121] Leu LS, Cook PF. Kinetic Mechanism of Serine Transacetylase from Salmonella typhimurium. Biochemistry. 1994;33:2667–2671.

[122] Annunziato G, Pieroni M, Benoni R, et al. Cyclopropane-1,2-dicarboxylic acids as new tools for the biophysical investigation of O-acetylserine sulfhydrylases by fluorimetric methods and saturation transfer difference (STD) NMR. J. Enzyme Inhib. Med. Chem. 2016;31:78–87.

[123] Spyrakis F, Singh R, Cozzini P, et al. Isozyme-specific ligands for O-acetylserine sulfhydrylase, a novel antibiotic target. PLoS One. 2013;8:e77558.

[124] Annunziato G, Franko N, Pieroni M, et al. Integration of Enhanced Sampling Methods with Saturation Transfer Difference Experiments to Identify Protein Druggable Pockets. J. Chem. Inf. Model. 2018;58:710–723.

[125] Mozzarelli A, Bettati S, Pucci AM, et al. Catalytic competence of O-acetylserine sulfhydrylase in the crystal probed by polarized absorption microspectrophotometry. J. Mol. Biol. 1998;283:135–146.

[126] Martins PM, Rocha F, Damas AM. Understanding water equilibration fundamentals as a step for rational protein crystallization. PLoS One. 2008;3:e1998.

[127] Richter MF, Drown BS, Riley AP, et al. Predictive compound accumulation rules yield a broad-spectrum antibiotic. Nature. 2017;545:299–304.

[128] Magalhães J, Franko N, Annunziato G, et al. Refining the structure_activity relationships of 2-phenylcyclopropane carboxylic acids as inhibitors of O-acetylserine sulfhydrylase isoforms. J. Enzyme Inhib. Med. Chem. 2019;34:31–43.

[129] Huczyński A, Janczak J, Stefańska J, et al. Synthesis and antimicrobial activity of amide derivatives of polyether antibiotic—salinomycin. Bioorg. Med. Chem. Lett. 2012;22:4697–4702.

[130] Fu J, Cheng K, Zhang Z, et al. Synthesis, structure and structure–activity relationship analysis of caffeic acid amides as potential antimicrobials. Eur. J. Med. Chem. 2010;45:2638–2643.

[131] Spyrakis F, Felici P, Bayden AS, et al. Fine tuning of the active site modulates specificity in the interaction of O-acetylserine sulfhydrylase isozymes with serine acetyltransferase. Biochim. Biophys. Acta - Proteins Proteomics. 2013;1834:169–181.

[132] Magalhães J, Franko N, Annunziato G, et al. Discovery of novel

fragments inhibiting O-acetylserine sulphhydrylase by combining scaffold hopping and ligand–based drug design. J. Enzyme Inhib. Med. Chem. 2018;33:1444–1452.

[133] Ke Y-Y, Coumar MS, Shiao H-Y, et al. Ligand efficiency based approach for efficient virtual screening of compound libraries. Eur. J. Med. Chem. 2014;83:226–235.

[134] Hopkins AL, Groom CR, Alex A. Ligand efficiency: a useful metric for lead selection. Drug Discov. Today. 2004;9:430–431.

[135] Alexeev D, Baxter RL, Campopiano DJ, et al. Suicide inhibition of α-oxamine synthases: structures of the covalent adducts of 8-amino-7-oxononanoate synthase with trifluoroalanine. Org. Biomol. Chem. 2006;4:1209.

[136] Passera E, Campanini B, Rossi F, et al. Human kynurenine aminotransferase II - reactivity with substrates and inhibitors. FEBS J. 2011;278:1882–1900.

[137] Poulin R, Lu L, Ackermann B, et al. Mechanism of the irreversible inactivation of mouse ornithine decarboxylase by α-difluoromethylornithine. Characterization of sequences at the inhibitor and coenzyme binding sites. J. Biol. Chem. 1992;267:150–158.

[138] Cook PF, Hara S, Nalabolu S, et al. pH Dependence of the Absorbance and 31P NMR Spectra of O-Acetylserine Sulfhydrylase in the Absence and Presence of O-Acetyl-L-Serine. Biochemistry. 1992;31:2298–2303.

[139] Tai CH, Nalabolu SR, Simmons JW, et al. Acid-Base Chemical Mechanism of (9-Acetylserine Sulfhydrylases-A and -B from pH

Studies. Biochemistry. 1995;34:12311–12322.

[140] Wang E, Walsh C. Suicide substrates for the alanine racemase of Escherichia coli B. Biochemistry. 1978;17:1313–1321.

[141] Turner RJ, Weiner JH, Taylor DE. Tellurite-mediated thiol oxidation in Escherichia coli. Microbiology. 1999;145:2549–2557.

[142] Schelle MW, Bertozzi CR. Sulfate metabolism in mycobacteria. ChemBioChem. 2006;7:1516–1524.

[143] Álvarez R, Neumann G, Frávega J, et al. CysB-dependent upregulation of the Salmonella Typhimurium cysJIH operon in response to antimicrobial compounds that induce oxidative stress. Biochem. Biophys. Res. Commun. 2015;458:46–51.

[144] Kredich NM. Regulation Salmonella of L-Cysteine typhimurium Biosynthesis in Salmonella typhimurium. Biol. Chem. 1971;246:3474–3484.

[145] Campanini B, Benoni R, Bettati S, et al. Moonlighting O-acetylserine sulfhydrylase: New functions for an old protein. Biochim. Biophys. Acta. 2015;1854:1184–1193.

[146] Kredich NM. The molecular basis for positive regulation of cys promoters in Salmonella typhimurium and Escherichia coli. Mol. Microbiol. 1992;6:2747–2753.

[147] Neuwald AF, Krishnan BR, Brikun I, et al. cysQ, a gene needed for cysteine synthesis in Escherichia coli K-12 only during aerobic growth. J. Bacteriol. 1992;174:415–425.

[148] Fan F, Vetting MW, Frantom PA, et al. Structures and mechanisms of the mycothiol biosynthetic enzymes. Curr. Opin. Chem. Biol. 2009;13:451–459.

[149] Imlay JA, Linn S. Mutagenesis and Stress Responses Induced in Escherichia coli by Hydrogen Peroxide. J. Bacteriol. 1987;169:2967–2976.

[150] Zhao Y, Nickels LM, Wang H, et al. OxyR-regulated catalase activity is critical for oxidative stress resistance, nodulation and nitrogen fixation in Azorhizobium caulinodans. FEMS Microbiol. Lett. 2016;363:1–8.

[151] Müller A, Eller J, Albrecht F, et al. Allicin induces thiol stress in bacteria through S-allylmercapto modification of protein cysteines. J. Biol. Chem. 2016;291:11477–11490.

[152] Hansen RE, Winther JR. An introduction to methods for analyzing thiols and disulfides: Reactions, reagents, and practical considerations. Anal. Biochem. 2009;394:147–158.